Aus der

Klinik und Poliklinik für Psychiatrie und Psychotherapie

Klinikum der Ludwig-Maximilians-Universität München

Paving the way to investigate white matter pathology in schizophrenia with hiPSC-derived models

Dissertation
zum Erwerb des Doctor of Philosophy (Ph.D.)
an der Medizinischen Fakultät der
Ludwig-Maximilians-Universität München

vorgelegt von
Dr. med. Florian Joachim Raabe

aus
Augsburg

Jahr
2022

_____

Mit Genehmigung der Medizinischen Fakultät der
Ludwig-Maximilians-Universität München

Erstes Gutachten: Prof. Dr. Moritz Roßner

Zweites Gutachten: Prof. Dr. Andrea Schmitt

Drittes Gutachten: Prof. Dr. Rebecca Schennach

Viertes Gutachten: Prof. Dr. Leonhard Schilbach

Dekan: Prof. Dr. med. Thomas Gudermann

Tag der mündlichen Prüfung: 21.12.2022

Affidavit

Affidavit

Raabe, Florian
_____
Surname, first name

_____
Street

_____
Zip code, town, country

I hereby declare, that the submitted thesis entitled:

Paving the way to investigate white matter pathology in schizophrenia with hiPSC-derived models

is my own work. I have only used the sources indicated and have not made unauthorised use of services of a third party. Where the work of others has been quoted or reproduced, the source is always given.

I further declare that the submitted thesis or parts thereof have not been presented as part of an examination degree to any other university.
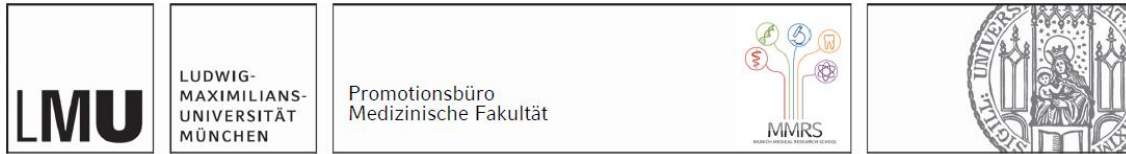
Munich, 04.04.2022   Florian Raabe
_____   _____
Place, date   Signature doctoral candidate

Confirmation of congruency

LMU LUDWIG-MAXIMILIANS-UNIVERSITÄT MÜNCHEN	Promotionsbüro Medizinische Fakultät	MMRS	

Confirmation of congruency between printed and electronic version of the doctoral thesis

Raabe, Florian
_____
Surname, first name

_____
Street

_____
Zip code, town, country

I hereby declare that the electronic version of the submitted thesis, entitled:

Paving the way to investigate white matter pathology in schizophrenia with hiPSC-derived models

is congruent with the printed version both in content and format.

Munich, 04.04.2022   Florian Raabe
_____   _____
Place, date   Signature doctoral candidate

Table of content

List of abbreviations

DTI   =   Diffusion tensor imaging

FA   =   Fractional anisotropy

GWAS   =   recent genome-wide association studies

hiPSC   =   human induced pluripotent stem cells

ICC   =   Immunocytochemistry

MIMICSS =   Multimodal Imaging in chronic Schizophrenia Study

mMRI   =   multimodal Magnetic Resonance Imaging

PMBCs   =   Peripheral blood mononuclear cells

scRNAseq =   single cell RNA sequencing

TMT-A   =   Trail Making Test parts A

TMT-B   =   Trail Making Test parts B

VLMT   =   Verbal Learning Memory Test

Abbreviation transcription factors

S   =   SOX10 =   SRY-box 10

O   =   OLIG2 =   oligodendrocyte transcription factor 2

N   =   *NKX6.2* =   NK6 homeobox 2

List of publications

Raabe, F. J., Stephan, M., Waldeck, J. B., Huber, V., Demetriou, D., Kannaiyan, N., . . . Rossner, M. J. (2022). Expression of Lineage Transcription Factors Identifies Differences in Transition States of Induced Human Oligodendrocyte Differentiation. *Cells, 11*(2). doi:10.3390/cells11020241

Yamada, S., Takahashi, S., Malchow, B., Papazova, I., Stocklein, S., Ertl-Wagner, B., . . . **Raabe, F. J.**, Keeser, D. (2021). Cognitive and functional deficits are associated with white matter abnormalities in two independent cohorts of patients with schizophrenia. Eur Arch Psychiatry Clin Neurosci. doi:10.1007/s00406-021-01363-8 **(shared last author)**

Gebicke-Haerter, P. J., Leonardi-Essmann, F., Haerter, J. O., Rossner, M. J., Falkai, P., Schmitt, A., & **Raabe, F. J.** (2021). Differential gene regulation in the anterior cingulate cortex and superior temporal cortex in schizophrenia: A molecular network approach. *Schizophrenia Research, 232*, 1-10. doi:10.1016/j.schres.2021.04.014

Adorjan, K., Pogarell, O., Streb, D., Padberg, F., Erdmann, C., Koller, G., **Raabe, F.**, . . . Falkai, P. (2021). Role of psychiatric hospitals during a pandemic: introducing the Munich Psychiatric COVID-19 Pandemic Contingency Plan. *BJPsych Open, 7*(2), e41. doi:10.1192/bjo.2020.167

Raabe, F. J., Wagner, E., Weiser, J., Brechtel, S., Popovic, D., Adorjan, K., . . . Koller, G. (2020). Classical blood biomarkers identify patients with higher risk for relapse 6 months after alcohol withdrawal treatment. Eur Arch Psychiatry Clin Neurosci. doi:10.1007/s00406-020-01153-8

Falkai, P., **Raabe, F.**, Bogerts, B., Schneider-Axmann, T., Malchow, B., Tatsch, L., . . . Schmitt, A. (2020). Association between altered hippocampal oligodendrocyte number and neuronal circuit structures in schizophrenia: a postmortem analysis. Eur Arch Psychiatry Clin Neurosci. doi:10.1007/s00406-019-01067-0 **(shared first author)**

Raabe, F.J.; Slapakova, L.; Rossner, M.J.; Cantuti-Castelvetri, L.; Simons, M.; Falkai, P.G.; Schmitt, A (2019). Oligodendrocytes as A New Therapeutic Target in Schizophrenia: From Histopathological Findings to Neuron-Oligodendrocyte Interaction. Cells, 8, doi:10.3390/cells8121496.

Papiol, S., Keeser, D., Hasan, A., Schneider-Axmann, T., **Raabe, F.**, Degenhardt, F., . . . Falkai, P. (2019). Polygenic burden associated to oligodendrocyte precursor cells and radial glia influences the hippocampal volume changes induced by aerobic exercise in schizophrenia patients. Transl Psychiatry, 9(1), 284. doi:10.1038/s41398-019-0618-z

Raabe, F. J., Galinski, S., Papiol, S., Falkai, P. G., Schmitt, A., & Rossner, M. J. (2018). Studying and modulating schizophrenia-associated dysfunctions of oligodendrocytes with patient-specific cell systems. NPJ Schizophr, 4(1), 23. doi:10.1038/s41537-018-0066-4

Wagner, E., **Raabe, F.**, Martin, G., Winter, C., Plorer, D., Krause, D. L., . . . Pogarell, O. (2018). Concomitant drug abuse of opioid dependent patients in maintenance treatment detected with a multi-target screening of oral fluid. Am J Addict. doi:10.1111/ajad.1273 **(shared first author)**

Kern, C., Kortum, K., Muller, M., **Raabe, F.**, Mayer, W. J., Priglinger, S., & Kreutzer, T. C. (2016). Correlation between weather and incidence of selected ophthalmological diagnoses: a database analysis. Clin Ophthalmol, 10, 1587-1592. doi:10.2147/OPTH.S107656

Zimmermann, C. A., Hoffmann, A., **Raabe, F.**, & Spengler, D. (2015). Role of mecp2 in experience-dependent epigenetic programming. Genes (Basel), 6(1), 60-86. doi:10.3390/genes6010060

Raabe, F. J., & Spengler, D. (2013). Epigenetic Risk Factors in PTSD and Depression. Front Psychiatry, 4, 80. doi:10.3389/fpsyt.2013.00080

1.   Introductory summary

1.1   Schizophrenia – clinical background

Schizophrenia is a severe, disabling neuropsychiatric disease with a high individual, social and economic global burden (James et al., 2018; Vos et al., 2020) and a lifetime prevalence just below 1% (McGrath, Saha, Chant, & Welham, 2008). Clinically, schizophrenia is characterized by positive symptoms such as hallucinations and delusion, negative symptoms such as affect flattening and lack of motivation, and cognitive deficits such as impaired working memory, reduced executive functioning and diminished attention (McCutcheon, Reis Marques, & Howes, 2020). Interestingly, "Dementia praecox" was the initial terminology for schizophrenia that was made popular by the founder of modern psychiatry and previous head of the Department of Psychiatry and Psychotherapy at the LMU Munich Emil Kraepelin (Kraepelin, 1899), and that implicated already the importance of cognitive dysfunction in schizophrenia (Falkai et al., 2015). On the treatment level, the "dopamine hypothesis" that was born in the 1960ies, explained the positive symptoms in schizophrenia based on hyperactive release of dopamine in mesolimbic structures (Brisch et al., 2014) and paved the way for most antipsychotic medications that are effective to treat the positive symptoms. Unfortunately, current antipsychotic medication and other substances in clinical trials do not substantially improve the negative and cognitive symptoms which are both more likely linked to disturbed cortical circuits (Goff, Hill, & Barch, 2011; McCutcheon et al., 2020) and to the functional outcome of the diseases (Green, Horan, & Lee, 2019). Therefore, to successfully improve patient outcomes and overcome the lack of efficacy of current treatments, therapies with novel modes of action are needed.

Importantly, schizophrenia is a highly heterogeneous diseases and the individual degree of affected clinical domains as well as the disease course differ between affected individuals (Falkai, Schmitt, & Cannon, 2011). By definition, the diagnosis of schizophrenia is based on operationalized clusters of symptoms that suffer from a lack of biological biomarkers that are meaningful enough to distinguish between other psychiatric diagnoses (McCutcheon et al., 2020). Overall, disentangling the neurobiological background of schizophrenia is needed to improve diagnosis and to develop innovative treatment strategies. Understanding the mechanisms underlying disturbed cognition in schizophrenia will completely change the view on this severe mental illness. In my thesis, I set the methodological basics to investigate potential oligodendroglial- and myelin-based dysfunctional mechanisms in patient representative subgroups. Pending positive results this research strategy may foster new myelin-based treatments.

1.2 Structural alterations, white matter pathology and oligodendroglial dysfunction in schizophrenia

Imaging studies revealed that schizophrenia spectrum disorders are associated with significant global and widespread alterations in brain structure (Haijma et al., 2013; van Erp et al., 2018), microstructure (Kelly et al., 2018), and connectivity (Brandl et al., 2019; Klauser et al., 2017; Li et al., 2017) which is supported by electrophysiological measurements (Schmitt, Hasan, Gruber, & Falkai, 2011).

These structural alterations are not only linked to neuronal dysfunction but also to changes of oligodendroglial lineage cells. A previous ENIGMA multicenter study that applied diffusion tensor imaging (DTI) in 4322 participants revealed widespread microstructural differences of the white matter in patients suffering from schizophrenia (Kelly et al., 2018) that were independent of the received antipsychotic treatment. Based on the analysis of several DTI-parameters, Kelly et al. concluded that the revealed white matter pathology in schizophrenia was most likely driven by aberrant myelination (Kelly et al., 2018).

The most abundant and prominent cells of the white matter are oligodendrocytes and their precursor cells. Oligodendrocytes provide the electric insulation from neuronal axons that enables the fast, saltatory transmission of action potentials along the axon (Nave, 2010). However, the biological function of the oligodendroglial lineage is not restricted to the commonly known myelination of neuronal cells. Oligodendrocytes are essential for the metabolic support to neuronal cells and perisomatic oligodendrocytes are electrically coupled to neuronal cells influencing the neuronal excitability of excitatory and inhibitory neurons via K+ buffering (Fields & Dutta, 2019; Micu, Plemel, Caprariello, Nave, & Stys, 2018; Simons & Nave, 2015). Moreover, there is a vibrant neuroglial crosstalk and the thickness of myelination is for example also dependent on neuronal activity which is important for complex processes such as learning and the brain's lifelong plasticity (Fields & Dutta, 2019).

Besides neurological diseases such as Multiple Sclerosis and Leukodystrophy that are characterized by neuroinflammation and neurodegeneration, schizophrenia has been associated with dysfunctions of oligodendrocyte precursor cells and oligodendrocytes (Raabe et al., 2019). Series of studies with different techniques clearly point out alterations of the white matter in schizophrenia (Bernstein, Steiner, Guest, Dobrowolny, & Bogerts, 2015; Cassoli et al., 2015) and post mortem studies provided good evidence for decreased oligodendrocyte number, disturbed oligodendrocyte precursor cells, altered oligodendroglial gene expression and impaired myelination in schizophrenia (Raabe et al., 2019).

Of note, oligodendrocyte impairments disturb axonal myelination which leads to deficits of the saltatory action potential propagation (fast conduction of nerve impulses) and which could impair cognitive performance (Fields, 2008). There is some evidence that disturbed white matter is associated with impaired cognition in patients with schizophrenia (Kuroki et al., 2006; Lim et al., 2006) and individuals at high-risk for schizophrenia (Kristensen et al., 2019). Furthermore, genetic variants of CNPase (2',3'-Cyclic-nucleotide 3'-phosphodiesterase) and MAG (Myelin-associated

glycoprotein) were associated with disturbed white matter and impaired cognition (Voineskos et al., 2013).

Overall, the above described findings indicate a dysfunctional oligodendroglial lineage and white matter pathology that might contribute to the pathophysiology of schizophrenia.

1.3   Genetic underpinnings of schizophrenia

Due to the heterogeneity of schizophrenia, the investigation of the underlining genetic aetiology has been faced several difficulties. Already decades ago, it was suggested that the presumed high genetic heritability would mainly stem from polygenetic mechanisms (Gottesman & Shields, 1967). Meanwhile, the genetic heritability of schizophrenia based on a large scale twin study (n = 31.524 twin pairs) has been estimated to be about 79% (Hilker et al., 2017) and recent genome-wide association studies (GWAS) identified 270 distinct risk loci (Pardinas et al., 2018; Ripke, Walters, & O'Donovan, 2020; Schizophrenia Working Group of the Psychiatric Genomics, 2014).

Importantly, schizophrenia associated GWAS loci are common variants of single-nucleotide polymorphism (SNP), that are abundant in the population, with an individual low effect size (Pardinas et al., 2018; Ripke et al., 2020; Schizophrenia Working Group of the Psychiatric Genomics, 2014).

Functional genomic pathway analysis intended to identify overarching pathways and common biological processes that are affected by the genetics of schizophrenia. Hereby synapse and immune pathways have been highlighted to be involved in schizophrenia *(The Network Pathway Analysis Subgroup of the Psychiatric Genomics, 2015; Wang et al., 2018)*. Pathway analyses with cell-type resolution using single cell RNAseq (scRNAseq) and single nuclear RNAseq (snRNAseq) identified a broad range of schizophrenia risk genes that were suggested to primarily affect excitatory and inhibitory neurons (Skene et al., 2018). However, also serial risk SNPs have been associated, on a less prominent degree compared to neuronal cells, with human oligodendroglial pathways (Duncan et al., 2014; Skene et al., 2018; Tansey & Hill, 2018).

Of note, GWAS-driven pathway analysis are not definite because:

I)   Transcriptomic studies on human *post mortem* brain that aim to provide cell type-specific RNA transcriptomes are technically restricted to snRNAseq with nuclear transcriptomes. This limits the analysis of transcripts that participate in cellular processes;

II)   low abundance transcripts, that code for example for transcription factors or components involved in signalling, might be underrepresented in certain cell type, e.g. in oligodendroglial cells compared to myelin-dependent transcripts;

III)   specific genes in pathway analysis that are linked to a certain cell-type are linked due to the highest gene expression in the certain cell-type. However, a certain gene could have relevant functions in other cell-types with lower expression as well;

IV)   transcripts that have not be identified to be cell type specific could nevertheless be (dys)functional in different classes of cells

(see Review in Appendix A (Raabe et al., 2018)).

In sum, genetic analysis provides evidence that the primary affected cell types in schizophrenia are neuronal cell types and it is discussed whether the oligodendroglial lineage is secondary disturbed due to primary neuronal deficits that are mediated by the neuroglial crosstalk or whether there are also cell-autonomous oligodendroglial defects in schizophrenia (see Review in Appendix A (Raabe et al., 2018)).

1.4   Human induced pluripotent stem cells

The advent of the human-derived induced pluripotent stem cell (hiPSC) technology (Takahashi & Yamanaka, 2006) combined with the technology to differentiate hiPSCs to principally any cell type of the brain, including those from the oligodendroglial lineage (Goldman & Kuypers, 2015) provides the unique possibility to study neuronal, glial cells and their networks "in a dish", which might push the boarders of translational research in neuropsychiatric diseases (Soliman, Aboharb, Zeltner, & Studer, 2017) (see also Review in Appendix A (Raabe et al., 2018)).

So far, several hiPSC-based studies highlighted neuronal dysfunction in schizophrenia and could reveal disturbed neuronal development, inhibited connectivity and impaired synapse function in neuronal cells from patients with schizophrenia (Prytkova & Brennand, 2017; Rasanen, Tiihonen, Koskuvi, Lehtonen, & Koistinaho, 2022; Soliman et al., 2017).

In contrast, only two recent hiPSC-based studies have investigated glial impairments in cohorts of sporadic schizophrenia and indicated a cell-autonomous disturbed oligodendroglial development and function in schizophrenia (McPhie et al., 2018; Windrem et al., 2017). The study of Windrem et al. was based on a very small cohort of only four affected patients with childhood-onset schizophrenia and revealed disturbed transcriptomic profiles that affect several signalling, developmental and oligodendrocyte differentiation pathways. Moreover, the authors found an impaired myelination capacity of glial progenitor cells derived from patients (Windrem et al., 2017). Additionally, McPhie et al. performed a very limited analysis with six affected patients that was restricted to immunocytochemistry only, and could provide some evidence that the development of the oligodendroglial lineage is impaired in schizophrenia (McPhie et al., 2018).

However, both studies were based on very protracted differentiation approaches that need 65 – 200 Days to be completed. These protracted differentiation approaches limit subsequent dissection of underlying mechanisms, to perform pharmaceutical or genetic high-throughput rescue experiments, or the application of hiPSC-technology in larger scale translational research setting (see Review in Appendix A (Raabe et al., 2018)). Finally, none of these paper provided translational data to which extend the in vitro data are associated with clinical relevant in vivo phenotypes.

1.6   Aims of the PhD Project

To investigate potential cell-autonomous disturbances of oligodendrocytes in schizophrenia, the key research tasks based on the agreement with the thesis advisory committee were:

a) Stratify candidate individuals with schizophrenia and controls without mental disorder of the deeply phenotyped cohort for subsequent translational hiPSC-based investigations.
b) Set up a neurobiological test system with accelerated oligodendrocyte differentiation approach that is suited to perform scaled case-control experiments.

1.7   Setting up a translational cohort

To study schizophrenia in patient-derived neurobiological test systems, our research group at the Department of Psychiatry, LMU Munich, has set up the *Multimodal Imaging in Chronic Schizophrenia Study* (MIMICSS) that provided a translational deeply phenotyped clinical cohort of individuals with schizophrenia (n=65), unaffected relatives (n=22) and controls (n=52). Patients, unaffected relatives and healthy controls were deeply phenotyped by an intensive assessment of psychopathology (PANSS, CGI, GAF, BDI-II, SANS, SAS-II), cognition (VLMT, TMT-A, TMT-B, Digit-Span-Task, DSST, d2 Test), and multimodal MRI imaging (structural MRI: T1, T2, DTI; fMRI: Resting State, language task, attention task). From a substantial part of the participants, I could organize to get peripheral blood mononuclear cells (PMBCs) that were banked in liquid nitrogen and that allowed subsequent hiPSC reprogramming (Ethikkommission München, Projekt-Nr.: 17-880).

## 1.8   Investigating polygenic driven disease mechanism in hiPSC-derived neurons

In a two centre collaboration project together with the *Lab for Genomics of Complex Diseases (Head: Michael Ziller), at the Department of Translational Research, Max Planck Institute of Psychiatry, Munich, Germany,* we investigated the highly polygenic nature (Pardinas et al., 2018; Ripke et al., 2020; Schizophrenia Working Group of the Psychiatric Genomics, 2014) of mental diseases in general and schizophrenia in particular using hiPSC. For this study, that is now in the submission process (Hausruckinger*, Raabe* et al., in submission, *contributed equally), I served as shared-first author.

We hypothesized that the aggregated effects of distinct genetic risk factor combinations found in each patient would functionally converge onto common biological mechanisms. In order to test this hypothesis, we first generated a large hiPSC cohort of 104 individual donors with and without mental illness: n = 38 patients with schizophrenia, n = 20 patients with bipolar disorder, n = 8 patients with major depression, and n = 38 neurotypical healthy controls. 42 individuals of this hiPSC cohort were from the PBMC cohort of MIMICSS.

After the generation of the 106 hiPSCs lines, we performed an extensive quality control including digital karyotyping using microarrays, immunocytochemistry (ICC) analysis of key pluripotency

markers, and assessment of differentiation potential by embryoid body (EB) formation followed by RNA-sequencing and lineage marker analysis. Moreover, the genetic analysis confirmed the absence of enriched copy number variations that were previously associated with schizophrenia in most of the donors and revealed a highly heterogeneous distribution of GWAS based common genetic variant risk factors for schizophrenia (Hausruckinger*, Raabe* et al., in submission, *contributed equally).
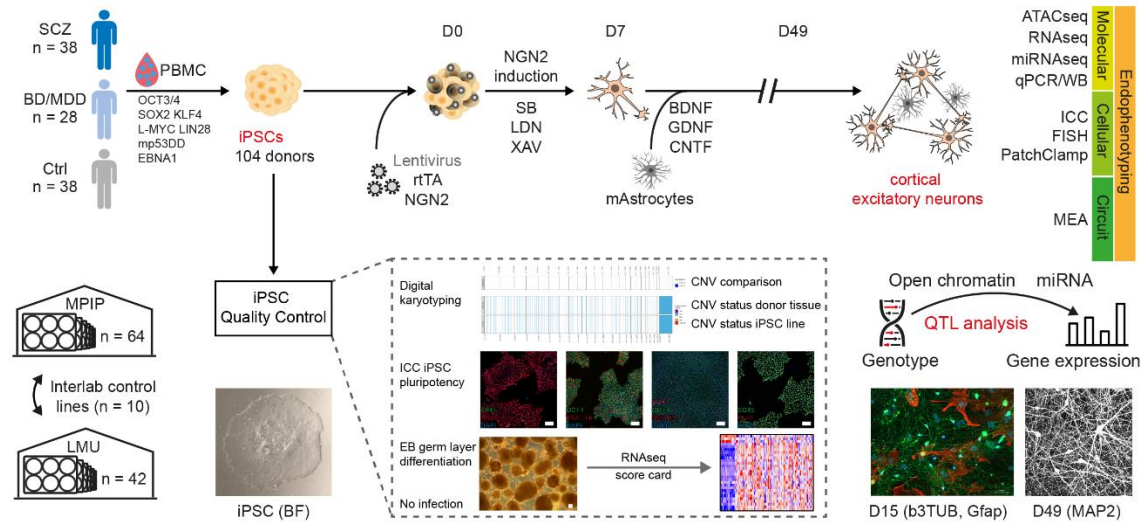
Figure 1: Study overview and quality control of iPSCs incl. genetic characterization. Schematic overview of iPSC line generation and differentiation to NGN2-directed cortical excitatory neurons (iNs), co-culturing with murine Astrocytes, and multi-modal endophenotyping after 49 days of differentiation which includes ATACseq, RNAseq, miRNAseq, qPCR, Western Blot (WB) on the molecular level, immunocytochemistry (ICC), fluorescence in situ hybridization (FISH) and electrophysiology by patch-clamp on a cellular level as well as multielectrode arrays (MEA) on the (micro)circuit level in a multicenter approach in order to perform a case-control study with patients affected with schizophrenia (SCZ), unipolar major depressive disorder (MDD), bipolar affective-disorder (BD) and healthy controls (Ctrl) to perform QTL analysis. iPSC characterization pipeline includes digital karyotyping (DK) using microarrays (Supplementary Fig. 1), immunocytochemistry (ICC) analysis of key pluripotency markers (Supplementary Fig. 2), and assessment of differentiation potential by embryoid body (EB) generation followed by RNA-Seq to perform score card assessment of the expressed germ layer signature. Infections with HIV, HCV, CMV and mycoplasma were excluded. Scale bars indicate 50μm.

Next, we applied a standardized in vitro neuronal differentiation using lentiviral overexpression of Neurogenin-2 (NGN2) for 49 days, followed by multi-omic profiling (RNAseq, ATACseq, miRNAseq) to perform quantitative trait analysis (QTL). Herby, we identified 1,891 genes, 2,992 chromatin peaks and 6 microRNAs that were modulated by the genetic variation in *cis* (i.e. SNP variants within promoters, enhancers, and intronic regions that regulate the expression level of the respective genes and miRNAs and that control chromatin accessibility).

In the following omics-based analysis, we investigated the differential expression of genes and mircoRNAs, and open chromatin between hiPSC-derived neurons from patients with schizophrenia and unaffected healthy controls. Hereby, we could identify 367 differential expressed genes and 67 differential expressed miRNAs. Interestingly, the identified genes did only partially overlap with GWAS hits for schizophrenia and were mostly subject of a complex

regulatory network of *cis-* and *trans*-acting factors. Moreover, we could reveal a dysregulation in the length of the 3'untranslated region (UTR) of many synapse related genes in hiPSC-derived neurons from patients with schizophrenia. For example, in SHANK3, a post-synaptic scaffold protein and known autism risk gene, the 3'UTR de-regulation of its mRNA expression was accompanied with an intracellular shift of *SHANK3* transcripts and SHANK3 protein localization. The associated cellular phenotype also included a reduced number of SHANK3-positive synapses and a disturbed microcircuit connectivity (Hausruckinger*, Raabe* et al., in submission, *contributed equally).

This comprehensive multi-level study of molecular and cellular endophenotyping showed that complex polygenic mechanisms converge on common pathways disrupted in schizophrenia, although individual patients have different polygenic backgrounds.

1.9   Association of white matter integrity with cognition and functional outcome in schizophrenia (Paper I)

To identify patient representative with presumed white matter pathology based on clinical deep phenotyping within the translational cohort, I teamed up with an imaging team (Shinichi Yamada, Shun Takahashi and Daniel Keeser) at the Department of Psychiatry, LMU Munich to analyse the deep phenotyped cohort.

For the study "Cognitive and functional deficits are associated with white matter abnormalities in two independent cohorts of patients with schizophrenia" (see Paper I (Yamada et al., 2021)), we used the available DTI datasets from 52 healthy controls and 50 patients and corresponding phenotype data. This allowed us to study the association of white matter integrity with cognition in schizophrenia and their impact on the functional outcome to pave the way for a meaningful subgroup stratification. To be able to reproduce our findings, we got the possibility to validate our findings in a clinical cohort (27 healthy controls and 48 patients) that was recruited at the University Medical Center Göttingen.

We calculated an overall cognition composite score based on the Verbal Learning Memory Test (VLMT), and the Trail Making Tests (TMT-A and TMT-B) covering diverse cognitive domains (verbal long and short term memory, executive function, attention, and cognitive flexibility) to allow a separation in two groups of patients: patients with better cognitive performance and patients with impaired cognitive performance (for details see Paper I (Yamada et al., 2021)).
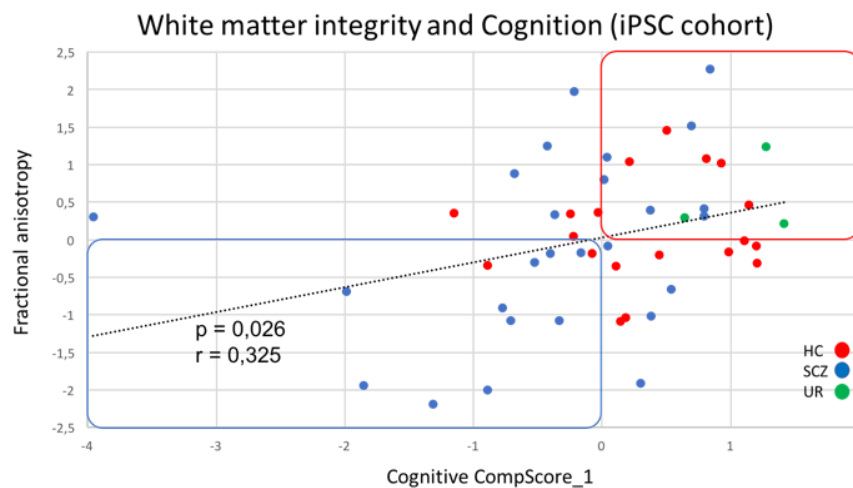
To determine the white matter integrity with DTI, we assessed the fractional anisotropy (FA) of the white matter tracts of the brain. Hereby, we could reveal significant altered atlas-defined regions in the white matter tracts in patients that, however, differed in their degree between both cohorts. In further analysis that were not restricted to non-brain-atlas defined regions but included the whole brain white matter skeleton, we could reveal significant lower FA in patients with lower cognitive performance compared to healthy controls. Finally, we could highlight an annotation of

the white matter integrity and the functional outcome using Global Assessment of Functioning (GAF) score (for details see Paper I (Yamada et al., 2021)).

My individual contributions to the paper are described in the respective contribution chapter (2.1 Contribution to Paper I).

1.10 Stratification based on white matter integrity and cognitive performance for a translational hiPSC cohort

Based on the clinical study (Yamada et al., 2021), I performed a stratification to identify candidate patients from whom we have PMBCs and hiPSCs and might be suited for translational experiments to investigate a potential oligodendroglial contribution.

Figure 2: Stratification of patients with schizophrenia, unaffected relatives and healthy controls based on cognition performance and white matter integrity. White matter integrity determined based on the individual fractional anisotropy (FA) of the white matter skeleton and composite score of the cognitive performance. Patients with cognitive impairments and reduced white matter integrity (blue marked quarter) were identified beside healthy controls and patients with high cognitive functioning and normal white matter integrity (red marked quarter). HC = healthy control, SCZ = schizophrenia, UR = unaffected relatives. Association calculated with person correlation using SPSS.

Within the translational cohort, I could replicate the significant association (Pearson correlation, r = 0.325, p = 0.026) of the cognitive performance versus FA deficits of the white matter tracts, which could be indicative for impaired myelination (Chang et al., 2017; Kelly et al., 2018). Hereby, I was able to identify schizophrenia patient with cognitive impairments and white matter pathology (= reduced FA) in contrast to patients and controls with high cognitive performance and no white matter pathology (**Figure 1**, unpublished data).

1.11 Barriers of oligodendrocyte differentiation from hiPSC

However, to investigate the oligodendroglial contribution in schizophrenia, there is also a need of robust and fast protocols to generate hiPSC-derived oligodendrocytes and their precursor cells. The initial strategies to generate oligodendrocytes from pluripotent stem cells applied

combinations of small molecules that stimulate or limit certain signaling pathways to foster oligodendroglial differentiation (Goldman & Kuypers, 2015; Lopez Juarez, He, & Richard Lu, 2016). However, a major disadvantage and limitation of the chemical differentiation strategies are the lengthy protocols, which need 65 – 200 days to be completed, and therefore limit scaled translational applications and are less suitable for potentially diagnostic approaches (see Review of Appendix A (Raabe et al., 2018)).

The "directed differentiation" is an alternative approach to generate differentiated cells. The principle is to force the overexpression of lineage-specific transcription factors that determines the hiPSC to differentiate towards an intended cell lineage (Oh & Jang, 2019) (see also Review of Appendix A (Raabe et al., 2018)).

Recently developed protocols for the differentiation of oligodendroglial cells from hiPSC (Ehrlich et al., 2017; Garcia-Leon et al., 2018; Pawlowski et al., 2017) used the transcriptions factors *SOX10* (SRY-box 10, abbreviated here as S) alone or (different) combination with the additional transcription factors *OLIG2* (oligodendrocyte transcription factor 2, abbreviated here as O) and *NKX6.2* (NK6 homeobox 2, abbreviated here as N).

Garcia et al. identified S alone to be most effective for the differentiation of oligodendrocytes (Garcia-Leon et al., 2018). Pawlowski et al. used SO to produce hiPSC-derived oligodendrocytes (Pawlowski et al., 2017). In contrast, the study Ehrlich et al. suggested that combining all three transcription factors (SON) might be most sufficient to generate oligodendrocytes (Ehrlich et al., 2017).

Unfortunately, additional to the application of distinct transcription factor combinations, the previous protocols differed also regarding several experimental settings that limits the direct comparison of the applied transcriptions factor combinations:

I)   The applied neural patterning approach, which was applied before the transcription factor overexpression, varied in terms of the time length and condition (free-floating vs. attached cell culture) of the neuronal patterning.

II)   The studies made use of different lentiviral constructs to overexpress the lineage transcription factors. Ehrlich et al. (2017) combined all transcription factors as a multicistronic unit within one lentiviral construct. Garcia et al. (2018) used individual lentiviral constructs without any antibiotic selection step for each individual transcription factor. The latter approach might reduce robustness and efficacy of the integration of several transcription factor compared to the application of only one single transcription factors.

III)   Previous studies did not investigate transcriptomics at single cell resolution that could more precisely address questions regarding cellular homogeneity and heterogeneity

1.12 Dissecting directed oligodendrocyte differentiation from hiPSC (Paper II)

To validate which protocol might be suitable for disease modelling, I initiated as first-author a study to compare S-, SO- and SON-directed oligodendroglial differentiation with a single and identical lentivirus backbone and with monolayer cell culture that are considered to be better standardisable and scalable for disease modelling (see Paper II (Raabe et al., 2022)).

The study "Expression of Lineage Transcription Factors Identifies Differences in Transition States of Induced Human Oligodendrocyte Differentiation" (see Paper II (Raabe et al., 2022)) was based on immunocytochemistry (ICC) and scRNAseq analysis. This study revealed that SON-directed differentiation might be better applied for studies that aim to investigate more mature oligodendrocytes in contrast to S alone that could be better for studies that investigate oligodendrocyte precursor biology.

To compare the differentiation potential on the protein level, I established ICC - based analysis that also contained a morphological quantification. Thereby, the ICC analysis could highlight that SON-directed differentiation allowed the generation of a higher amount of late-stage O4+ oligodendrocyte precursor cells (*O4-Antigens are sulfatides*) compared to SO and S. Moreover, SON-directed differentiation provided a faster generation of mature MBP+ (*myelin basic protein*) oligodendrocytes compared to S. Furthermore SON-directed oligodendrocytes displayed a more mature morphology in the quantitative morphological analysis (for details, see Paper II (Raabe et al., 2022)).

To study the transcriptome at single cell resolution, I established scRNAseq of the hiPSC-derived oligodendroglial cells. The analysis of the applied scRNAseq could address dissect questions regarding the heterogeneity of the culture conditions and allowed to investigate cell-type and transcription factor dependent pathways (for details, see Paper II (Raabe et al., 2022)).

Further, the transcriptomic analysis revealed that the maturation grade of the oligodendroglial cells was dependent on the expression level of the lentiviral constructs directing S- and SON differentiation underlining the construct validity of the applied approach (for details, see Paper II).

Furthermore, unsupervised hierarchical clustering highlighted the co-clustering of the hiPSC-derived oligodendroglial cells with primary murine oligodendrocyte precursor cells and mature oligodendrocytes (for details, see Paper II (Raabe et al., 2022)).

Addressing the maturation stage, the single cell RNA sequencing analysis also revealed a much higher percentage of oligodendrocytes in the SON-directed differentiation compared to the S-directed oligodendroglial differentiation. Furthermore, the SON-directed oligodendrocytes expressed higher levels of late-stage oligodendrocyte marker genes compared to the S-directed differentiation (for details, see Paper II (Raabe et al., 2022)).

Moreover, RNA velocity analysis indicated that S-derived oligodendrocyte precursor cells escape to a much higher degree the oligodendroglial differentiation path as compared to SON-directed

oligodendrocyte precursor cells and that S-derived oligodendroglial cells are less mature than those generated with SON (for details, see Paper II (Raabe et al., 2022)).

My individual contributions to the study are described in the respective contribution chapter (2.2 Contribution to Paper II).

1.13 Paving the way to investigate white matter pathology in schizophrenia with hiPSC-derived models

Until recently, research on the biological causes of psychiatric disorders was mainly limited to imaging studies, genetic and molecular analysis of peripheral tissues (mainly blood), and studies on postmortem brain samples (see Review in Appendix A (Raabe et al., 2018)). The advent of hiPSC technology may help to overcome several of those limitations and promises to expand the boarders of biological psychiatry.

In my PhD projects, I stressed two major bottlenecks of translational psychiatry using hiPSC-based neurobiological test systems.

One bottleneck is the selection of disease-representative patients from whom hiPSCs should be generated and applied to investigate diseases-relevant biology. The generation of a deeply phenotyped cohort using multimodal imaging and neurocognitive testing served as the basis for the initiated translational cohort at the Stem Cell Unit from the Department of Psychiatry, LMU Munich, to study schizophrenia relevant biology, including the oligodendroglial contribution, in human-derived cellular test systems. The clinical study "Cognitive and functional deficits are associated with white matter abnormalities in two independent cohorts of patients with schizophrenia" (Paper I (Yamada et al., 2021)) provided the basis for the applied patient stratification to investigate a potential oligodendroglial contribution in schizophrenia in a future project.

Another bottleneck is the availability of robust neurobiological test systems and established test readouts. The study "Expression of Lineage Transcription Factors Identifies Differences in Transition States of Induced Human Oligodendrocyte Differentiation" (Paper II (Raabe et al., 2022)) provided a robust and fast method (22 days) to generate mature oligodendrocytes. Herby, I established a modified approach for the lentiviral differentiation construct. In contrast to previous studies in which the lentiviral infection was performed after the initial neuronal patterning (Ehrlich et al., 2017; Garcia-Leon et al., 2018), I established the lentiviral infection already at the hiPSC stage that can easily be amplified, frozen and banked, and applied en masse for future case-control cohort experiments, genetic or compound screenings.

Based on my PhD project, I paved the way to investigate the oligodendroglial contribution of white matter pathology in schizophrenia with patients-derived hiPSC-based models in stratified diseases-relevant subgroups in our lab. Of note, the origin of white matter pathology in schizophrenia could also be due to primary neuronal deficits and the subsequent disturbed neuroglial crosstalk. However, the co-cultivation of hiPSC-based neurons and oligodendrocytes

might also specifically help to address the question of primary cellular cause and secondary contribution.

Investigating disease-relevant subgroups using the hiPSC technology promises to overcome current limitations of biological psychiatry in order to dissect cellular and molecular disease mechanisms in patient-derived models. In addition, new treatment strategies aimed at enhancing oligodendrocyte proliferation and differentiation should be tested in these in-vitro human cellular models.

2. Contribution to the PhD publications and Appendix

2.1 Contribution to Paper I

Yamada, S., S. Takahashi, B. Malchow, I. Papazova, S. Stocklein, B. Ertl-Wagner, B. Papazov, U. Kumpf, T. Wobrock, K. Keller-Varady, A. Hasan, P. Falkai, E. Wagner, **F. J. Raabe (shared last author),** and D. Keeser. "Cognitive and Functional Deficits Are Associated with White Matter Abnormalities in Two Independent Cohorts of Patients with Schizophrenia." *Eur Arch Psychiatry Clin Neurosci*. https://dx.doi.org/10.1007/s00406-021-01363-8.

For the clinical study that focused on cognitive impairments in schizophrenia and their association with structural alteration of the white matter using DTI, I served as shared-last and corresponding author.

The larger of the two cohorts within the study, the Multimodal Imaging in chronic Schizophrenia Study (MIMICSS), was assembled at the Department of Psychiatry and Psychotherapy, LMU Munich, Germany. Hereby, I did patient recruitment and clinical characterization and organized the mMRI investigations and the neurocognitive testing. For the study that focused on cognition, functional deficits and structural alteration, I was part of the core team who conceptualized the study. Hereby I defined the exclusion and inclusion criteria for the study and set up the cognitive metrics that was subsequent applied by the formal analysis team that I supervised. Moreover, I performed the data visualization and wrote the initial draft with the core team. Finally, I organized as corresponding author the manuscript handling with the other coauthors and managed the submission and publishing process.

2.2 Contribution to Paper II

Raabe, F. J., M. Stephan, J. B. Waldeck, V. Huber, D. Demetriou, N. Kannaiyan, S. Galinski, L. V. Glaser, M. C. Wehr, M. J. Ziller, A. Schmitt, P. Falkai, and M. J. Rossner. "Expression of Lineage Transcription Factors Identifies Differences in Transition States of Induced Human Oligodendrocyte Differentiation." *Cells* 11, no. 2. https://dx.doi.org/10.3390/cells11020241.

For the preclinical study that focused on the directed differentiation of oligodendrocytes and their precursor cell from human induced pluripotent stem cells (hiPSC) I served as first-author.

I conceptualized the study, established the core parts of the applied approach and methodology, such lentiviral infection with differentiation constructs, hiPSC-derived directed oligodendroglial differentiation, immunocytochemistry (ICC) experiments, ICC co-localization analysis, ICC-morphological analysis, single cell RNA sequencing (scRNAseq) in the lab and organized funding for the study. Moreover, I planned and performed the experiments for the study. For the transcriptomics analysis, I defined the settings and genes of interests which were analyzed together with the second author Marius Stephan who provided his well-established transcriptomic analysis scripts and did the formal analysis. Finally, I conducted the data visualization, designed the figures, and wrote the initial first draft manuscript.

2.4 Contribution to Appendix A

Raabe, F. J., S. Galinski, S. Papiol, P. G. Falkai, A. Schmitt, and M. J. Rossner. "Studying and Modulating Schizophrenia-Associated Dysfunctions of Oligodendrocytes with Patient-Specific Cell Systems." *NPJ Schizophr* 4, no. 1: 23. https://dx.doi.org/10.1038/s41537-018-0066-4.

This review paper served as preview for the planned PhD projects, provided the conceptional backgroup of the attempt to study oligodendrocyte biology in schizophrenia with patient-derived hiPSC-based neurobiological test systems. I served as first author who was involved in the conventionalization of the review, performed the literature search, did the figure visualization, and wrote the initial first draft. Important: Appendix A does not contain original data and provides background for the two original papers.

3.   Paper I

Cognitive and functional deficits are associated with white matter abnormalities in two independent cohorts of patients with schizophrenia

Shinichi Yamada[1,2,#], Shun Takahashi[1,2,3], Berend Malchow[1,4], Irina Papazova[5], Sophia Stöcklein[6], Birgit Ertl-Wagner[7], Boris Papazov[6], Ulrike Kumpf[1], Thomas Wobrock[4,8], Katriona Keller-Varady[9], Alkomiet Hasan[5], Peter Falkai[1], Elias Wagner[1], Florian J. Raabe[1,10,*,#], Daniel Keeser[1,6,11*,#]

[1] Department of Psychiatry and Psychotherapy, University Hospital, LMU Munich, Munich, Germany
[2] Department of Neuropsychiatry, Wakayama Medical University, Wakayama, Japan
[3] Clinical Research and Education Center, Asakayama General Hospital, Sakai, Japan
[4] Department of Psychiatry and Psychotherapy, University Medical Center Göttingen, Göttingen, Germany
[5] Department of Psychiatry Psychotherapy and Psychosomatics, Medical Faculty, University of Augsburg, Augsburg, Germany
[6] Department of Radiology, University Hospital, LMU Munich, Munich, Germany
[7] Department of Diagnostic Imaging, Division of Neuroradiology, The Hospital for Sick Children, Toronto, Canada
[8] Department of Psychiatry and Psychotherapy, County Hospitals Darmstadt-Dieburg, Gross-Umstadt, Germany
[9] Institute of Sports Medicine, Hannover Medical School, Hannover, Germany
[10] International Max Planck Research School for Translational Psychiatry (IMPRS-TP), Munich, Germany
[11] NeuroImaging Core Unit Munich (NICUM), University Hospital, LMU Munich, Munich, Germany
* These authors contributed equally

Corresponding authors: Florian.Raabe@med.uni-muenchen.de, Daniel.Keeser@med.uni-muenchen.de

ORIGINAL PAPER

Cognitive and functional deficits are associated with white matter abnormalities in two independent cohorts of patients with schizophrenia

Shinichi Yamada[1,2] · Shun Takahashi[1,2,3] · Berend Malchow[1,4] · Irina Papazova[5] · Sophia Stöcklein[6] ·
Birgit Ertl-Wagner[7] · Boris Papazov[6] · Ulrike Kumpf[1] · Thomas Wobrock[4,8] · Katriona Keller-Varady[9] ·
Alkomiet Hasan[5] · Peter Falkai[1] · Elias Wagner[1] · Florian J. Raabe[1,10] · Daniel Keeser[1,6,11]

Abstract

Background Significant evidence links white matter (WM) microstructural abnormalities to cognitive impairment in schizophrenia (SZ), but the relationship of these abnormalities with functional outcome remains unclear.

Methods In two independent cohorts (C1, C2), patients with SZ were divided into two subgroups: patients with higher cognitive performance (SZ-HCP-C1, $n = 25$; SZ-HCP-C2, $n = 24$) and patients with lower cognitive performance (SZ-LCP-C1, $n = 25$; SZ-LCP-C2, $n = 24$). Healthy controls (HC) were included in both cohorts (HC-C1, $n = 52$; HC-C2, $n = 27$). We compared fractional anisotropy (FA) of the whole-brain WM skeleton between the three groups (SZ-LCP, SZ-HCP, HC) by a whole-brain exploratory approach and an atlas-defined WM regions-of-interest approach via tract-based spatial statistics. In addition, we explored whether FA values were associated with Global Assessment of Functioning (GAF) scores in the SZ groups.

Results In both cohorts, mean FA values of whole-brain WM skeleton were significantly lower in the SCZ-LCP group than in the SCZ-HCP group. Whereas in C1 the FA of the frontal part of the left inferior fronto-occipital fasciculus (IFOF) was positively correlated with GAF score, in C2 the FA of the temporal part of the left IFOF was positively correlated with GAF score.

Conclusions We provide robust evidence for WM microstructural abnormalities in SZ. These abnormalities are more prominent in patients with low cognitive performance and are associated with the level of functioning.

Keywords Cognitive deficits · Fractional anisotropy · Global functioning · Schizophrenia · Replication · Confirmation

Abbreviations

DTI	Diffusion tensor imaging	STM	Short-term memory
FA	Fractional anisotropy	SZ	Schizophrenia
FSL	FMRIB software library	SZ-HCP	Schizophrenia with higher cognitive performance
HC	Healthy controls		
IFOF	Inferior fronto-occipital fasciculus	SZ-LCP	Schizophrenia with lower cognitive performance
GAF	Global assessment of functioning		
PANSS	Positive and negative syndrome Scale	TBSS	Tract-based spatial statistics
		TMT-A	Trail Making Test part A
		TMT-B	Trail Making Test part B
		LTM	Long-term memory
		WM	White matter

Shinichi Yamada, Florian J. Raabe and Daniel Keeser contributed equally.

✉ Florian J. Raabe
  florian.raabe@med.uni-muenchen.de

✉ Daniel Keeser
  daniel.keeser@med.uni-muenchen.de

Extended author information available on the last page of the article

◯ Springer

Introduction

Schizophrenia (SZ) is a severe neuropsychiatric disorder that is associated with poor social [1–3] and occupational functioning [3, 4]. This poor functioning is related to neurocognitive impairment [5–8]. Neurocognitive impairments can be present from the at-risk period to the chronic stages of SZ [9], but not all patients are affected by cognitive deficits. The fifth edition of *Diagnostic and Statistical Manual of Mental Disorders (DSM-V)* describes a broad range of severities of cognitive impairment in SZ, ranging from intact to severe [10]. However, the question remains unanswered whether the different levels of impairment correlate with different neurobiological characteristics. Understanding the relationship between the degree of cognitive impairment and the underlying neurobiology is key in developing innovative neural targets to improve functional outcomes in SZ.

The disconnection hypothesis in SZ has been put forward in the form of various disconnection theories, such as disconnection of fronto-temporal regions [11, 12], formation of cortico-thalamo-cerebellar loops [13], and crossing of interhemispheric fibers in the corpus callosum [14]. White matter (WM) fibers connect brain regions structurally and functionally [15, 16], including the cortices associated with various cognitive domains [17, 18]. WM microstructural abnormalities can be revealed by diffusion tensor imaging (DTI) because the DTI signal is sensitive to the movement of water molecules and WM microstructures were shown to represent directional information of water molecules [19–21] in postmortem animal studies [22–24] and human brain dissections [25–27]. Recently, the ENIGMA Schizophrenia DTI Working Group conducted the largest international multicenter study to date; it included 4322 patients with SZ from 29 independent international cohorts and highlighted a disturbed WM integrity in widespread regions [28]. Previous studies have supported the importance of WM integrity decline for cognitive impairment [29–31] and functioning in SZ [3, 32]. However, to our knowledge, the relationship between WM integrity, cognitive function, and global functioning in SZ has not yet been investigated with the same analytical methods and replicated in two independent samples with different MRI parameters.

Therefore, we performed a replication study that applied a whole-brain exploratory approach and atlas-defined WM regions-of-interest approach via tract-based spatial statistics (TBSS) in two different cohorts. In the present study, we aimed to robustly identify microstructural differences in WM in patients with SZ subdivided into groups with good and poor cognitive performance. Moreover, we aimed to investigate the relationship

between regions-of-interest (ROIs) selected on the basis of exploratory findings and functional outcomes in SZ. We hypothesized that brain WM microstructure in SZ is more severely disturbed in patients with poor cognitive performance and poor functioning.

Methods

Participants

Participants in cohort (1) were recruited from the University Hospital, LMU Munich, Germany. This study was approved by the local ethics committee of the University Hospital, LMU Munich (project number: 17–13), and written informed consent was obtained from all participants. The patients were diagnosed by two independent, experienced psychiatrists using the criteria of the *International Statistical Classification of Diseases and Related Health Problems, 10th revision (ICD-10)* [33]. Individuals with no current or past mental illness (according to the MINI Plus Interview [34]) were recruited into the HC group. Most patients were treated with antipsychotic medication, daily dosage of antipsychotic was calculated using the chlorpromazine equivalent method [35] and additional treatment with antidepressants and/or a benzodiazepines was assessed. In all patients, symptom severity was determined with the Positive and Negative Syndrome Scale (PANSS) [36] and level of functioning with the Global Assessment of Functioning (GAF) [37]. GAF scores were demeaned (subtracting the group mean from the individual scores, thus, the new mean is zero) to avoid overestimated associations. Parts of cohort (1) individuals were included in previous studies [38–40]. Participants from cohort (2) were recruited at the Department of Psychiatry and Psychotherapy of the University Medical Center Göttingen, and were assessed with the baseline in a previous longitudinal study [41, 42].

The demographic and clinical characteristics of the study participants in cohorts (1) and (2) are shown in Table 1. Each cohort consisted of patients with SZ and HC. In each cohort, the participants with SZ were evenly divided into a group with higher cognitive performance (HCP) and one with lower cognitive performance (LCP) on the basis of the cognitive composite score, as described in below. Cohort (1) comprised 52 HC and 50 patients with SZ, evenly subdivided into an HCP group (SZ-HCP-C1 group, $n = 25$) and LCP group (SZ-LCP-C1 group; $n = 25$), and cohort (2) comprised 27 HC and 48 patients with SZ subdivided into an HCP group (SZ-HCP-C2 group, $n = 24$) and LCP group (SZ-LCP-C2 group, $n = 24$).

Table 1 Demographic and clinical characteristics in cohort (1) and (2)

	Cohort (1)							Cohort (2)						
	HC (n=52)	SZ (n=50)	p	SZ-HCP-C1 (n=25)	SZ-LCP-C1 (n=25)	p	Post hoc comparisons (HC vs SZ-HCP-C1)(HC vs SZ-LCP-C1)(SZ-HCP-C1 vs SZ-LCP-C1)	HC (n=27)	SZ (n=48)	p	SZ-HCP-C2 (n=24)	SZ-LCP-C2 (n=24)	p	Post hoc comparisons (HC vs SZ-HCP-C2)(HC vs SZ-LCP-C2)(SZ-HCP-C2 vs SZ-LCP-C2)
Age, y, mean (sd)	32.07 (10.95)	35.16 (11.26)	0.164[a]	32.56 (9.19)	37.76 (12.66)	0.097[b]		36.62 (10.91)	35.2 (12.4)	0.642[a]	31.91 (10.65)	38.66 (13.30)	0.127[b]	
Sex, n, male/female	39/13	42/8	0.261[c]	20/5	22/3	0.416[c]		18/9	33/15	0.852[c]	16/8	17/7	0.307[c]	
Hand preference, n, right/left	46/6	46/4	0.547[c]	24/1	22/3	0.531[c]		21/6	42/6	0.270[c]	21/3	21/3	0.544[c]	
Duration of school education, y, mean (sd)	12.27 (1.269)	11.52 (2.187)	0.036*[a]	11.76 (1.942)	11.28 (2.424)	0.068[b]	(0.702)(0.070)(1.000)	11.96 (1.372)	11.66	0.425[a]	12.58 (1.442)	10.75 (1.648)	<0.001[b]	(0.424)(0.015*)(<0.001***)
Duration of illness, y, mean (sd)		8.920 (9.023)		7.600 (7.852)	10.24 (10.04)	0.306[a]			9.916 (8.867)		7.791 (8.005)	12.04 (9.336)	0.097[a]	
PANSS positive score, mean (sd)		13.96 (5.409)		13.92 (5.015)	14.00 (5.880)	0.959[a]			14.33 (6.302)		13.75 (5.712)	14.91 (6.915)	0.527[a]	
PANSS negative score, mean (sd)		16.98 (5.235)		15.00 (4.627)	18.96 (5.135)	0.006**[a]			20.16 (9.198)		19.33 (8.297)	21.00 (10.12)	0.536[a]	
PANSS general score, mean (sd)		30.44 (8.435)		19.32 (7.695)	31.56 (9.133)	0.353[a]			37.33 (16.76)		33.04 (14.49)	41.62 (18.04)	0.076[a]	
PANSS total score, mean (sd)		61.38 (16.67)		58.24 (15.446)	64.52 (17.55)	0.186[a]			71.83 (29.98)		66.12 (25.8)	77.54 (33.21)	0.190[a]	
Demean GAF, mean (sd)		55.77 (9.66)		58.38 (9.588)	53.16 (9.186)	0.055[a]			59.93 (11.93)		61.75 (12.42)	58.12 (11.38)	0.298[a]	
STM score, z scores, mean (sd)	0.516 (0.915)	−0.537 (0.794)	<0.001[a]	−0.067 (0.691)	−1.007 (0.592)	<0.001[b]	(0.010**)(<0.001***)(<0.001***)	0.276 (0.873)	−0.155 (1.051)	0.074[a]	0.440 (0.942)	−0.751 (0.792)	<0.001[b]	(1.000)(<0.001***)(<0.001***)
LMT score, z scores, mean (sd)	0.543 (0.667)	−0.564 (0.989)	<0.001[a]	0.142 (0.604)	−1.271 (0.727)	<0.001[b]	(0.052)(<0.001***)(<0.001***)	0.234 (0.857)	−0.132 (1.067)	0.131[a]	0.485 (0.746)	−0.749 (0.988)	<0.001[b]	(0.924)(<0.001***)(<0.001***)
TMT-A, time (s), z scores, mean (sd)	−0.467 (0.858)	0.488 (0.914)	<0.001[a]	0.013 (0.791)	0.963 (0.781)	<0.001[b]	(0.054)(<0.001***)(<0.001***)	−0.267 (0.632)	0.150 (1.144)	0.045*[a]	−0.578 (0.739)	0.879 (1.011)	<0.001[b]	(0.518)(<0.001***)(<0.001***)
TMT-B, time (s), z scores, mean (sd)	−0.420 (0.498)	0.437 (1.199)	<0.001[a]	−0.244 (0.487)	1.119 (1.315)	<0.001[b]	(1.000)(<0.001***)(<0.001***)	−0.293 (0.965)	0.165 (1.001)	0.058[a]	−0.466 (0.503)	0.797 (0.981)	<0.001[b]	(1.000)(<0.001***)(<0.001***)

Table 1 (continued)

	Cohort (1)							Cohort (2)						
	HC (n=52)	SZ (n=50)	p	SZ-HCP-C1 (n=25)	SZ-LCP-C1 (n=25)	p	Post hoc comparisons (HC vs SZ-HCP-C1)(HC vs SZ-LCP-C1)(SZ-HCP-C1 vs SZ-LCP-C1)	HC (n=27)	SZ (n=48)	p	SZ-HCP-C2 (n=24)	SZ-LCP-C2 (n=24)	p	Post hoc comparisons (HC vs SZ-HCP-C2)(HC vs SZ-LCP-C2)(SZ-HCP-C2 vs SZ-LCP-C2)
Cognitive composite score, z scores, mean (sd)	0.487 (0.548)	−0.507 (0.760)	<0.001[a]	0.076 (0.375)	−1.090 (0.574)	<0.001[b]	(0.005**) (<0.001***) (<0.001***)	0.268 (0.565)	−0.150 (0.826)	0.022*[a]	0.492 (0.471)	−0.794 (0.557)	<0.001[b]	(0.417) (<0.001***) (<0.001***)
Daily dose of antipsychotics, CPZ equivalents, mean (sd)		472.1 (325.6)		437.4 (265.2)	506.8 (379.0)	0.456[a]			548.9 (545.4)		600.0 (646.3)	497.8 (429.9)	0.522[a]	
Antidepressant, n, with/without		8/42		3/22	5/20	0.440[c]			11/37		5/19	6/18	0.731[c]	
Benzodiazepine, n, with/without		7/43		2/23	5/20	0.221[c]			6/41		1/23	5/19	0.080[c]	

Significant differences among the three groups are marked. Values marked with ***, ** and * are significant at $p < 0.001$, $p < 0.01$, and $p < 0.05$, respectively

HC healthy controls, *SZ* schizophrenia, *HCP* high cognitive performer, *LCP* low cognitive performer, *SD* standard deviation, *PANSS* Positive and Negative Syndrome Scale, *GAF* Global Assessment of Functioning, *CPZ equivalents* chlorpromazine equivalents

[a] Independent samples *t* test

[b] Analysis of variance and Bonferroni's post hoc test

[c] Chi-square test

Neuropsychological measurements in cohorts (1) and (2)

We used neurocognitive instruments that are related to functional deficits in SZ [7, 30, 43]. Neurocognitive function was assessed by experienced psychologists with the short-term memory (STM) and long-term memory (LTM), which were obtained from previous factor analyses of the Verbal Learning Memory Test [44], and the Trail Making Test parts A (TMT-A) and B (TMT-B) [45]. Z scores, that consisted of number of remembered words (STM, LTM, high score = good performance), and seconds to complete task (TMT-A, TMT-B, high score = poor performance), were used for the neuropsychological tests. Within each cohort, a cognitive composite score was calculated with the following equation: $\{(STM\ z\ scores) + (LTM\ z\ scores) + (-1) \times (TMT\text{-}A\ z\ scores) + (-1) \times (TMT\text{-}B\ z\ scores)\}/4$.

Magnetic resonance imaging data acquisition and DTI parameters in cohort (1)

All magnetic resonance imaging (MRI) examinations were performed with a 3.0 T MR scanner (Magnetom Skyra, Siemens Healthcare, Erlangen, Germany) with a standard 20-channel phased-array head coil. DTI was performed with 64 non-collinear diffusion-encoding directions and the following parameters: repetition time, 9600 ms; echo time, 95 ms; field of view, 244 mm; voxel size, $2.0 \times 2.0 \times 2.0$ mm; slice thickness, 2.0 mm; 65 slices; and multiple diffusion weighting b values ($b = 1000$ s/mm^2 and $b = 0$).

MRI data acquisition and DTI parameter in cohort (2)

All MRI examinations were performed with a 3.0 T MR scanner (Magnetom TIM Trio, Siemens Healthcare, Erlangen, Germany) with a standard 8-channel phased-array head coil. DTI was performed with 12 non-collinear diffusion-encoding directions and the following parameters: repetition time, 6500 ms; echo time, 96 ms; field of view, 256 mm; voxel size, $2.0 \times 2.0 \times 2.0$ mm; slice thickness, 2.0 mm; 49 slices; and multiple diffusion weighting b values ($b = 1000$ s/mm^2 and $b = 0$).

Imaging analysis in cohorts (1) and (2)

DTI data were processed with TBSS programs [46] in the FMRIB software Library (FSL), version 6.0.0. [47]. The Brain Extraction Tool was used to create a binary mask from the non-diffusion-weighted data, and the diffusion tensor and associated parameters such as fractional anisotropy (FA) maps were calculated with the DTIFIT program implemented in the FSL. Nonlinear transformation and affine registration were performed to normalize all FA data into a standard space with the nonlinear registration tool FNIRT [48]. Normalized FA images were averaged to create a mean FA image, and a mean FA skeleton was created by taking the centers of all tracts common to all participants. The voxel values of each participant's FA map were projected onto the skeleton by searching the local maxima along the perpendicular direction from the skeleton. The resulting data were fed into the voxel-wise statistical analysis described in Sect. 2.5.

Statistical analyses in cohorts (1) and (2)

In each cohort, differences in demographic and clinical characteristics between the HC and SZ groups were analyzed by independent samples t tests for continuous variables (age, duration of school education, the z score of four neurocognitive tests and the cognitive composite score) and chi-square tests for categorical variables (sex distribution and hand preference), with a significance level of $\alpha < 0.05$. Differences in demographic and clinical characteristics between the SZ-HCP and SZ-LCP groups in each cohort were analyzed with independent samples t tests for continuous variables (duration of illness, PANSS subscores, GAF scores, chlorpromazine daily dose equivalents) and chi-square tests for the number of patients taking medication, with a significance level of $\alpha < 0.05$. Differences in demographic and clinical characteristics between the HC, SZ-HCP, and SZ-LCP groups in each cohort were analyzed by analysis of variance and Bonferroni's post hoc test for continuous variables (age, duration of school education, and the z scores of each neurocognitive test) and chi-square tests for categorical variables (sex distribution and hand preference), with a significance level of $\alpha < 0.05$. Group differences in demographic and clinical characteristics between the SZ groups in cohorts (1) and (2) were analyzed by independent samples t tests for continuous variables (age and duration of school education) and chi-square tests for categorical variables (sex distribution and hand preference), with a significance level of $\alpha < 0.05$. All statistical analyses were performed with IBM SPSS statistics 20.

Whole-brain exploratory approach

Voxel-wise statistics of the skeletonized FA data were applied using randomize in FSL, version 6.0.0. The HC and SZ groups were compared by an analysis of covariance design, with age and sex as nuisance covariates. We randomly performed permutation-based testing with 5000 permutations and inference by threshold-free cluster enhancement (TFCE) with a threshold of less than 0.05. The mean FA values of the whole skeleton in the HC, SZ-HCP, and SZ-LCP groups were examined for differences by analysis of variance and Bonferroni's post hoc test, with age and sex as covariates, with a significance level of $\alpha < 0.05$.

Atlas-defined WM regions-of-interest approach

For atlas-based segmentation, all extracted skeletons were overlaid with the Johns Hopkins University DTI-based WM Atlas in FSL [49, 50]. Differences of the mean FA values in 20 ROIs in the HC and SZ groups were examined by independent samples t tests, with age and sex as covariates, with significance set at $p < 0.00125$. ($= 0.05/40$ WM tracts because 20 WM tracts were examined in each cohort). The mean FA values of 20 ROIs in the HC, SZ-HCP, and SZ-LCP groups were examined for differences by analysis of variance and Bonferroni's post hoc test, with age and sex as covariates and significance set at $p < 0.00125$ ($= 0.05/40$ WM tracts because 20 WM tracts were examined in each cohort). In the voxels with a statistical difference in the mean FA values of 20 ROIs, voxel-wise multiple regression analyses were performed with TBSS to examine the relationship between FA values and demean GAF scores. We used 5000 permutations to calculate FA values using age and sex as covariates. Spearman's rank correlation test was carried out between the demeaned GAF scores and mean FA values of the voxels that were statistically significant in the voxel-wise multiple regression analysis.

Results

Demographic and clinical characteristics in cohorts (1) and (2)

Table 1 illustrates demographic and clinical characteristics of both cohorts. In cohort (1), no differences were observed in age, sex, or hand preference between the HC and SZ groups, however, duration of school education was significantly lower in the SZ group than in the HC group. Age, sex, hand preference, and duration of school education were not different between the HC, SZ-HCP, and SZ-LCP groups. Furthermore, duration of illness, PANSS positive, general, and total scores, GAF scores, chlorpromazine daily dose equivalents, and the number of patients taking an antidepressant or benzodiazepine were not different between the SZ-HCP and SZ-LCP groups. However, the SZ-LCP group had significantly higher PANSS negative scores than the SZ-HCP group ($p < 0.01$).

In cohort (2), no differences in age, sex, hand preference, or duration of school education were observed between the HC and SZ groups. Age, sex, and hand preference were not different between the HC, SZ-HCP, and SZ-LCP groups, but duration of school education was significantly lower in the SZ-LCP group than in the SZ-HCP group ($p < 0.001$). No significant differences were found between the SZ-HCP and SZ-LCP groups with regard to the duration of illness, PANSS subscales, GAF scores, chlorpromazine daily dose

equivalents, and the number of patients taking an antidepressant or benzodiazepine.

Further analyses of demographic and clinical characteristics between the SZ groups in cohorts (1) and (2) are shown in Supplementary Table 1. The SZ group in cohort (2) had significantly higher PANSS negative, general, and total scores than the SZ group in cohort (1) ($p < 0.05$).

Group comparison of FA in cohorts (1) and (2)

Whole-brain exploratory approach

In cohort (1), the FA values in the SZ group were significantly lower than those in the HC group in the left temporal basal areas ($p < 0.05$, Fig. 1a). The mean FA of the whole-brain WM skeleton was significantly lower in the SZ-LCP group than in the HC group ($p < 0.05$, Fig. 1c).

In cohort (2), the FA values in the SZ group were significantly lower than those in the HC group in widespread regions ($p < 0.05$, Fig. 1b). The mean FA of the whole-brain WM skeleton was significantly lower in the SZ-HCP and SZ-LCP groups than in the HC group ($p < 0.05$, Fig. 1d).

#### Atlas-defined WM regions-of-interest approach

The results of our analysis of the significant differences in WM skeleton mean FA in patients and HC in the major WM tracts as defined by the Johns Hopkins University WM Atlas are shown in Table 2. In both cohorts, the WM skeleton mean FA values in the SZ and SZ-LCP groups were significantly lower than those in the HC group in the left IFOF (Fig. 1, Table 2), i.e., significant cognition-related FA reductions in SZ were found in the left IFOF.

Finally, multiple regression analysis revealed that in cohort (1), FA values in the frontal part of the left IFOF were significantly associated with the demean GAF scores ($r = 0.472$, $p < 0.001$, Fig. 2a,c); and in cohort (2), FA values in the temporal part of the left IFOF were significantly associated with the demean GAF scores ($r = 0.336$, $p = 0.022$, Fig. 2b,d), i.e., significant positive associations were found between the cognitive-related FA and the demean GAF scores in the fronto-temporal part of the left IFOF in SZ.

Discussion

Our results provide robust evidence of WM microstructural abnormalities in patients with SZ, especially in those patients with lower cognitive performance (SZ-LCP). Second, in the SZ group we found a significant positive relationship between cognition-related FA values in the fronto-temporal part of the left IFOF and the GAF score.
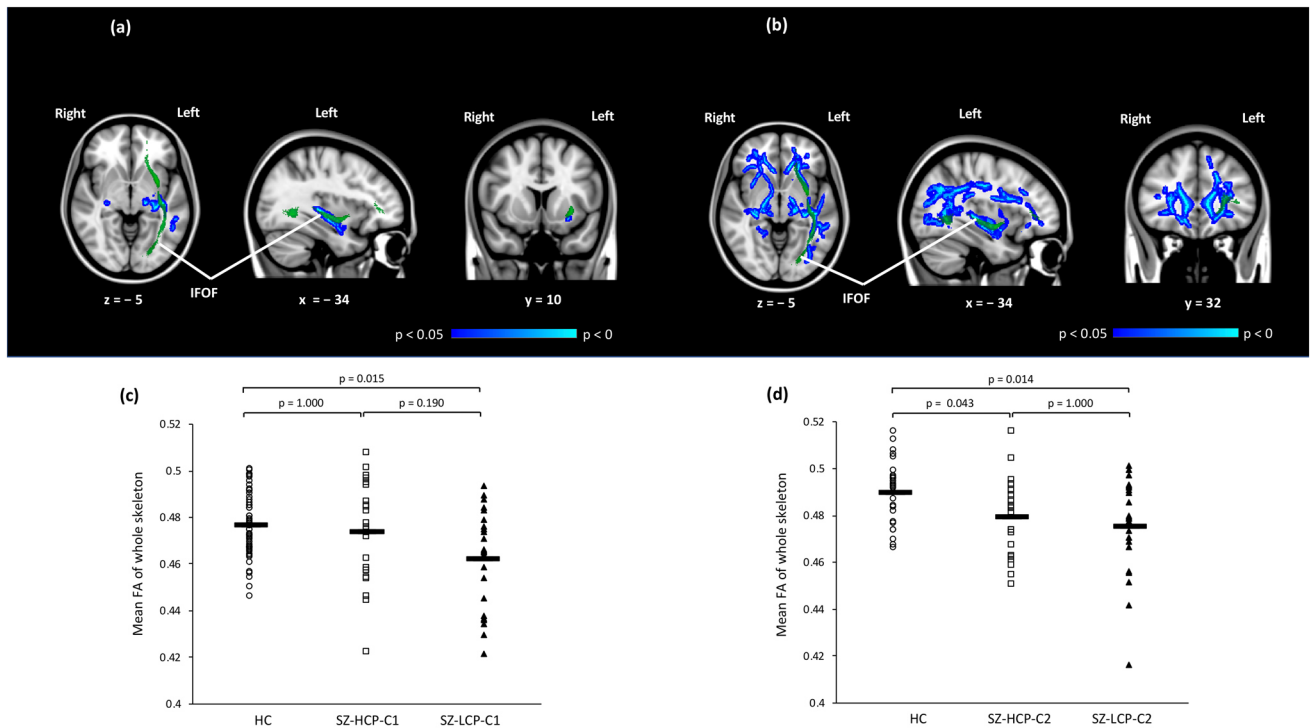
Fig. 1 a Difference in fractional anisotropy (FA) values between the healthy controls (HC) and schizophrenia (SZ) groups in cohort (1). Blue to light blue voxels indicate regions where the FA values were significantly lower in the SZ group than in the HC group ($p < 0.05$). **b** Difference in FA values between the HC and SZ groups in cohort (2). Blue to light blue voxels indicate regions where the FA values were significantly lower in the SZ group than in the HC group ($p < 0.05$). **c** Differences in mean fractional anisotropy (FA) values of whole-brain white matter (WM) skeleton in healthy controls (HC) and in patients with schizophrenia with higher cognitive performance (SZ-HCP-C1) and lower cognitive performance (SZ-LCP-C1) in cohort (1). The circles represent mean FA values of the whole skeleton in the HC group; the squares represent mean FA values of the whole skeleton in the SZ-HCP-C1 group; and the triangles represent mean FA values of the whole skeleton in the SZ-LCP-C1 group. **d** Differences in mean FA values of whole-brain WM skeleton in the HC, SZ-HCP-C2, and SZ-LCP-C2 groups in cohort (2). The circles represent mean FA values of the whole skeleton in the HC group; the squares represent mean FA values of the whole skeleton in the SZ-HCP-C2 group; and the triangles represent mean FA values of the whole skeleton in the SZ-LCP-C2 group. *FA* fractional anisotropy, *HC* healthy controls, *SZ* schizophrenia, *SZ-HCP-C1* patients with schizophrenia and higher cognitive performance in cohort (1), *SZ-HCP-C2* patients with schizophrenia and higher cognitive performance in cohort (2), *SZ-LCP-C1* patients with schizophrenia with lower cognitive performance in cohort (1), *SZ-LCP-C2* patients with schizophrenia with lower cognitive performance in cohort (2)

Our results are consistent with previous findings which revealed that WM volumes were significantly smaller in patients with SZ with cognitive impairment than in healthy individuals but WM volumes in patients without cognitive impairment were not [51]. Moreover, Pérez-Iglesias et al. [52] reported that patients with SZ with cognitive impairment showed a significantly greater decrease in FA values than patients without cognitive impairment.

In this study, we could replicate in two independent cohorts of patients with SZ, that especially patients with poor cognitive performance were affected by WM microstructural abnormalities. Moreover, cognition-related WM abnormalities, which were mainly found in fronto-temporal parts of the left IFOF, were related to general, social, and occupational functioning.

It is worth emphasizing here that in our study FA was measured with different MRI scan parameters in two independent cohorts. A clinical application of structural MRI in clinical trials requires a certain robustness of readouts across different scanners and protocols, despite all biological and technical variability.

The advantage of the current study is the replication of our findings in two independent cohorts and thus increases generalizability. Therefore, our results provide robust evidence that emphasizes the relevance of large reductions in FA as indicating a neurobiological mechanism of SZ in patients with severe cognitive impairment. Beyond the group comparison, the future goal is to find a framework for individual patients [53] to allow MRI images from individuals to be directly compared with a reference. In particular, the increase in the use of MRI-based outcome measurements in clinical trials [54] requires a more precise definition and standardization, especially considering assessments of individuals.

Table 2 Differences in fractional anisotropy in the Johns Hopkins University White-Matter Tractography Atlas-based tract

	Cohort (1) HC	SZ	p	SZ-HCP-C1	SZ-LCP-C1	p	Post hoc comparison (HC vs SZ-HCP-C1)(HC vs SZ-LCP-C1)(SZ-HCP-C1 vs SZ-LCP-C1)	Cohort (2) HC	SZ	p	SZ2-HCP-C2	SZ-LCP-C2	p	Post hoc comparisons (HC vs SZ-HCP-C2)(HC vs SZ-LCP-C2)(SZ-HCP-C2 vs SZ-LCP-C2)
Left anterior thalamic radiation, mean (sd)	0.482 0.015	0.472 0.019	0.005*	0.475 0.020	0.486 0.017	0.013*	(0.154)(0.013*)(1.000)	0.449 0.014	0.442 0.025	0.083	0.449 0.025	0.435 0.025	0.013*	(1.000)(0.015*)(0.054)
Right anterior thalamic radiation, mean (sd)	0.471 0.018	0.461 0.018	0.031*	0.463 0.019	0.459 0.018	0.072		0.437 0.015	0.431 0.024	0.155	0.436 0.026	0.427 0.023	0.117	
Left cingulum cingulate gyrus, mean (sd)	0.634 0.031	0.618 0.032	0.046*	0.628 0.028	0.609 0.034	0.020*	(1.000)(0.019*)(0.147)	0.609 0.029	0.603 0.041	0.394	0.612 0.039	0.594 0.042	0.143	
Right cingulum cingulate gyrus, mean (sd)	0.592 0.032	0.574 0.044	0.067	0.579 0.040	0.570 0.048	0.168		0.566 0.037	0.561 0.043	0.438	0.566 0.041	0.555 0.046	0.517	
Left cingulum hippocampus, mean (sd)	0.559 0.044	0.549 0.063	0.554	0.561 0.061	0.537 0.064	0.087		0.509 0.049	0.489 0.049	0.020*	0.482 0.057	0.496 0.039	0.043*	(0.043*)(0.551)(1.000)
Right cingulum hippocampus, mean (sd)	0.562 0.062	0.554 0.063	0.735	0.555 0.079	0.554 0.061	0.670		0.502 0.050	0.493 0.049	0.178	0.492 0.052	0.493 0.047	0.400	
Left corticospinal tract, mean (sd)	0.637 0.020	0.630 0.020	0.100	0.631 0.022	0.628 0.019	0.253		0.585 0.025	0.582 0.028	0.790	0.590 0.026	0.574 0.028	0.195	
Right corticospinal tract, mean (sd)	0.637 0.021	0.632 0.025	0.369	0.632 0.029	0.633 0.022	0.575		0.602 0.026	0.593 0.031	0.309	0.598 0.029	0.588 0.032	0.481	
Forceps major, mean (sd)	0.706 0.019	0.694 0.031	0.094	0.694 0.031	0.693 0.032	0.247		0.692 0.022	0.679 0.027	0.034*	0.685 0.028	0.674 0.025	0.057	
Forceps minor, mean (sd)	0.584 0.023	0.567 0.027	<0.001***	0.574 0.028	0.56 0.025	0.002**	(0.033*)(0.003**)(1.000)	0.577 0.029	0.566 0.022	0.120	0.577 0.027	0.554 0.025	0.017*	(1.000)(0.021*)(0.049*)
Left inferior fronto-occipital fascicles, mean (sd)	0.560 0.023	0.534 0.023	<0.001***	0.537 0.021	0.531 0.025	<0.001***	(1.000)(<0.001***)(1.000)	0.530 0.021	0.517 0.025	0.014*	0.528 0.025	0.507 0.019	<0.001***	(1.000)(<0.001***)(0.007**)
Right inferior fronto-occipital fascicles, mean (sd)	0.551 0.023	0.540 0.023	0.055	0.545 0.018	0.536 0.027	0.102		0.525 0.021	0.516 0.028	0.112	0.528 0.027	0.503 0.022	<0.001***	(1.000)(0.002**)(0.002**)

Table 2 (continued)

	Cohort (1) HC mean	sd	SZ mean	sd	p	SZ-HCP-C1 mean	sd	SZ-LCP-C1 mean	sd	p	Post hoc comparison (HC vs SZ-HCP-C1) (HC vs SZ-LCP-C1) (SZ-HCP-C1 vs SZ-LCP-C1)	Cohort (2) HC mean	sd	SZ mean	sd	p	SZ2-HCP-C2 mean	sd	SZ-LCP-C2 mean	sd	p	Post hoc comparisons (HC vs SZ-HCP-C2) (HC vs SZ-LCP-C2) (SZ-HCP-C2 vs SZ-LCP-C2)
Left inferior longitudinal fascicles, mean (sd)	0.555	0.023	0.533	0.027	<0.001***	0.536	0.024	0.531	0.030	0.004**	(0.020*) (0.008**) (1.000)	0.515	0.025	0.504	0.024	0.053	0.512	0.024	0.495	0.02	0.020*	(1.000) (0.017**) (0.130)
Right inferior longitudinal fascicles, mean (sd)	0.573	0.023	0.563	0.029	0.115	0.566	0.026	0.560	0.033	0.274		0.524	0.024	0.515	0.026	0.183	0.527	0.024	0.503	0.024	0.006**	(1.000) (0.014*) (0.011*)
Left superior longitudinal fascicles, mean (sd)	0.522	0.023	0.506	0.024	0.006*	0.507	0.026	0.505	0.024	0.023*	(0.044*) (0.076) (1.000)	0.497	0.025	0.487	0.025	0.097	0.490	0.026	0.484	0.024	0.245	
Right superior longitudinal fascicles, mean (sd)	0.522	0.025	0.511	0.025	0.100	0.507	0.027	0.516	0.023	0.102		0.512	0.027	0.503	0.028	0.158	0.509	0.028	0.497	0.027	0.183	
Left superior longitudinal fascicles, temporal part, mean (sd)	0.568	0.027	0.553	0.027	0.023	0.552	0.027	0.553	0.027	0.068		0.536	0.029	0.527	0.029	0.211	0.527	0.032	0.527	0.026	0.420	
Right superior longitudinal fascicles, temporal part, mean (sd)	0.560	0.031	0.553	0.028	0.290	0.549	0.027	0.558	0.028	0.256		0.541	0.031	0.534	0.028	0.305	0.538	0.031	0.529	0.025	0.445	
Left uncinate fascicles, mean (sd)	0.549	0.036	0.521	0.032	<0.001***	0.526	0.033	0.516	0.029	0.003**	(0.038*) (0.004**) (1.000)	0.487	0.028	0.481	0.028	0.239	0.487	0.034	0.476	0.035	0.209	
Right uncinate fascicles, mean (sd)	0.582	0.033	0.562	0.038	0.027	0.562	0.038	0.561	0.039	0.084		0.524	0.035	0.513	0.039	0.125	0.515	0.042	0.511	0.037	0.286	

One-way ANOVA and Bonferroni's post hoc test with age and sex as covariates. Significant differences among the three groups are marked. Values marked with ***, ** and * are significant at $p < 0.05/40 = 0.00125$, $p < 0.01$ and $p < 0.05$, respectively
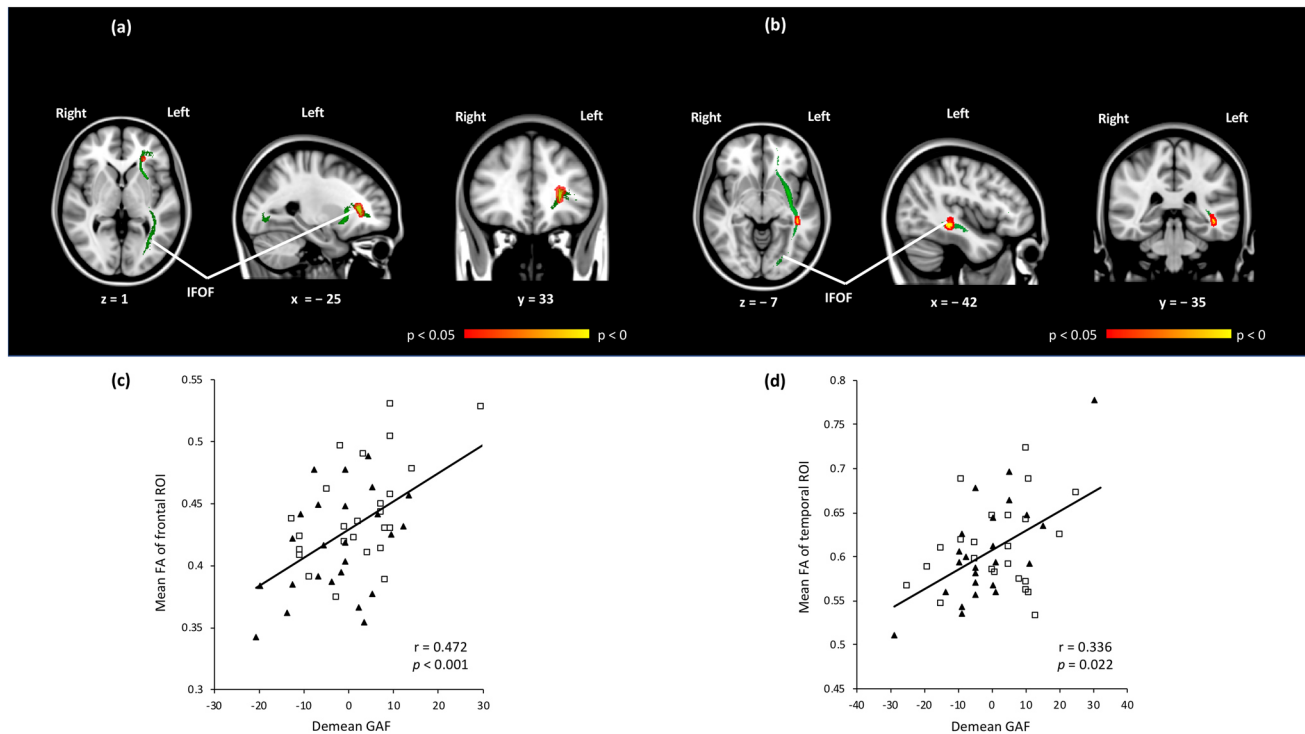
Fig. 2 a Red-yellow voxels indicate a significant positive relation between the fractional anisotropy (FA) values in the left inferior fronto-occipital fasciculus (IFOF) and the demean Global Assessment of Functioning (GAF) scores in the schizophrenia (SZ) group in cohort (1). **b** Red-yellow voxels indicate a significant positive relation between the FA values in the left IFOF and the demean GAF scores in the SZ group in cohort (2). **c** Scatter plot showing the relation of the demean Global Assessment of Functioning (GAF) scores and mean fractional anisotropy (FA) values of the voxels that showed a statistically significant correlation in voxel-wise multiple regression analysis in **a**. The squares represent patients with schizophrenia and higher cognitive performance in cohort (1), and the triangles represent the group of patients with schizophrenia and lower cognitive performance in cohort (1). **d** Scatter plot showing the relation of the demean GAF scores and mean FA values of the voxels that reached a statistically significant correlation in voxel-wise multiple regression analysis in **b**. The squares represent patients with schizophrenia and higher cognitive performance in cohort (2), and the triangles represent patients with schizophrenia and lower cognitive performance in cohort (2). *FA* fractional anisotropy, *GAF* global assessment of functioning, *IFOF* inferior front-occipital fascicles, *SZ* schizophrenia, *ROI* region of interest

In its atlas-based analysis, the current study found a significant positive relationship in both cohorts between cognition-related FA, mainly in the fronto-temporal part of the left IFOF, and demean GAF scores in patients. The IFOF is the longest associative bundle and connects the occipital cortex, superior parietal lobule, and temporal basal areas to the frontal lobe [55, 56]. Moreover, the fronto-temporal part of the left IFOF is the region of greater interest in SZ: As early as the last century, Wernicke [57] and Kraepelin [58] suggested the importance of the fronto-temporal network in the neuropathology of SZ, and later brain investigations with various neuroimaging methods reinforced this idea [12, 59, 60]. Previous DTI findings implicated prefrontal and temporal lobes [61–63] and the fiber tracts connecting these regions [64] in SZ. Our current finding of an association of the anisotropic reductions in the left IFOF with the cognitive composite and reduced GAF scores may be seen as confirming some previous reports from other DTI studies in SZ that used other cognitive test batteries [31, 65]. In summary, this

replication study in a cohort from our previous studies [41, 42] and a new cohort extends previous work [31, 65]. We demonstrated that the origin of neurocognitive deficits and poor functional outcomes in patients with SZ may be related to neurobiological abnormalities in the left IFOF of brain networks in the temporal and frontal cortex.

An interesting finding from our analysis of the whole skeleton is that the FA values in widespread regions were significantly lower in the SZ group than in the HC group in cohort (2) but not in cohort (1). Another interesting finding from our atlas-based analysis is that we found a significant positive relation between the FA values and the demean GAF scores in the temporal part of the left IFOF in cohort (2) but in the frontal part of the left IFOF in cohort (1), i.e., the local regions in the left IFOF could not be replicated in both cohorts. This discrepancy between the independent cohorts might be explained, at least in part, by some factors affecting FA, such as differences in symptom severity for SZ [28], the use of different channel

head coils in MRI research [66] and other dimensions (e.g. aggression or impulsivity[67]) that were not included in the present study.

Some limitations of this study must be noted. First, the patients were taking a variety of pharmacological agents not only at the time of scanning, but prior to the scanning (i.e., lifetime use of medication). Second, they were evenly divided with regard to the cognitive composite score and could not be classified according to unique score criteria (e.g., > 1 SD below the normative mean), though previous findings show that approximately one quarter of schizophrenia have similar cognitive performance as healthy [51]. Future studies are necessary using a greater number of patients, who are classified according to unique score criteria, with limited medication exposure and matched lifetime use of medication to confirm the results of our study.

The main strength of this study is the replication approach that used independent samples with different MRI parameters. The results provide a foundation for developing the neurobiological basis of cognitive function, which could serve as a functional proxy in SZ and other psychiatric disorders. Of particular importance will be the design of an approach to transform individual changes of the structural and functional connectome towards a clinical application. Here, cognition and functionality for psychiatric disorders will also play an important role across diagnoses.

Declarations

References

1. Burns T, Patrick D (2007) Social functioning as an outcome measure in schizophrenia studies. Acta Psychiatr Scand 116:403–418. https://doi.org/10.1111/j.1600-0447.2007.01108.x
2. Morrison RL, Bellack AS (1987) Social functioning of schizophrenic patients: clinical and research issues. Schizophr Bull 13:715–725. https://doi.org/10.1093/schbul/13.4.715
3. Wojtalik JA, Smith MJ, Keshavan MS, Eack SM (2017) A systematic and meta-analytic review of neural correlates of functional outcome in schizophrenia. Schizophr Bull 43:1329–1347. https://doi.org/10.1093/schbul/sbx008
4. Tsang HWH, Leung AY, Chung RCK et al (2010) Review on vocational predictors: a systematic review of predictors of vocational outcomes among individuals with schizophrenia: an update since 1998. Aust N Z J Psychiatry 44:495–504. https://doi.org/10.3109/00048671003785716
5. Fett A-KJ, Viechtbauer W, Dominguez M-G et al (2011) The relationship between neurocognition and social cognition with functional outcomes in schizophrenia: A meta-analysis. Neurosci Biobehav Rev 35:573–588. https://doi.org/10.1016/j.neubiorev.2010.07.001
6. Green MF (2016) Impact of cognitive and social cognitive impairment on functional outcomes in patients with schizophrenia. J Clin Psychiatry 77:20
7. Green MF, Kern RS, Braff DL, Mintz J (2000) Neurocognitive deficits and functional outcome in schizophrenia: are we measuring the "right stuff"? Schizophr Bull 26:119–136
8. Zaragoza Domingo S, Bobes J, García-Portilla M-P et al (2015) Cognitive performance associated to functional outcomes in stable outpatients with schizophrenia. Schizophr Res Cogn 2:146–158. https://doi.org/10.1016/j.scog.2015.03.002
9. Falkai P, Schmitt A (2019) The need to develop personalized interventions to improve cognition in schizophrenia. World Psychiatry 18:170. https://doi.org/10.1002/wps.20650
10. Association AP, Association AP (2013) Diagnostic and statistical manual of mental disorders: DSM-5, 5th edn. American Psychiatric Association, Washington, D.C.
11. Friston KJ (1999) Schizophrenia and the disconnection hypothesis. Acta Psychiatr Scand 99:68–79. https://doi.org/10.1111/j.1600-0447.1999.tb05985.x
12. Friston KJ, Frith CD (1995) Schizophrenia: a disconnection syndrome. Clin Neurosci 3:89–97

13. Andreasen NC (1999) A unitary model of schizophrenia: Bleuler's "Fragmented Phrene" as Schizencephaly. Arch Gen Psychiatry 56:781–787. https://doi.org/10.1001/archpsyc.56.9.781

14. Crow TJ, Paez P, Chance SA (2007) Callosal misconnectivity and the sex difference in psychosis. Int Rev Psychiatry 19:449–457. https://doi.org/10.1080/09540260701486282

15. Fields RD (2008) White matter in learning, cognition and psychiatric disorders. Trends Neurosci 31:361–370. https://doi.org/10.1016/j.tins.2008.04.001

16. Wheeler AL, Voineskos AN (2014) A review of structural neuroimaging in schizophrenia: from connectivity to connectomics. Front Hum Neurosci 8:653. https://doi.org/10.3389/fnhum.2014.00653

17. Baars BJ, Franklin S, Ramsøy TZ (2013) Global workspace dynamics: cortical "binding and propagation" enables conscious contents. Front Psychol. https://doi.org/10.3389/fpsyg.2013.00200

18. Duncan J, Owen AM (2000) Common regions of the human frontal lobe recruited by diverse cognitive demands. Trends Neurosci 23:475–483. https://doi.org/10.1016/S0166-2236(00)01633-7

19. Basser PJ, Mattiello J, LeBihan D (1994) MR diffusion tensor spectroscopy and imaging. Biophys J 66:259–267. https://doi.org/10.1016/S0006-3495(94)80775-1

20. Le Bihan D, Breton E (1985) Imagerie de diffusion in vivo par résonance magnétique nucléaire. Comptes rendus de l'Académie des sciences Série 2. Mécanique Phys Chim Sci Univ Sci Terre 301:1109–1112

21. Moseley ME, Cohen Y, Kucharczyk J et al (1990) Diffusion-weighted MR imaging of anisotropic water diffusion in cat central nervous system. Radiology 176:439–445. https://doi.org/10.1148/radiology.176.2.2367658

22. Dauguet J, Peled S, Berezovskii V et al (2007) Comparison of fiber tracts derived from in-vivo DTI tractography with 3D histological neural tract tracer reconstruction on a macaque brain. Neuroimage 37:530–538

23. Thiebaut de Schotten M, Dell'Acqua F, Forkel SJ et al (2011) A lateralized brain network for visuospatial attention. Nat Neurosci 14:1245–1246. https://doi.org/10.1038/nn.2905

24. Thiebaut de Schotten M, Dell'Acqua F, Valabregue R, Catani M (2012) Monkey to human comparative anatomy of the frontal lobe association tracts. Cortex 48:82–96. https://doi.org/10.1016/j.cortex.2011.10.001

25. Basser PJ, Pajevic S, Pierpaoli C et al (2000) In vivo fiber tractography using DT-MRI data. Magn Reson Med 44:625–632

26. Catani M, Dell'Acqua F, Vergani F et al (2012) Short frontal lobe connections of the human brain. Cortex 48:273–291. https://doi.org/10.1016/j.cortex.2011.12.001

27. Dell'Acqua F, Catani M (2012) Structural human brain networks: hot topics in diffusion tractography. Curr Opin Neurol 25:375–383

28. Kelly S, Jahanshad N, Zalesky A et al (2018) Widespread white matter microstructural differences in schizophrenia across 4322 individuals: results from the ENIGMA Schizophrenia DTI Working Group. Mol Psychiatry 23:1261–1269

29. Castro-de-Araujo LFS, Allin M, Picchioni MM et al (2018) Schizophrenia moderates the relationship between white matter integrity and cognition. Schizophr Res 199:250–256. https://doi.org/10.1016/j.schres.2018.03.033

30. Kochunov P, Coyle TR, Rowland LM et al (2017) Association of white matter with core cognitive deficits in patients with schizophrenia. JAMA Psychiatr 74:958–966

31. Roalf DR, Ruparel K, Verma R et al (2013) White matter organization and neurocognitive performance variability in schizophrenia. Schizophr Res 143:172–178. https://doi.org/10.1016/j.schres.2012.10.014

32. Mitelman SA, Torosjan Y, Newmark RE et al (2007) Internal capsule, corpus callosum and long associative fibers in good and poor outcome schizophrenia: a diffusion tensor imaging survey. Schizophr Res 92:211–224. https://doi.org/10.1016/j.schres.2006.12.029

33. ICD-10 Version:2010. https://icd.who.int/browse10/2010/en. Accessed 16 July 2021

34. Sheehan DV, Lecrubier Y, Sheehan KH et al (1998) The Mini-International Neuropsychiatric Interview (MINI): the development and validation of a structured diagnostic psychiatric interview for DSM-IV and ICD-10. J Clin Psychiatry 59(Suppl 20):22–33

35. Woods SW (2003) Chlorpromazine equivalent doses for the newer atypical antipsychotics. J Clin Psychiatry 64:663–667. https://doi.org/10.4088/jcp.v64n0607

36. Kay SR, Fiszbein A, Opler LA (1987) The positive and negative syndrome scale (PANSS) for schizophrenia. Schizophr Bull 13:261–276

37. Endicott J, Spitzer RL, Fleiss JL, Cohen J (1976) The global assessment scale. A procedure for measuring overall severity of psychiatric disturbance. Arch Gen Psychiatry 33:766–771. https://doi.org/10.1001/archpsyc.1976.01770060086012

38. Beller E, Keeser D, Wehn A et al (2019) T1-MPRAGE and T2-FLAIR segmentation of cortical and subcortical brain regions—an MRI evaluation study. Neuroradiology 61:129–136. https://doi.org/10.1007/s00234-018-2121-2

39. Trossbach SV, Hecher L, Schafflick D et al (2019) Dysregulation of a specific immune-related network of genes biologically defines a subset of schizophrenia. Transl Psychiatry 9:1–16. https://doi.org/10.1038/s41398-019-0486-6

40. Papazova I (2021) Predicting cognition in schizophrenia applying machine learning to structural MRI data. PhD Thesis, Ludwig-Maximilians-Universität München

41. Malchow B, Keller K, Hasan A et al (2015) Effects of endurance training combined with cognitive remediation on everyday functioning, symptoms, and cognition in multiepisode schizophrenia patients. Schizophr Bull 41:847–858. https://doi.org/10.1093/schbul/sbv020

42. Malchow B, Keeser D, Keller K et al (2016) Effects of endurance training on brain structures in chronic schizophrenia patients and healthy controls. Schizophr Res 173:182–191. https://doi.org/10.1016/j.schres.2015.01.005

43. Harvey PD, Green MF, Keefe RS, Velligan DI (2004) Cognitive functioning in schizophrenia: a consensus statement on its role in the definition and evaluation of effective treatments for the illness. J Clin Psychiatry 65:361–372

44. Müller H, Hasse-Sander I, Horn R et al (1997) Rey auditory-verbal learning test: structure of a modified german version. J Clin Psychol 53:663–671. https://doi.org/10.1002/(sici)1097-4679(199711)53:7%3c663::aid-jclp4%3e3.0.co;2-j

45. Reitan R, Wolfson D (1993) The Halstead-Reitan neuropsychology battery: theory and clinical interpretation. Hardcover Neuropsychology

46. Smith SM, Jenkinson M, Johansen-Berg H et al (2006) Tract-based spatial statistics: voxelwise analysis of multi-subject diffusion data. Neuroimage 31:1487–1505. https://doi.org/10.1016/j.neuroimage.2006.02.024

47. Smith SM, Jenkinson M, Woolrich MW et al (2004) Advances in functional and structural MR image analysis and implementation as FSL. Neuroimage 23(Suppl 1):S208-219. https://doi.org/10.1016/j.neuroimage.2004.07.051

48. Andersson JL, Jenkinson M, Smith S (2007) Non-linear registration, aka Spatial normalisation FMRIB technical report TR07JA2. FMRIB Anal Group Univ Oxf 2:e21

49. Mori S, Wakana S, van Zijl PCM, Nagae-Poetscher LM (2005) MRI atlas of human white matter. Elsevier

50. Wakana S, Caprihan A, Panzenboeck MM et al (2007) Reproducibility of quantitative tractography methods applied to cerebral

white matter. Neuroimage 36:630–644. https://doi.org/10.1016/j.neuroimage.2007.02.049

51. Wexler BE, Zhu H, Bell MD et al (2009) Neuropsychological near normality and brain structure abnormality in schizophrenia. Am J Psychiatry 166:189–195. https://doi.org/10.1176/appi.ajp.2008.08020258

52. Pérez-Iglesias R, Tordesillas-Gutiérrez D, McGuire PK et al (2010) White matter integrity and cognitive impairment in first-episode psychosis. Am J Psychiatry 167:451–458. https://doi.org/10.1176/appi.ajp.2009.09050716

53. Dubois J, Adolphs R (2016) Building a science of individual differences from fMRI. Trends Cogn Sci 20:425–443. https://doi.org/10.1016/j.tics.2016.03.014

54. Sadraee A, Paulus M, Ekhtiari H (2021) fMRI as an outcome measure in clinical trials: A systematic review in clinicaltrials.gov. Brain Behav 11:02089. https://doi.org/10.1002/brb3.2089

55. Martino J, Brogna C, Robles SG et al (2010) Anatomic dissection of the inferior fronto-occipital fasciculus revisited in the lights of brain stimulation data. Cortex 46:691–699. https://doi.org/10.1016/j.cortex.2009.07.015

56. Sarubbo S, De Benedictis A, Maldonado IL et al (2013) Frontal terminations for the inferior fronto-occipital fascicle: anatomical dissection, DTI study and functional considerations on a multi-component bundle. Brain Struct Funct 218:21–37. https://doi.org/10.1007/s00429-011-0372-3

57. Wernicke C (1906) Grundriss der Psychiatrie in klinischen Vorlesungen. Thieme

58. Kraepelin E (1919) Dementia praecox and paraphrenia. Livingstone

59. McGuire PK, Frith CD (1996) Disordered functional connectivity in schizophrenia. Psychol Med 26:663–667. https://doi.org/10.1017/s0033291700037673

60. Weinberger DR (1987) Implications of normal brain development for the pathogenesis of schizophrenia. Arch Gen Psychiatry 44:660–669. https://doi.org/10.1001/archpsyc.1987.01800190080012

61. Ellison-Wright I, Bullmore E (2009) Meta-analysis of diffusion tensor imaging studies in schizophrenia. Schizophr Res 108:3–10. https://doi.org/10.1016/j.schres.2008.11.021

62. Kubicki M, McCarley R, Westin C-F et al (2007) A review of diffusion tensor imaging studies in schizophrenia. J Psychiatr Res 41:15–30. https://doi.org/10.1016/j.jpsychires.2005.05.005

63. Pettersson-Yeo W, Allen P, Benetti S et al (2011) Dysconnectivity in schizophrenia: where are we now? Neurosci Biobehav Rev 35:1110–1124. https://doi.org/10.1016/j.neubiorev.2010.11.004

64. Zalesky A, Fornito A, Seal ML et al (2011) Disrupted axonal fiber connectivity in schizophrenia. Biol Psychiatry 69:80–89. https://doi.org/10.1016/j.biopsych.2010.08.022

65. Liu X, Lai Y, Wang X et al (2013) Reduced white matter integrity and cognitive deficit in never-medicated chronic schizophrenia: a diffusion tensor study using TBSS. Behav Brain Res 252:157–163. https://doi.org/10.1016/j.bbr.2013.05.061

66. Panman JL, To YY, van der Ende EL et al (2019) Bias introduced by multiple head coils in MRI research: an 8 channel and 32 channel coil comparison. Front Neurosci 13:729. https://doi.org/10.3389/fnins.2019.00729

67. Tesli N, Westlye LT, Storvestre GB et al (2021) White matter microstructure in schizophrenia patients with a history of violence. Eur Arch Psychiatry Clin Neurosci 271:623–634. https://doi.org/10.1007/s00406-019-00988-0

Authors and Affiliations

Shinichi Yamada[1,2] · **Shun Takahashi**[1,2,3] · **Berend Malchow**[1,4] · **Irina Papazova**[5] · **Sophia Stöcklein**[6] · **Birgit Ertl-Wagner**[7] · **Boris Papazov**[6] · **Ulrike Kumpf**[1] · **Thomas Wobrock**[4,8] · **Katriona Keller-Varady**[9] · **Alkomiet Hasan**[5] · **Peter Falkai**[1] · **Elias Wagner**[1] · **Florian J. Raabe**[1,10] · **Daniel Keeser**[1,6,11]

1 Department of Psychiatry and Psychotherapy, University Hospital, LMU Munich, Munich, Germany

2 Department of Neuropsychiatry, Wakayama Medical University, Wakayama, Japan

3 Clinical Research and Education Center, Asakayama General Hospital, Sakai, Japan

4 Department of Psychiatry and Psychotherapy, University Medical Center Göttingen, Göttingen, Germany

5 Department of Psychiatry Psychotherapy and Psychosomatics, Medical Faculty, University of Augsburg, Augsburg, Germany

6 Department of Radiology, University Hospital, LMU Munich, Munich, Germany

7 Division of Neuroradiology, Department of Diagnostic Imaging, The Hospital for Sick Children, Toronto, Canada

8 Department of Psychiatry and Psychotherapy, County Hospitals Darmstadt-Dieburg, Gross-Umstadt, Germany

9 Institute of Sports Medicine, Hannover Medical School, Hannover, Germany

10 International Max Planck Research School for Translational Psychiatry (IMPRS-TP), Munich, Germany

11 NeuroImaging Core Unit Munich (NICUM), University Hospital, LMU Munich, Munich, Germany

4.   Paper II

Expression of Lineage Transcription Factors Identifies Differences in Transition States of Induced Human Oligodendrocyte Differentiation

Florian J. Raabe [1,2], Marius Stephan [1,2,3], Jan Benedikt Waldeck [1], Verena Huber [1], Damianos Demetriou [1], Nirmal Kannaiyan [1,3], Sabrina Galinski [1,3], Laura V. Glaser [4], Michael C. Wehr [1,3], Michael J. Ziller [5,6], Andrea Schmitt [1,7], Peter Falkai [1] and Moritz J. Rossner [1,3]*

[1] Department of Psychiatry and Psychotherapy, University Hospital, LMU Munich, 80336 Munich, Germany
[2] International Max Planck Research School for Translational Psychiatry (IMPRS-TP), 80804 Munich,
Germany
[3] Systasy Bioscience GmbH, 81669, Munich, Germany.
[4] Department of Computational Molecular Biology, Max Planck Institute for Molecular Genetics, 14195 Berlin, Germany
[5] Max Planck Institute of Psychiatry, 80804 Munich, Germany
[6] Department of Psychiatry, University of Münster, 48149 Münster, Germany
[7] Laboratory of Neurosciences (LIM-27), Institute of Psychiatry, University of São Paulo (USP), São Paulo-SP 05403-903, Brazil

* Correspondence: Moritz.Rossner@med.uni-muenchen.de

Expression of Lineage Transcription Factors Identifies Differences in Transition States of Induced Human Oligodendrocyte Differentiation

Florian J. Raabe [1,2], Marius Stephan [1,2,3], Jan Benedikt Waldeck [1], Verena Huber [1], Damianos Demetriou [1], Nirmal Kannaiyan [1,3], Sabrina Galinski [1,3], Laura V. Glaser [4], Michael C. Wehr [1,3], Michael J. Ziller [5,6], Andrea Schmitt [1,7], Peter Falkai [1] and Moritz J. Rossner [1,3,*]

1 Department of Psychiatry and Psychotherapy, University Hospital, LMU Munich, 80336 Munich, Germany;
Florian.Raabe@med.uni-muenchen.de (F.J.R.); marius.stephan@med.uni-muenchen.de (M.S.);
Benedikt.Waldeck@med.uni-muenchen.de (J.B.W.); Venena.Huber@med.uni-muenchen.de (V.H.);
Damianos.Demetriou@med.uni-muenchen.de (D.D.); Nirmal.Kannaiyan@med.uni-muenchen.de (N.K.);
Sabrina.Galinski@med.uni-muenchen.de (S.G.); Michael.Wehr@med.uni-muenchen.de (M.C.W.);
Andrea.Schmitt@med.uni-muenchen.de (A.S.); Peter.Falkai@med.uni-muenchen.de (P.F.)
2 International Max Planck Research School for Translational Psychiatry (IMPRS-TP), 80804 Munich, Germany
3 Systasy Bioscience GmbH, 81669 Munich, Germany
4 Department of Computational Molecular Biology, Max Planck Institute for Molecular Genetics,
14195 Berlin, Germany; glaser@molgen.mpg.de
5 Max Planck Institute of Psychiatry, 80804 Munich, Germany; michael_ziller@psych.mpg.de
6 Department of Psychiatry, University of Münster, 48149 Münster, Germany
7 Laboratory of Neurosciences (LIM-27), Institute of Psychiatry, University of São Paulo (USP),
São Paulo 05403-903, Brazil
* Correspondence: Moritz.Rossner@med.uni-muenchen.de

Abstract: Oligodendrocytes (OLs) are critical for myelination and are implicated in several brain disorders. Directed differentiation of human-induced OLs (iOLs) from pluripotent stem cells can be achieved by forced expression of different combinations of the transcription factors SOX10 (S), OLIG2 (O), and NKX6.2 (N). Here, we applied quantitative image analysis and single-cell transcriptomics to compare different transcription factor (TF) combinations for their efficacy towards robust OL lineage conversion. Compared with S alone, the combination of SON increases the number of iOLs and generates iOLs with a more complex morphology and higher expression levels of myelin-marker genes. RNA velocity analysis of individual cells reveals that S generates a population of oligodendrocyte-precursor cells (OPCs) that appear to be more immature than those generated by SON and to display distinct molecular properties. Our work highlights that TFs for generating iOPCs or iOLs should be chosen depending on the intended application or research question, and that SON might be beneficial to study more mature iOLs while S might be better suited to investigate iOPC biology.

Keywords: directed differentiation; oligodendrocytes; human pluripotent stem cells; hiPSC; scR-NAseq; RNA velocity

1. Introduction

Myelinating oligodendrocytes (OLs) are essential for saltatory nerve conduction in the central nervous system and are involved in the metabolic support of neurons and modulation of neuronal excitability [1,2]. OLs are derived from oligodendrocyte precursor cells (OPCs) and both cell types are considered heterogeneous populations with regional specifications and functionally different states [3–6]. Moreover, OL dysfunction is associated with several major neurological diseases, e.g., multiple sclerosis, leukodystrophy, stroke, and schizophrenia [1,7]. The advent of human-induced pluripotent stem cells (hiPSCs)

paved the way for generating hiPSC-derived OPCs (hiPSC OPCs) and hiPSC-derived OLs (hiPSC OLs) that improved our understanding of human biology and enabled dissection of pathophysiological mechanisms, including cell-based therapies [8,9].

Initial protocols applied small molecules and peptides but took 75 to 200 days to generate hiPSC OPCs and hiPSC OLs [8,9], thus limiting larger-scaled studies such as compound screens or large cohort investigations [10]. A subsequent, more rapid strategy used overexpression of lineage-specific transcription factors (TFs), which forces oligodendroglial differentiation and allows generation of induced OPCs (iOPCs) and iOLs within 20 to 30 days [8,9]. Most protocols identified overexpression of SRY-box 10 (SOX10) as sufficient for iOL generation [11–13] and overexpression of SOX9 alone was also recently shown to be an efficient approach [14]. Garcia-León et al., suggested that SOX10 (referred to as S) alone is most efficient for iOL generation [13]. In contrast, Ehrlich et al., showed that the combination SON–consisting of S, oligodendrocyte transcription factor 2 (OLIG2, referred to as O), and the NK6 homeobox 2 (NKX6.2, referred to as N)–enriched the yield of iOLs [11] and allowed direct reprogramming of human fibroblasts [15]. In addition, Pawlowski et al., applied the combination SO to generate iOLs from embryonic stem cells [12]. Nonetheless, iOLs displayed transcriptional similarities to primary OLs and allowed axonal myelination in vitro and in vivo [11,13]. Despite these functional and morphological similarities between studies, several experimental conditions beyond the different TF combinations varied, preventing direct comparison of the findings. First, the neural patterning strategies applied before initiating TF overexpression differed: Garcia et al., performed neural induction on a monolayer [13], whereas Ehrlich et al., performed free-floating embryoid body formation with neural patterning and applied different combinations of small molecules [11]. Second, different configurations of the TF-expressing lentivirus constructs were applied: Ehrlich et al., expressed all TFs as multicistronic units, however, Garcia et al., used combinations of individual TFs expressing lentiviral constructs, which likely reduced the efficacy of multi-TF combinations in generating iOLs compared with that of single TFs. Moreover, to date, no studies have addressed the fate and heterogeneity of individual iOPCs and iOL populations.

Therefore, we systematically compared S-, SO- and SON-directed differentiation of individual oligodendroglial lineage cells by using a streamlined protocol in which all TF combinations were expressed from an identical lentivirus backbone and all cell culture conditions were standardized. We show that S-, SO- and SON-directed differentiation were all sufficient to generate high yields of O4[+] iOPCs, however, SON provided significant more yield than SO and S. Further investigations with S and SON show that SON allows an earlier generation of MBP[+] iOLs with higher yields and more complex morphology. Subsequent scRNAseq experiments including RNA velocity analysis reveals a fastened directed oligodendroglial differentiation using SON and higher maturation stages of SON-iOLs compared to S-iOLs. We show that scRNAseq including RNA analysis is not limited to dissecting a static stage but allows to dissect the time-dependent dynamics of directed differentiation and highlights that SON-directed differentiation might be better suited for research with a focus on more mature iOL.

2. Materials and Methods

2.1. Lentiviral Vectors

The cDNA sequences of human SOX10 (S), SOX10-P2A-OLIG2 (SO) and SOX10-P2A-OLIG2-T2A-NKX6.2 (SON) were synthesized as plasmids (GenScript, Piscataway, NJ, USA), with each open reading frame flanked by attB1 and attB2 sites for Gateway recombination cloning. Synthesized genes were recombined into pDONR/Zeo (Thermo Fisher Scientific, Waltham, MA, USA, #12535035) to yield Entry clones. Entry clones were finally recombined into pINDUCER21-puro_Gateway-3xFLAG (Addgene, Watertown, MA, USA, plasmid #172981). HEK293 cells (ATCC) were used for lentivirus production. S-, SO- and SON-lentiviral vectors (12 μg of each) were transfected with packaging plasmids psPAX2 (Addgene plasmid #12260, 9 μg) and pMD2.G (Addgene plasmid #12259, 4 μg)

with 4 µg polyethylenimine per 1 µg plasmid-DNA (Polysciences, Warrington, FL, USA, #9002-98-6). Then, 48 h after lentiviral transfection, the culture medium was collected, filtered through a 0.45 µM PVDF filter, precipitated with PEG-it (System Biosciences, Palo Alto, CA, USA, #LV810A-1) according to the manufacturer's instructions, resuspended in DPBS, and stored at −80 °C for further use.

2.2. HiPSC Lines, HiPSC Cultivation and Lentiviral Transfection

hiPSC were derived from the hiPSC biobank at the Department of Psychiatry and Psychotherapy, University Hospital, LMU Munich, Munich, Germany. hiPSC were generated from PBMCs according to a previous protocol [16]. Conventional hiPSC verification included validation of pluripotency by immunocytochemistry (Tra1-60, NANOG, OCT4, SOX2), genomic integrity by digital karyotyping [17] (pipeline available at https://gitlab.mpcdf.mpg.de/luciat/cnv_detection.git, last accessed 28 June 2021), and successful differentiation into all three germ layers [18]. hiPSC were tested negative for HIV, HCV, CMV (by Synlab, Munich, Germany) and free of Mycoplasma infections (by Eurofins, Ebersberg, Germany). All used hiPSC lines and passaging numbers are annotated in Table S1. Technical experiments were performed with line PSYLMUi001-A, SON-directed oligodendroglial differentiation efficiency was replicated with six independent hiPSC lines as annotated in Table S1.

hiPSCs were cultivated in feeder-free conditions with iPS-Brew (Miltenyi Biotec, Bergisch Gladbach, Germany, #130-104-368) on Vitronectin (Thermo Fisher Scientific, Waltham, MA, USA, #A14700). Lentiviral transfection was performed in iPS-Brew, supplemented with 1 µM Y-27632 (Rock-Inhibitor, Selleckchem, Houston, USA, #S 1049) and plated with 5×10^4 cells/cm^2. Selection with 1 ug/mL puromycin (Thermo Fisher Scientific, Waltham, MA, USA, #A1113803) was performed 48 h after transfection. We performed the first passage after transfection with Accutase (Sigma-Aldrich, St. Louis, USA, #A6964) and single cells. Subsequent passaging for expansion or maintenance was performed as hiPSC clump passaging with 0.5 µM EDTA (Thermo Fisher Scientific, Waltham, MA, USA, #15575-020). An overview of used materials is annotated in Table S2. Independent experiments were based on independent lentiviral infections.

2.3. Neural Induction

Neural induction and oligodendroglial differentiation were performed according to published protocols [13,19] with the modification that lentiviral transduction was performed before and not after neural induction (Figure 1A). At least one passage before neural induction, the hiPSC medium was changed to mTeSR1 (StemCell, Vancouver, Canada, #85850). Two days before neural induction, hiPSCs were singularized with Accutase, resuspended in mTeSR1, supplemented with 1× RevitaCell (Thermo Fisher Scientific, Waltham, MA, USA, #A2644501), and plated at a cell density of 2×10^4 cells/cm^2 on 12- and 24-well plates (Corning, New York, NJ, USA, #CORN3513 and #CORN3526) coated with Matrigel (BD Bioscience, San Jose, CA, USA, #354277). Two days after cultivation in mTESR1, neural induction was initiated by medium exchange to N2B27, which consists of DMEM/F-12 with GlutaMAX™ (Gibco, brand of Thermo Fisher Scientific, Waltham, MA, USA, #31331028), 1× N2 (Gibco, #17502048), 1× NEAA (Gibco, #11140035), 50 µM Mercaptoethanol (Gibco, #21985023) and 25 µg/mL Insulin (Sigma, #I9278), supplemented with 10 µM SB431542 (StemCell, Vancouver, Canada, #72232), 1 µM LDN193189 (StemCell, Vancouver, Canada, #72147) and 0.1 µM retinoic acid (RA)(Sigma-Aldrich, St. Louis, MO, USA, #R2625-50MG). A daily full media change of 0.5 mL per 24 wells and 1 mL per 12 wells was performed and media volume was doubled after day 4 of neural induction. From day 8 after neural induction, daily media change was performed with N2B27 supplemented with 0.1 µM RA and 1 µM SAG (Millipore, Burlington, MA, USA, #566660) until day 12.
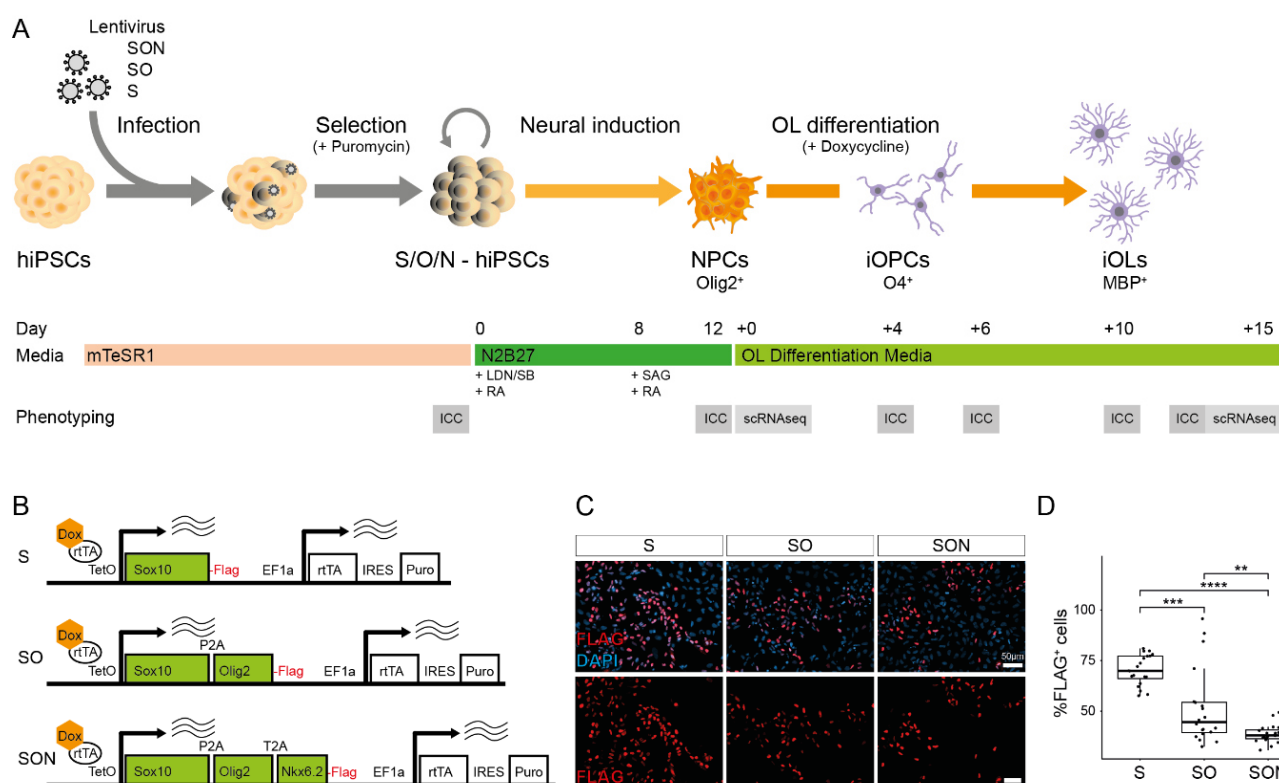
Figure 1. Experimental overview and applied constructs. (**A**) Experimental overview of directed differentiation of induced oligodendrocytes (iOLs) and their precursor cells (iOPC) from human induced pluripotent stem cells (hiPSCs). (**B**) Scheme of lentiviral vectors expressing the transcription factors (TF) SON (SOX10-OLIG2-NKX6.2), SO (SOX10-OLIG2) and S (SOX10). (**C**) Representative images of FLAG$^+$ hiPSCs 48 h after doxycycline induction. Scale bar: 50 μm. (**D**) Quantification of the percentage of FLAG$^+$ cells 48 h after doxycycline induction. Mean ± SD of FLAG$^+$ cells: 70.3% ± 7.5% in S-hiPSCs, 51.6% ± 18.7% in SO-hiPSCs and 38.7% ± 4.5% in SON-hiPSCs. Illustrated with box (quartiles) and whisker (largest/smallest observation within hinge ± 1.5× interquartile range) plot. Each dot represents one analyzed field of view (n = 20 per condition) from one independent experiment. Statistical analysis by Kruskal–Wallis test ($p < 0.0001$) and post hoc Mann–Whitney U test. ** $p < 0.01$, *** $p < 0.001$, **** $p < 0.0001$.

2.4. Oligodendroglial Differentiation

Twelve- or twenty-four-well plates were coated with PLO/Laminin. First, 50 μg/mL poly-L-ornithine (Sigma, P4957) in DPBS (ThermoFisher Scientific, Waltham, MA, USA, #1419009400) was coated overnight at 37 °C. Then, 3× washing steps were performed with DPBS, and plates were incubated overnight with 10 μg/mL mouse laminin (Sigma, #L2020) at 37 °C. Day 12 NPCs were passaged as single cells upon Accutase treatment and were seeded at a density of 150,000 cells/cm^2 in N2B27 supplemented with 0.1 μM RA, 1 μM SAG (Millipore, #566660), and 1× RevitaCell. The next day, directed OL differentiation was initiated by adding OL differentiation medium (OL-DM), which consists of N2B27 supplemented with 10 ng/mL PDGF-AA (PeproTech, brand of Thermo Fisher Scientific, Waltham, MA, USA, #100-13A), 10 ng/mL IGF1 (PeproTech, #100-11), 5 ng/mL HGF (PeproTech, #100-39), 10 ng/mL NT3 (Peprotech, #AF-450-03), 0.1 ng/mL Biotin (Sigma, #B4639), 1 mM dbcAMP (Sigma, #D0627), 60 ng/mL T3 (Sigma, #T6397) and 1 μg/mL doxycycline (Clontech, brand of Takara Bio, Shiga, Japan, #NC0424034). Full media change was performed every second day and puromycin selection was performed from Day + 2 to Day + 4 by supplementing media with 1 μg puromycin (ThermoFisher Scientific, Waltham, MA, USA, #A1113803). Cells were passaged at Day + 10 or cryopreserved for further use. Singularized cells were resuspended in OL-DM, supplemented with 1× RevitaCell and

mixed 1:1 with cooled ProFreeze CDM (Lonza, Basel, Switzerland, #BEBP12-769E) for freezing purposes. Cells were stored overnight in a freezing container (Nalgene Mr. Frosty) at −80 °C and subsequently placed in liquid nitrogen.

2.5. O4 Microbeads Purification

To select O4$^+$ cells, we performed microbead purification with anti-O4 microbeads (Miltenyi Biotec, #130-096-670) according to the manufacturer's instructions.

2.6. Immunofluorescence Staining and Imaging Analysis

Before fixation, cells were washed with PBS. Then, they were fixed with 4% PFA for 10 min at room temperature (RT). Subsequently, 3× washing with PBS was performed. Permeabilization and blocking were performed with 0.1% Triton and 5% goat serum in PBS for 60 min at RT. Triton was omitted for O4 staining. Primary antibodies were added in PBS supplemented with 0.1% Triton and 1% goat serum and incubated overnight at 4 °C. On the next day, the primary antibody solution was removed by 3× PBS washing. The respective secondary antibodies in PBS were added and the cells were incubated for 60 min at RT. The secondary antibody solution was removed by 3× PBS washing and nuclei were counterstained with DAPI, which was added during the second washing step. Finally, samples were washed 1× with water and mounted onto microscope slides. Imaging was performed on an Axio Observer.Z1 (Zeiss) inverted microscope and fields of view (FOV) were taken at randomly defined but fixed positions for each well at 20× magnification. Image analysis was performed with the Fiji [20] and its plugin Simple Neurite Tracer [21]. Average values per FOV were used for subsequent statistical analysis.

2.7. Single-Cell RNA Sequencing and Data Analysis
2.7.1. Sample Processing

Cells were detached and singularized with Accutase supplemented with DNAse1 (Merck, Darmstadt, Germany, #DN25-1G), cell aggregates were removed with 30 μm Pre-Separation Filters (Miltenyi Biotec, Bergisch-Gladbach, Germany #130-041-407), and cells were kept on ice in cold PBS with 1% BSA. Small aliquots of the samples were stained with trypan blue and cell density, viability, and multiplet rate were determined in an improved Neumann counting chamber. The density was adjusted to 2500 cells/μL. The multiplet rate was less than 7% in all samples.

2.7.2. Library Preparation

The single-cell libraries were prepared with the SureCell WTA 3′ Kit (Illumina, San Diego, CA, USA) on a ddSEQ Single-Cell Isolator (Bio-Rad, Hercules, USA) in accordance with the manufacturer's protocol. Library quality and yield were evaluated with a high-sensitivity DNA kit on a Bioanalyzer 2100 (Agilent, Santa Clara, CA, USA) according to the manufacturer's specifications.

2.7.3. Sequencing

Libraries for scRNAseq experiments were sequenced on a NextSeq550 (Illumina) in paired-end mode with 69 cycles in Read1 and 80 cycles in Read2. Subsequently, the sequencing data were demultiplexed with bcl2fastq (Illumina).

2.7.4. Upstream Analysis of scRNAseq Data

Reads were quality-checked with FastQC (v0.11.9). Barcodes in Read1 were identified, added to the Read2 BAM file as an XC tag, and quality-checked with the ddSeeker tool [22], which found that 91% of barcodes were good quality in all samples. The tagged BAM files were further processed with Drop-seq tools (v2.3.0). A metabundle was created with the Ensembl annotation release 100 of the GRCh38 human genome (*create_Drop-seq_reference_metadata*). A non-human fragment (3′LTR and WPRE) and the 3xFLAG-Tag

region of the expression constructs were added to the genome FASTA and GTF to determine the construct expression levels. The data were filtered for rejected barcodes. The reads were sorted by query name, and the BAM files were converted back to FASTQ for mapping. Read2 was mapped by using the STAR aligner (v2.7.5) with default settings. Aligned data were merged with the unaligned but barcode-tagged data. Functional annotation was added and any remaining substitution and synthesis errors in the cell barcodes were repaired to create the final BAM file. Digital gene expression data were extracted (*Digital Expression*) for the 2000 most abundant cell barcodes in each sample. The threshold was chosen to be well beyond the cut-off suggested by the knee plot generated by ddSeeker's *make_graphs.R*.

In the RNA velocity analysis pipeline, to acquire separate count matrices for spliced and unspliced reads we estimated counts with DropEst (v0.8.6) instead of Drop-seq's *Digital Expression*. The following command was used, in accordance with the suggestions of the developers of Velocyto [23]: *dropest -m -V -b -f -g%GTF file from Drop-seq metabundle% -L eiEIBA -m -c %FILEPATH%/dropEst/configs/drop_seq_velocyto.xml.* Note that the barcode tag was changed from *BC* to *XC* in *drop_seq_velocyto.xml* to make the Drop-seq output compatible with Dropest.

2.7.5. Downstream Analysis of scRNAseq Data

The scRNAseq data were further processed with the R (v4.0.4) package *Seurat* (v4.0.1) [24]. The UMI count tables were imported in R, and Seurat objects were created for each sample. We filtered for features expressed in at least three cells in each dataset and for cells with at least 200 features in the first step. Mitochondrial RNA content was determined by grepping for "^MT-" (*PercentageFeatureSet*). We filtered the cells further for barcodes with less than 5% mitochondrial RNA content, at least 1700 UMI counts in the NPC and SON sample and 1000 counts in the S sample, and a minimum of 1000 detected features. After these filtering steps, 1194 cells were left in total.

2.7.6. Normalization of scRNAseq Data

All datasets were merged into one object. To check for artifacts potentially introduced by merging, we additionally performed all analyses on each sample dataset individually. The data were normalized by the single-cell transform procedure (*SCTransform*) [25], which regressed out the percentage of mitochondrial transcripts.

2.7.7. Dimension Reduction and Clustering of scRNAseq Data

Dimension reduction was performed as a principal component analysis (*RunPCA*). The previously identified 3000 most variable features (*FindVariableFeatures*) were used as input. The first 30 principal components were computed. Based on an elbow plot, as suggested in Macosko et al., 2015, we decided to use the first 15 principal components for downstream analysis. We performed SNN graph-based clustering with a resolution of 0.23 (*FindNeighbors, FindClusters*); this clustering returned 5 distinct clusters of cells. Next, we computed a UMAP embedding (*RunUMAP;* wrapper function for integration of the *Python* library *umap-learn*; [26]). Later in the project, we revisited the clustering and increased the resolution to 0.28, which split the iOPC cluster into two subclusters, which we then used for differential expression analysis.

2.7.8. Integration with Bulk RNAseq Data

To integrate our data with publicly available bulk RNA-seq data, we followed the procedure from Ng et al. [14]. We used a primary cell dataset from mouse brain tissue because human datasets are commonly based on postmortem samples. The dataset is available on the Gene Expression Omnibus website under the accession number GSE52564 [27]. Briefly, we created an average expression table and excluded features that were expressed in less than 10% of all cells in our dataset. The filtering step was introduced to avoid artifacts resulting from bad coverage inherent to single-cell RNA-seq data and low expres-

sion. The resulting list was then filtered for variably expressed genes in our dataset; such genes were computed as differential expression with a minimum log2-fold change of 0.25 (*FindAllMarkers*). This step improved the signal-to-noise ratio and reduced potential batch effects. Next, we filtered the reference dataset and our dataset for mouse/human homologs. Finally, a list of about 3000 features was entered into the analysis. From our datasets, we excluded all iOPC cells in the NI Day + 0 sample because of their low number and their high probability of being misclustered NPCs. From the reference dataset neurons, we retained myelinating oligodendrocytes (MO), newly formed oligodendrocytes (NFO), and oligodendrocyte progenitor cells (OPC). First, we calculated feature variability (*rowVars*) with the *DESeq2 R* package [28] for variance stabilization (*VarianceStabilizingTransformation;* vst). Then, we used the 2000 most variable features for the downstream analysis. A principal component analysis (PCA) was performed to check for batch effects and other artifacts, and Manhattan distances were calculated between samples and features. These distances were used for hierarchical clustering and shown in heatmaps. Additionally, Spearman correlation coefficients were calculated to ensure that our data correlated appropriately with the reference data.

2.7.9. Differential Expression Analysis

Differential gene expression was analyzed with *Seurat v3* [29]. Genes were selected for expression in a minimum of 10% of all cells included in the analysis and for variability between groups. The data used were normalized but not integrated because the integration procedure smoothens expression differences, which leads to the underestimation of transcriptional differences. The results were tested in a Wilcoxon rank-sum test, and p values were adjusted with the Bonferroni procedure. Marker genes for characterization of the clusters were identified with a minimum log2-fold change in average expression (avg_log2FC) of 0.25 between the respective cluster and background (*FindAllMarkers()*). In pairwise comparisons between clusters, an avg_log2FC threshold of 1 was chosen because the lower threshold used for marker identification produced a high level of noise in downstream analyses.

2.7.10. Analysis of Maturation Marker Load and Construct Expression

Construct counts based on the 3′LTR-WPRE sequence were included in the *sctransform* regression model for normalization (see Section 2.7.6.) and used for construct expression equivalent. The FLAG tag region was not detected in the sequencing data.

For the maturation marker load, a set of genes with increasing levels of expression during oligodendrocyte-lineage differentiation [9] and that were detected with scRNAseq was chosen, specifically: *CNP, CD9, CLDN11, GALC, PLP1, MAG, MAL, MBP, MOBP,* and *MYRF*. The normalized expression level of these genes was then summarized for each cell. A Spearman correlation factor between construct expression level and marker load was computed and tested for S and SON Day + 15 samples.

2.7.11. Hypergeometric Gene Ontology Term Enrichment Analysis

For hypergeometric enrichment analyses of gene ontology (GO) terms, we used the GOrilla online tool [30]. Unranked gene lists were compared, of which one comprised all genes that entered the respective differential expression analysis (background) and the other identified differentially expressed genes (target). Only process terms went into the analysis. Enriched terms were filtered with an FDR-adjusted q-value threshold of 10^{-3} and a B value of less than 500.

2.7.12. RNA Velocity Analysis

For RNA velocity analysis, we first created a loom file for each sample from the Dropest output by using the command line *Python* implementation of the *velocyto* (v0.17.17) [23]. Next, we combined these loom files for downstream analysis. Additionally, we analyzed each sample independently to make sure that merging the samples

had not introduced major artifacts. We used the *scVelo Python* library [31] for the rest of the pipeline. We imported the combined loom file as anndata with the *anndata* library [32] and imported the cellIDs, UMAP coordinates, and cluster assignment from the *Seurat* pipeline. The cells were filtered for these IDs and their UMAP coordinates, and clusters were assigned. Further, the cells were filtered and normalized by using the default parameters with *pp.filter_and_normalize()*. Briefly, highly variable genes were selected, and the data were normalized by total library size and subsequently transformed to a logarithmic scale. For quality control, the fraction of unspliced transcripts was determined and found to be 13%, which is well within the lower range of 10% to 25% that is typically found in scRNAseq data. A fraction of this size is to be expected from a 3′ UTR-enriched RNA-seq dataset and is sufficient for RNA velocity estimation [31,33]. Moments were calculated and a full dynamic model was fitted to the data [31] (*tl.recover_dynamics()*, *tl.velocity(mode = "dynamical")*). This model was used to compute the velocity graph (*tl.velocity_graph()*).

2.7.13. Latent Time and PAGA Analysis

In addition, the gene-shared latent time was computed (*tl.latent_time()*) to create a pseudo-timeline that was used to inform cell-to-cell transition inference. A PAGA analysis was computed to find cluster-to-cluster transitions (*tl.paga_plot()*) [34]. Latent times were reimported in R to be used as a measure for maturity and were tested between samples with a Wilcoxon rank-sum test.

2.8. Statistics

Data were first tested for normal distribution with a Shapiro–Wilk test. We used both parametric (Student's *t*-test, ANOVA) and nonparametric analyses (two-sample Wilcoxon's rank-sum test, Kruskal–Wallis test, chi-squared test, Fisher's exact test), depending on the specific distribution properties of the data. Significance was set at * $p < 0.05$, ** $p < 0.01$, *** $p < 0.001$ and **** $p < 0.0001$.

3. Results

### 3.1. Generation of Stable S-/SO-/SON-Expressing hiPSCs and Neural Induction

To investigate TF-based differences of directed differentiation of iOPCs and iOLs with S [13], SO [12] and SON [11], we applied these TF combinations in accordance with the neural induction and differentiation protocol adapted from Garcia-Leon et al. [13,19] (Figure 1A). To allow a direct comparison, we cloned the three TFs combinations of S, SO, and SON into the same lentiviral backbone containing constitutive expression units for the reversed tetracycline transactivator (rtTA) [35] and a puromycin selection cassette (see Methods for details) (Figure 1B and Figure S1A). The human coding regions of *SOX10*, *OLIG2*, and *NKX6.2*, which were linked by the self-cleavage sites P2A and T2A, were under the control of the doxycycline-inducible operator (tetO) harboring a C-terminal FLAG-tag (Figure 1B and Figure S1A). We demonstrated the functionality of the constructs 48 h after doxycycline induction by examining infected hiPSCs with immunostainings, which showed higher numbers of FLAG⁺ cells with S than with SO and SON (Figure 1C,D), likely reflecting the size of the different constructs and reduced protein expression upon P2A- and T2A-mediated cleavage. According to our protocol (Figure 1A), infection was performed on the hiPSC level; subsequent puromycin selection was performed to enrich for S-, SO-, or SON-hiPSC and followed by neural induction to generate PAX6⁺ and OLIG2⁺ neural precursor cells (NPCs) (Figure S1B).

3.2. Graded Efficiency to Generate iOPCs by S-, SO- and SON-Directed Differentiation

We next tested whether S-, SO- and SON-directed differentiation differs in their potential to generate O4-positive (O4⁺) iOPCs as assessed by immunocytochemistry (ICC). All TF combinations generated high yields of O4⁺ cells + 4 and + 6 days after induction of oligodendroglial differentiation. SON provided higher yields than SO and S at both time

points (Figure 2A–D). At day + 4, 38.1% ± 14.6% of all cells stained positive for O4$^+$ with SON-directed differentiation, compared with 33.9% ± 13.3% with SO-directed and 28.6% ± 8.9% with S-directed differentiation (Figure 2B). At day + 6, 83.9% ± 14.6% of SON-directed, 74.4% ± 7.7% of SO-directed and 73.6% ± 8.1% of S-directed cells were O4$^+$ (Figure 2D). These results clearly show a graded potential (SON > SO > S) to generate oligodendroglial lineage cells.
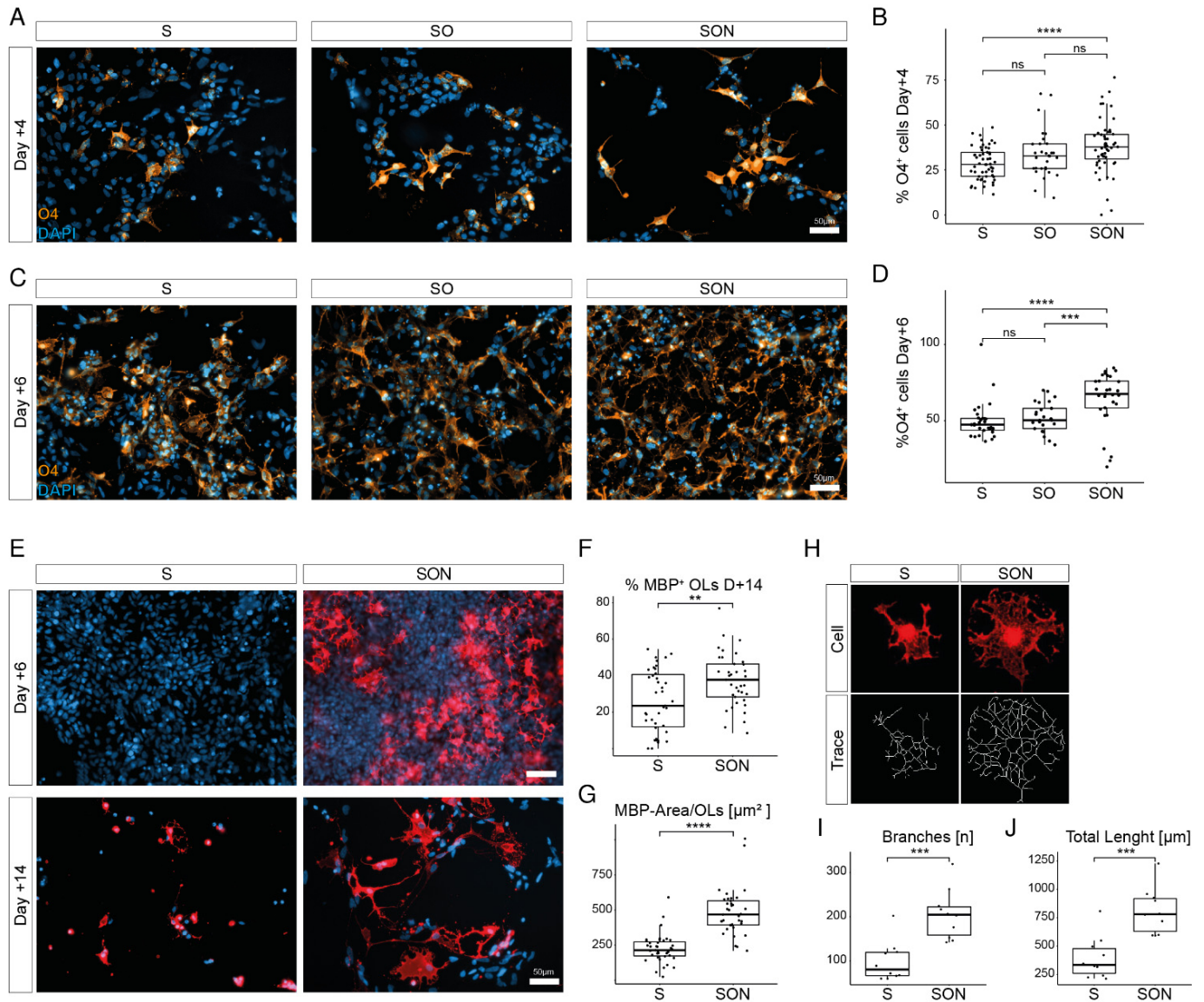
Figure 2. SON-directed differentiation leads to accelerated differentiation and morphologically highly ramified oligodendrocytes as compared with S-directed differentiation. (**A**) O4$^+$ (orange) iOPCs at Day + 4 of oligodendrocyte differentiation with S, SO and SON. Scale bar: 50 μm. (**B**) Quantification of O4$^+$ cells at Day + 4 illustrated with box-and-whisker plot. Each dot represents one analyzed field of view (*n* = 30–55 per condition) from two independent experiments. Statistical analysis by ANOVA (F = 8.02, *p* = 0.00051) and post hoc Tukey test. **** *p* < 0.001, ns = *p* > 0.05. (**C**) O4$^+$ (orange) iOPCs at Day + 6 of OL differentiation with S, SO and SON TFs. Scale bar: 50 μm. (**D**) Quantification of O4$^+$

cells at Day + 6 illustrated with a box-and-whisker plot. Each dot represents one analyzed field of view (n = 25–29 per condition) from two experiments. Statistical analysis by Kruskal–Wallis test (p = < 0.0001) and post hoc Mann–Whitney U test, *** p < 0.001, **** p < 0.0001, ns = p > 0.05. (**E**) MBP$^+$ iOLs appear at Day + 6 with SON-directed differentiation; no MBP$^+$ iOLs are detectable at this timepoint in the S condition. At Day + 14, SON- and S-MBP$^+$ cells are morphologically different. Representative images from two independent experiments. (**F**) Quantification of MBP$^+$ iOLs at Day + 14 illustrated with a box-and-whisker plot. Each dot represents one analyzed field of view (n = 37–39 fields of view per condition). Statistical analysis by Mann–Whitney U test. ** p < 0.01. Representative data from two independent experiments. (**G**) Quantification of average cell size of MBP$^+$ SON-iOLs compared with S-iOLs at Day + 14 of differentiation. Box-and-whisker plot; Each dot represents one analyzed field of view (n = 37–39 fields of view per condition). Statistical analysis by Mann–Whitney U test. **** p < 0.0001. Representative data from two independent experiments. (**H**) Illustration of representative individual cell assessments of S-iOLs and SON-iOLs with the Neurite simple tracer. (**I**) Quantification of the number of branches per MBP$^+$ cell (n = 10 analyzed cells per condition) illustrated by box-and-whisker plot. Statistical analysis by Mann–Whitney U test. *** p < 0.001. (**J**) Quantification of the total traced length per MBP$^+$ cell (n = 10 analyzed cells per condition) illustrated by box-and-whisker plot. Statistical analysis by Mann–Whitney U test. *** p < 0.001.

3.3. SON-Directed Differentiation Is Robust and Generates Mature iOLs More Efficiently Than S

To validate the robustness of our approach in generating O4$^+$ cells, we applied SON-directed differentiation from six independently generated iPSC lines from different donors (Figure S2). The analysis revealed comparable efficiencies for all samples, and we could highlight that an additional intermediate puromycin selection from day + 2 until day + 4 enriches the yield of O4$^+$ cells without the need for a mechanical purification step (Figure S2).

Given that the greatest differences were detected between SON and S, we compared these conditions in the subsequent analyses. Thus, we investigated the efficiency of SON- and S-directed differentiation in their potential to generate mature iOLs expressing the late-stage marker myelin basic protein (MBP). Compared with S-directed differentiation, SON-directed differentiation forced an earlier generation of MBP$^+$ iOLs (at day + 6) and yielded higher numbers at day + 14 (37.5% $\pm$ 14.7% vs. 26.0% $\pm$ 17.0%) (Figure 2E,F). SON generated iOLs that were highly significantly larger and had a more complex ramified OL morphology (Figure 2G–J).

3.4. Individual Transcriptomic Profiles Reveal a Higher Level of Maturation of iOLs upon SON Differentiation

To reveal the transcriptional architecture of individual induced cells, we applied single-cell RNA sequencing (scRNAseq) after completion of neural induction (NI Day + 0) and 15 days after S (S Day + 15) and SON (SON Day + 15) induction (Figure 1A). All samples were analyzed individually (NI Day + 0: n = 217 cells, S Day + 15: n = 577 cells, SON Day + 15: n = 400 cells) and for analyses purposes all 1194 cells were fused together to enable direct comparisons. Shared nearest neighbor (SNN) graph-based clustering identified separate populations of NPCs and neuronal cells, one iOPC cluster, and two distinct iOL clusters, iOL1 and iOL2 (Figure 3A,B). Subsequent statistical analysis revealed a highly significant ($p < 2.2 \times 10^{-16}$) cell cluster composition between the baseline sample NI Day + 0 (n = 217 cells) compared to differentiated samples S Day + 15 (n = 577 cells) and SON Day + 15 (n = 400 cells) as well as between the differentiated samples (Figure 3C, Table S5). This underlines the effect of the directed oligodendroglial differentiation per se as well as the impact on cell cluster composition when different combinations of directing transcription factors were applied (Figure 3A–C, Tables S4 and S5).
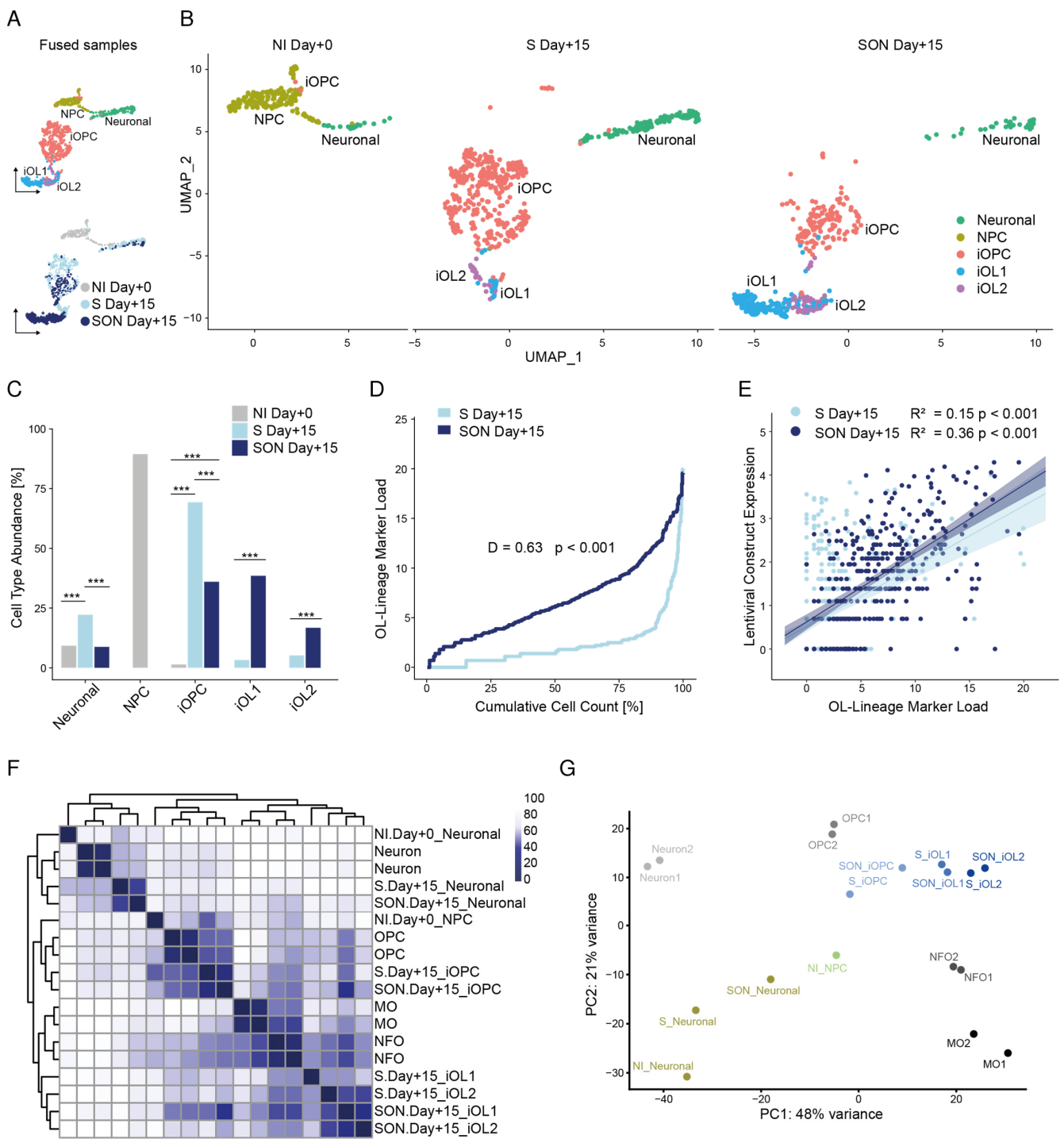
Figure 3. scRNAseq reveals higher level of maturation of oligodendroglial lineage cells, increased level of lentivirus dependent lineage commitment in SON-differentiation and co-clustering with primary OPCs and OLs. (**A**) UMAP embedding of integrated scRNAseq data of baseline sample (Day + 0) after neural induction (NI, *n* = 217 cells) and samples + 15 days after directed differentiation by SOX10 (S, *n* = 577 cells) and SOX10-OLIG2-NKX6.2 (SON, *n* = 400 cells). Top: UMAP dimension plot illustrates clusters of neural precursor cells (NPC, brown), neuronal cells (green), induced oligodendrocyte precursor cells (iOPCs, red), induced oligodendrocyte cluster 1 (iOL1, blue), and

induced oligodendrocyte cluster 2 (iOL2, violet). Bottom: UMAP dimension plot illustrated sample composition after neural induction (NI Day + 0, grey), 15 days after directed differentiation by SOX10 (S Day + 15, light blue), and SOX10-OLIG2-NKX6.2 (SON Day + 15, dark blue). (**B**) UMAP dimension plot, split by sample, showing clusters of neural precursor cells (NPC, brown), neuronal cells (green), induced oligodendrocyte precursor cells (iOPCs, red), induced oligodendrocyte cluster 1 (iOL1, blue), and induced oligodendrocyte cluster 2 (iOL2, violet). (**C**) Percentage of cells (*y*-axis) in each cluster (*x*-axis) from scRNAseq samples NI Day + 0 (grey), S Day + 15 (light blue), SON Day + 15 (dark blue) from B. Significant differences (*** $p < 0.001$) of the cell cluster abundance between annotated samples based on Fisher's exact tests. (**D**) Cumulative iOL lineage marker load (*y*-axis) across the ranked cells (*x*-axis) after + 15 days of directed differentiation by SOX10 (S Day + 15, light blue) and SOX10-OLIG2-NKX6.2 (SON Day + 15, dark blue). *p*-value indicates a significance difference in iOL lineage marker load distribution (Kolmogorov–Smirnov test, *p*-value < 0.001) across the cell population from the scRNAseq experiments after S- and SON-directed oligodendroglial differentiation with higher load in SON-expressing cells (Wilcoxon's rank-sum test, W = 44916, $p < 0.001$. (**E**) Linear regression model of the relationship between lentiviral construct expression (*y*-axis) and iOL lineage marker load (*x*-axis) across the cell populations of S- and SON-directed oligodendroglial differentiation from corresponding scRNAseq data. Spearman's R^2 coefficient of determination and respective significance value of the regression model is indicated in the plot. (**F**) Comparison of transcriptomes of samples from this study with published primary murine cells [27]. Heatmap of Manhattan sample distances and dendrograms from the corresponding unsupervised hierarchical clustering. Abbreviations for primary reference samples: MO, myelinating oligodendrocytes; NFO, newly formed oligodendrocytes; OPC, oligodendrocyte precursor cells. (**G**) Principal component analysis dimension plot showing the first two principal components. scRNAseq data points are colored, whereas reference murine samples are shown in black and grey scale, as indicated.

The most abundant cell types in the baseline neural induction Day + 0 sample were NPCs (89.4%) and neuronal cells (9.2%); a few cells were assigned to the iOPC cluster (1.4%) but no iOLs were detected (Figure 3A–C). The S-directed culture was dominated by the iOPC cluster (69.3%), and the proportion of iOL1 (3.3%) and iOL2 (5.2%) cells was much lower. In contrast, the sample from the SON-directed differentiation comprised a high fraction of iOL1 (38.5%) and iOL2 cells (16.8%), representing a significant ($p < 0.001$) 11- and 3-fold enrichment, respectively, over the S condition (Figure 3C). In contrast, the iOPC cluster was larger in S- compared to SON-directed oligodendroglial differentiation ($p < 0.001$; Figure 3C, Tables S4 and S5).

Next, we investigated the effect of S- versus SON-directed differentiation on the maturation state across the corresponding cell clusters. When plotting the cumulative OL-lineage marker load as a step function of the marker load rank, we observed that the SON-directed populations exhibited a different distribution of OL-lineage marker load (Kolmogorow-Smirnow-Test, *p*-value < 0.001) with generally higher load in SON-expressing cells (Wilcoxon's rank-sum test, W = 44916, $p < 0.001$, Figure 3D). Of note, in both directed differentiation approaches OL-Lineage marker load was significantly associated with the lentiviral construct expression ($p < 0.001$, Figure 3E). The correlation was higher in SON-directed differentiation ($R^2 = 0.36$) compared to S ($R^2 = 0.15$) indicating a stronger oligodendroglial determination using SON-directed differentiation (Figure 3E).

In both S- and SON-directed oligodendroglial differentiation, a small fraction of cells escaped the oligodendroglial lineage and differentiated towards a neuronal identity. However, this neuronal population was 2.5 times ($p < 0.001$) less abundant with SON-directed (8.8%) than with S-directed differentiation (22.2%) (Figure 3A–C).

3.5. Co-Clustering of S- and SON-Differentiated iOPCs and iOLs with Primary OPCs and OLs

To compare iOPCs and iOLs with primary OPCs and OLs, we calculated the average gene expression in each cluster and sample (Table S6) and performed unsupervised clustering of each sample's clusters with reference transcriptomic data that were obtained from FACS purified primary cells [27]. In the resulting dendrogram, we found three main clusters: One cluster grouped the iOL1 and iOL2 profiles together with newly formedmurine oligodendrocytes (NFO) and myelinating oligodendrocytes (MO) [27], a second cluster contained the iOPCs and NPCs together with the reference OPC samples (Figure 3F) and in the third cluster the neuronal cells clustered together with primary neurons. When we looked at the 50 most variable features in this unsupervised clustering, we found that 26 of those genes formed a gene set that separated the oligodendroglial samples from the neuronal cells (Figure S3). In this gene set, all iOL cluster profiles closely resembled the NFO and the expression profile MO of the reference sample. In a principal component analysis, the first principal component explained 48% of the total variance, and the samples were aligned in the presumable flow of differentiation, findings that underline the high similarity between the S-/SON-directed hiPSC-derived cells and primary oligodendroglial cells (Figure 3G).

3.6. Dedicated Gene Expression Profiles of Marker Genes Support Identities of Subclusters and Differential Efficiency of S and SON Conditions towards the Oligodendroglial Lineage

To further characterize cluster identities, we compared the expression and abundance of marker genes [9] in the dedicated NPC, iOPC, and iOL1 and iOL2 subclusters (Figure 4 and Figure S4, Tables S4–S7). The neural stem cell marker *PAX6* was highly expressed not only in a large proportion of NPCs but also in a substantial proportion of iOPCs. S-derived iOPCs expressed *PAX6* at higher frequencies as compared to SON iOPCs ($p < 0.001$) (Figure 4A–C). This enrichment towards NPC/S-iOPC was supported by violin plots showing the distribution of the averaged expression levels which was higher in S iOPCs over SON iOPCs ($p < 0.001$, Figure 4D). An overall similar profile was observed for an additional progenitor marker, *SOX3* (Figure S4A–D, Tables S4–S7). *SOX9*, an OPC stage-enriched TF, was predominantly expressed in S- and SON-iOPCs with no substantial differences within the respective clusters but a significantly higher number of *SOX9* expressing cells in the S-directed cluster compared to the SON condition ($p < 0.001$, Figure 4E–H). An overall similar, OPC-biased profile was obtained with *ST8SIA1* (the gene product stained with the prototypical OPC marker A2B5, Figure S4E–H, Tables S4–S7). *MBP* was selected as a marker for mature OLs and showed a strong increase in expression comparing iOPC and iOL1 clusters ($p < 0.001$) reaching the highest expressing levels in the iOL2 cluster ($p < 0.001$, Tables S4–S7). Moreover, SON iOPCs express low levels of *MBP* in contrast to S iOPCs ($p < 0.001$), but in S-derived cells, *MBP* was almost exclusively detected in iOL1 and iOL2 clusters (Figure 4I–L). Notably, some myelin genes expressed at the late stage, such as myelin-associated oligodendrocyte basic protein (*MOBP*), were robustly expressed only in the SON-derived iOL2 cell population and almost absent in S-derived cells (Figure 4M–P, Tables S4–S7). The higher level of expression of *MBP* and many other myelin marker genes, such as proteolipid protein 1 (*PLP1*) and galactosylceramidase (*GALC*, Figure S4I–P, Tables S4–S7), indicates that the iOL2 subcluster represents the most matured fraction of iOLs.
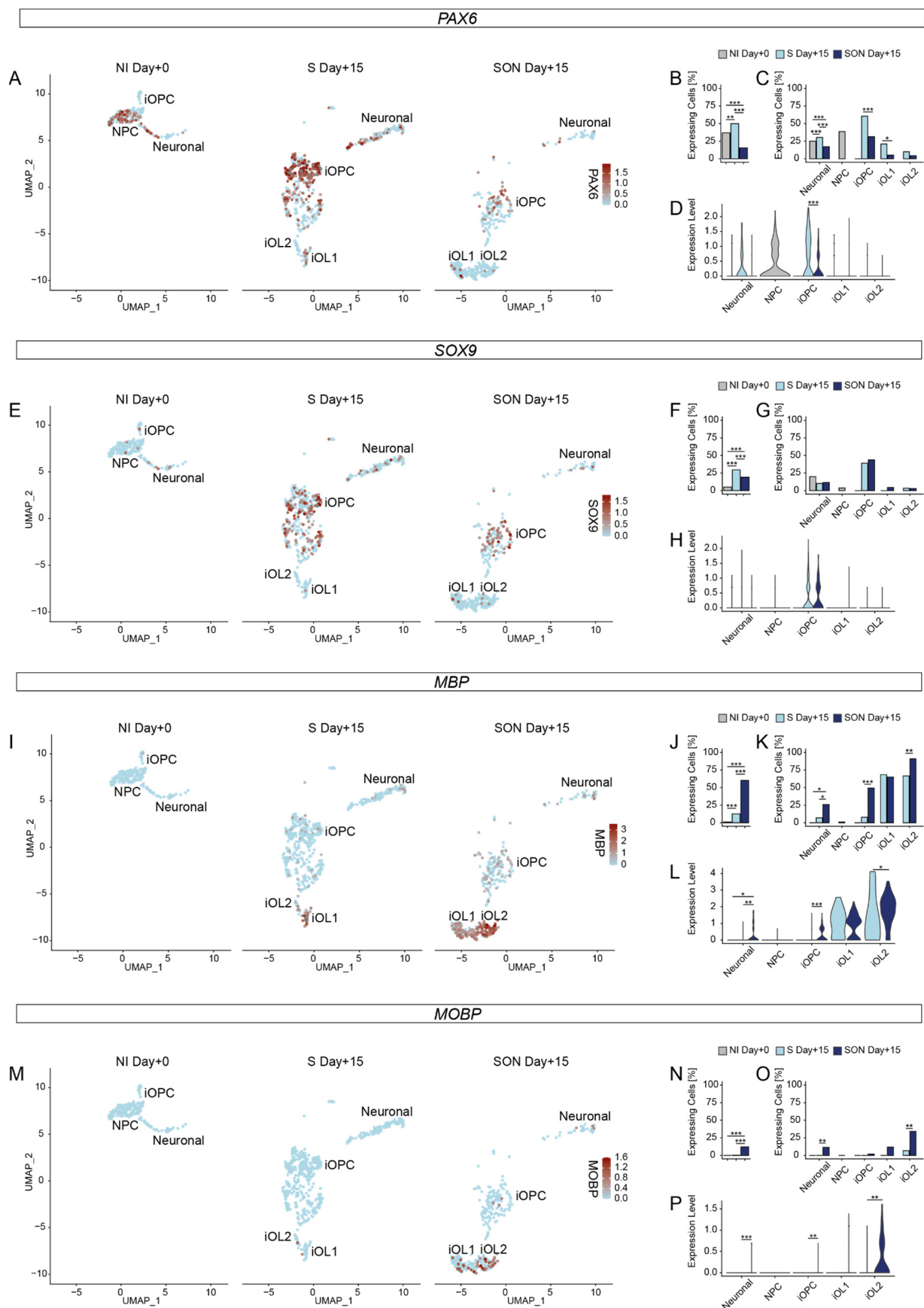
Figure 4. Marker gene expression verifies cluster identities and shows a mature oligodendrocyte phenotype in SON. (**A,E,I,M**) UMAP representation showing single-cell expression of selected marker

genes (**A**) *PAX6*, (**E**) *SOX9*, (**I**) *MBP*, (**M**) *MOBP* from scRNAseq of baseline sample after neural induction (NI Day + 0, *n* = 217 cells, one independent experiment) and samples after 15 days of directed differentiation by SOX10 (S Day + 15, *n* = 577 cells, one independent experiment) and SOX10-OLIG2-NKX6.2 (SON Day + 15, *n* = 400 cells, one independent experiment) with annotated cell clusters of neural precursor cells (NPC), neuronal cells, induced oligodendrocyte precursor cells (iOPCs), induced oligodendrocyte cluster 1 (iOL1) and induced oligodendrocyte cluster 2 (iOL2). Expression value per cell plotted according to the color intensity of the respective scale bar as indicated. (**B,F,J,N**) Bar plots illustrate the abundance of expressing cells for each sample. ** (*p*-value < 0.01), *** (*p*-value < 0.001) based on Fisher's exact tests (details provided in Table S5). (**C,G,K,O**) Bar plots illustrate the abundance of expressing cells for each cluster split by sample. * (*p*-value < 0.05), ** (*p*-value < 0.01), *** (*p*-value < 0.001) based on Fisher's exact tests (details provided in Table S5). (**D,H,L,P**) Violin plots of the normalized expression per sample within the respective cell type cluster. * (*p*-value < 0.05), ** (*p*-value < 0.01), *** (*p*-value < 0.001) based on Wilcoxon signed-rank test (details provided in Table S7).
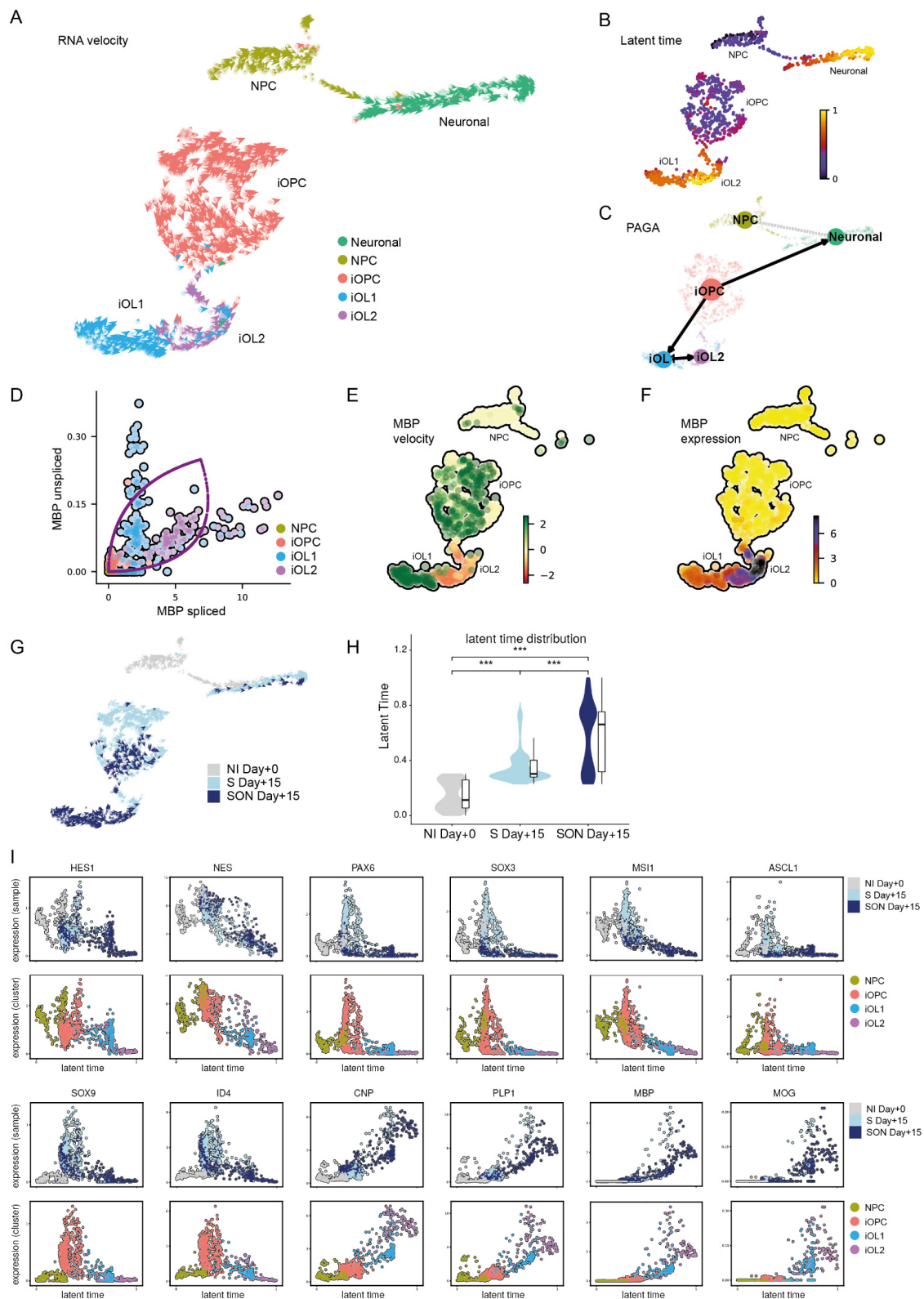
3.7. RNA Velocity Reveals Divergent Dynamics of Fate Decisions upon Induced Oligodendroglial Differentiation

To examine the transcriptional dynamics underlying the different processes and outcomes of S- and SON-directed differentiation, we applied the RNA velocity approach to model the splicing kinetics as a proxy of the status of individual cells along the differentiation trajectories [23]. Briefly, the direction and speed of transcriptional changes in single cells are estimated from the ratio of detected unspliced to detected spliced transcripts. This allows for the prediction of the future transcriptional state of a specific gene in a given cell. A higher than expected ratio of unspliced to spliced mRNAs signifies upregulation over steady-state expression levels because of the temporal delay between an increase in transcriptional rate and an increase in the amount of mature mRNAs as end products of splicing [23]. In turn, a lower than expected unspliced to spliced ratio indicates downregulation because of the temporal delay between a decrease in the transcriptional rate and degradation of mature mRNAs. The 'velocity' vectors represent the direction and speed of the transcriptional changes in each cell and estimate future cell kinetics by indicating the movement of the cell through transcriptional space during differentiation.

In our data, we first determined the proportion of detectable unspliced transcripts to ensure their suitability for this type of analysis. This value typically depends on the protocol used, data processing, read length, and cell types present in the sample [31,33]. In our samples, the overall proportion of unspliced counts was 13% (Figure S5A), which was well within the expected range [33]. We found small differences among clusters (Figure S5B) and between samples (Figure S5C) but the differences were all within a range of 11% (iOL1) to 16% (NPC).

When the 'velocity' vectors were superimposed on the UMAP dimension plot (Figure 3A), two main streams of cells—an oligodendroglial and a neuronal stream—emerged along differentiation pathways in our cultures (Figure 5A). Moreover, we looked at the gene-shared latent time, a recent pseudo-time concept that uses only transcriptional kinetics instead of a diffusion-based approach [31]. Here, we found two endpoints, one pathway in the direction of the neuronal cluster and one in the direction of the iOL2 cluster, again indicating the presence of two distinct lineages in the pooled S and SON samples (Figure 5B). Additionally, we used partition-based graph abstraction (PAGA) to identify transitions between clusters [34] (Figure 5C). These transitions confirmed the two major differentiation pathways in our samples: One pathway represented the oligodendroglial lineage, in which the cells transitioned from an OPC state to an early OL identity in the iOL1 cluster and then moved on to the more mature iOL2 cluster, and the other led to a neuronal identity. In this stream, cells in the neural induction baseline sample differentiated directly towards this direction. In contrast, in the S

and SON samples, where no NPCs were left, iOPCs transdifferentiated to a neuronal identity. These escaping iOPCs were also clearly visible in the vector plot (Figure 5A).

Figure 5. RNA velocity reveals the dynamics of fate decisions upon induced oligodendroglial differentiation. (**A**) RNA velocity vectors projected on the single-cell UMAP-based dimension plot

indicate direction and speed of individual cells in transcriptional space. (**B**) The gene-shared latent time identifies two endpoints of differentiation in the scRNAseq samples: One in the induced oligodendrocyte cluster 2 (iOL2) cluster and one in the neuronal cluster. (**C**) Partition-based graph abstraction (PAGA) plot visualizing transitions between clusters superimposed on the UMAP embedding reveals two differentiation paths: (1) the oligodendroglial lineage, in which the cells transition from iOPC to iOL1 to iOL2, and (2) the neuronal lineage from NPCs and iOPCs that escape the TF-directed oligodendroglial differentiation. (**D**) Dynamic model of MBP's transcriptional kinetics plotted on top of the scatter plot of unspliced and spliced transcript expression. (**E**) MBP velocity estimates indicating MBP mRNA induction (green) and repression (red). (**F**) MBP expression level. (**G**) Velocity vectors on UMAP embedding with sample color code: Sample after neural induction (NI Day + 0) in grey, S-directed differentiation (S Day + 15) in light blue and SON-directed differentiation (SON Day + 15) in dark blue, as indicated. (**H**) Latent time distribution between baseline (NI Day + 0), S-directed differentiation (S Day + 15), and SON-directed differentiation (SON Day + 15), illustrated with a violin and box- and-whisker plot. Pairwise comparisons were tested with Wilcoxon's rank-sum test. *** $p < 0.001$. (**I**) Latent time versus gene expression of stage-specific genes during oligodendrocyte differentiation. Individual cells colored by cluster and sample.

In addition, we analyzed the dynamic model and RNA velocity of individual 'velocity genes' (Figure 5I). An interesting example of a strong 'velocity gene' is *MBP*. The phase portrait visualizes unspliced and spliced transcripts overlayed with the corresponding dynamic model (Figure 5D). When examining the phase portrait of *MBP*, we noticed that most iOL1 cells were in an on state, i.e., upregulating *MBP* transcription, as indicated by a high positive ratio of unspliced to spliced transcripts (Figure 5E). In contrast, most iOL2 cells were close to a steady-state or negative velocity value, reflecting the endpoint of *MBP* upregulation (Figure 5E). However, the somewhat counterintuitive RNA velocity-derived model for the oligodendroglial differentiation path iOPC to iOL1 to iOL2 (Figure 5C,E) was in line with the elevated levels of spliced *MBP* mRNA level along this trajectory (Figure 5F,I).

We also detected clear differences in the differentiation processes between the S Day + 15 and SON Day + 15 samples (Figure 5G). Notably, the population of iOPCs moving towards the neuronal cluster was much more prominent in S-directed than in SON-directed oligodendroglial differentiation (Figure 5G, upper light blue half of the iOPC cluster). Moreover, the gene-shared latent time scores of each cell could be used as an indicator of maturity because in both samples the cells took a similar path in their differentiation to OLs. This was confirmed in an individual RNA velocity analysis of both samples, which eliminated the possibility that one sample could be interfering with the other (Figure S5D). When comparing the latent time scores between samples, the oligodendroglial lineage in the SON-expressing culture (median = 0.66; MAD = 0.31; n = 365) was found to be significantly more mature than that in the S-expressing culture (median = 0.30; MAD = 0.05; n = 449) [W = 42640; $p = 2.2 \times 10^{-16}$] (Figure 5H). This result was in line with the higher abundance of iOL1 and iOL2 cells in SON Day + 15.

Finally, we identified a series of differentiation marker genes from a previously published study [9] expressed in our samples and illustrated their transcriptional kinetics during OL differentiation as a gene expression level dependent on latent time (Figure 5I). This allowed us to show again the high overlap of a late gene-shared latent time point, the SON sample, and the iOL cluster identities (Figure 5I).

3.8. Characterisation of iOPC Subclusters

The RNA velocity analysis enabled us to clearly identify two distinct differentiation streams within the iOPC cluster that were moving in different directions (Figure 5G), a feature that was not detected in the first shared nearest neighbor (SNN)-based clustering result (Figure 3A,C). One subcluster followed the oligodendroglial lineage and was present in both S- and SON-directed differentiation and another partly escaped towards a neuronal lineage and was almost exclusively found in the S-directed differentiation (Figure 5G). Because of this observation, we increased the resolution of the SNN clustering to empir-

ically identify subpopulations in the sample. This approach allowed us to identify two iOPC subclusters that were illustrated in an RNA velocity plot color coded for the iOPC subclusters (Figure 6A and Figure S6A,B). The iOPC2 subcluster, which occurred in both conditions (18.2% in S Day + 15 and 32.0% in SON Day + 15), comprised mainly the iOPC population of the OPC-OL differentiation pathway (Figure 6A). In contrast, the iOPC1 subcluster was almost exclusively observed in S Day + 15 (51.1% in S Day + 15 and 4.2% in SON Day + 15) and comprised the stream of cells escaping towards the neuronal cluster, which likely represented a more volatile iOPC stage under the given culture condition (Figure 6A and Figure S6A,B). Of note, we analyzed the expression of the exogenous lentiviral construct via the scRNAseq-detecTable 3′LTR site (Figure S6C,D). Expression levels of exogenous constructs were higher and more homogenous in iOL1 and iOL2 compared to iOPC1, iOPC2, and the neuronal cluster. Furthermore, within iOPC1, iOPC2, iOL1, and iOL2, S-, or SON-construct expression were comparable.

To identify molecular signatures of the two iOPC stages, we compared the differential average gene expression in the S-iOPC1, S-iOPC2, and SON-iOPC2 subclusters (Figure 6B–F, Table S8). We found substantial differences in significantly deregulated genes between the iOPC1 and iOPC2 clusters in the comparisons of S-iOPC1 with S-iOPC2 (Figure 6B) and S-iOPC1 with SON-iOPC2 (Figure 6C). Notably, the progenitor markers PAX6 and SOX3 were expressed at a lower level in the iOPC2 cluster, indicating a higher maturation level (Figure 6B,C). In contrast, only very few genes were found to be differentially expressed in S-iOPC2 and SON-iOPC2, indicating that the iOPC2 cluster identity was independent of the condition and that it represents a rather homogenous entity (Figure 6D). This assumption was corroborated by the broad overlap of differentially expressed genes in both comparisons (Figure 6E,F). A comparison of SON-iOPC1 and SON-iOPC2 was deemed not advisable because of the low number of cells in the SON-iOPC1 cluster, which can be independently interpreted as an indicator of an increased drive of iOPC maturation mediated by SON compared with iOPC maturation mediated by S alone. This finding underlines that the directed OL differentiation driven by S was similar in both conditions, whereas the efficiency was higher with SON than with S. Furthermore, we performed a gene ontology term-based hypergeometric enrichment analysis for the comparisons of iOPC1 and iOPC2 (Table S9). Thereby we identified gene-sets relevant for the organization of the extracellular matrix as most significantly altered (Figure 6G), a result that is in line with several genes of the collagen family that were detected as being upregulated in the gene-by-gene analysis (Figure 6B,C).

These findings prompted us to hypothesize that structural differences may also be visible between S- and SON-generated iOPCs. Therefore, for both conditions we performed microbead purification to enrich O4$^+$ iOPCs at day + 10 and morphological analysis of O4$^+$ cells at day + 16. We thereby observed substantial morphological differences between S- and SON-directed O4$^+$ cells (Figure 6D) and a larger average cell size of SON-derived O4$^+$ cells compared with S-derived O4$^+$ cells (Figure 6H).

Overall, our results show that different combinations of TFs have a substantial effect on iOPC and iOL morphology, maturation stage, cell cluster composition, and lineage transition dynamics.

Figure 6. Characterization of iOPC subcluster formation induced by S- and SON-directed differentiation reveals profound differences in expression of extracellular matrix components. (**A**) Zoom-out

of oligodendroglial lineage clusters of RNA velocity vectors projected on UMAP dimension plot of iOPC1, iOPC2, iOL1, and iOL2 clusters of S Day + 15 and SON Day + 15. For a complete dimension plot including neuronal linage, see Figure S6A,B. (**B**) Differential gene expression (DGE) analysis of S-iOPC2 subcluster and S-iOPC1 subcluster illustrated with volcano plot. The average log2 fold change (log2FC) is shown on the *x*-axis and the negative log10 *p*-value ($-\log10(p)$) on the *y*-axis. Genes significantly upregulated (red) and downregulated (blue) in S-iOPC2 compared with S-iOPC1 are colored. The top 20 differentially expressed genes are labeled for up- and downregulation accordingly. (**C**) DGE analysis of SON-iOPC2 subcluster and S-iOPC1 subcluster illustrated with a volcano plot. Genes significantly upregulated (red) and downregulated (blue) in SON-iOPC2 compared with S-iOPC1 are colored. (**D**) DGE analysis of SON-iOPC2 subcluster and S-iOPC2 subcluster illustrated with a volcano plot. Genes significantly upregulated (red) and downregulated (blue) in SON-iOPC2 are colored. (**E**) Upregulated genes within iOPC subclusters shown in a Venn diagram. (**F**) Downregulated genes within iOPC subclusters shown in a Venn diagram. (**G**) Pathway enrichment analysis of iOPC subcluster comparison. (**H**) Representative images of O4$^+$ iOPCs after microbead purification. (**I**) Quantification of cell sizes of O4$^+$ iOPCs illustrated with a box-and-whisker plot. Dots correspond to analyzed fields of view (*n* = 25–26 per condition). Statistical analysis by two-sided *t*-test. **** *p* < 0.0001.

4. Discussion

In our comparative study, we confirmed that S-, SO- and SON-directed conversion are all sufficient to rapidly generate oligodendroglial lineage cells from hiPSCs. As a result of the side-by-side analysis at the single-cell resolution, we showed that the application of SON generated more O4$^+$ late-stage iOPCs and more mature and complex MBP$^+$ iOLs than the application of S alone, supporting previous observations [11]. S alone was most effective in generating a mixed population of iOPCs (see below). In agreement with previous studies [36,37], we observed a higher level of expression of smaller-sized constructs. However, an intermediate selection step performed in our protocol normalized these differences and allowed us to compare TF combinations irrespective of construct size. As mentioned above, a more recent study that used a systematic screen for lineage-converting TFs found that SOX9 was capable of inducing oligodendroglial cells on its own [14]. Thus, similar to other SOX family members, both SOX9 and SOX10 can be considered as pioneering TFs in the oligodendroglial lineage that prime critical steps essential for stem cell conversion [38]. SOX9 operates genetically upstream of SOX10 in the oligodendroglial lineage and—despite the fact that SOX9 can generate myelinating iOLs in a 3D system [14]—it remains an open question whether SOX9 might generate more earlier stage iOPCs than SOX10 in a cell-autonomous setting such as the one applied in this study. We observed substantial differences in iOPC and iOL heterogeneity and dynamics of differentiation between S- and SON-directed oligodendroglial differentiation. Despite the finding that OPC marker genes such as *SOX9*, *ST8SIA1*, *CNP*, *ID2* and *ID4* reached similar levels in S- and SON-iOPCs, the expression level of oligodendroglial maturation markers such as *GALC* and *MOBP* was higher in SON-iOLs than in S-iOLs under the applied conditions. Moreover, the cell cluster composition differed dramatically: Mature iOLs, that express *PLP1, GALC, MBP, MOBP,* were far more abundant upon SON-directed differentiation but the iOPC cluster was larger and more diverse in the S-directed condition (see below).

To improve purity and scalability, we introduced the lentivirus-encoded lineage transcription factors at the level of iPSC cultivation followed by two puromycin selection steps, one before and one after initiation of iOPC/iOL differentiation; this protocol was robust for different iPSC lines obtained from six different human donors. The advantage of this approach is that less lentivirus is needed and only infected S/O/N-hiPSCs are proliferative and can be amplified, frozen, banked, and recovered en masse at the time needed. In the future, this approach will be particularly suited to enable larger-

scaled case-control comparisons and may allow also genetic and compound screenings requiring high numbers of dedicated cells. Nonetheless, epigenetic lentivirus silencing is a confounding factor [39]. The drop of FLAG[+] hiPSCs after doxycycline induction is likely due to the loss of cleavage efficiencies by single versus double P2A/T2A element-containing constructs [40].

In both conditions (S and SON), the lentiviral construct expression level was associated with a higher level of OL-lineage marker load. However, SON-directed differentiation caused a much higher marker load underlining a more maturing oligodendroglial differentiation compared to S-directed differentiation in line with previous work [11].

On the iOPC/iOL level, lentiviral construct transcriptome levels within the clusters were comparable between S and SON indicating that the expression levels are unlikely to cause cluster diversity and that this diversity is most likely attributed to the different TF combinations. However, expression levels were higher in iOL clusters compared to iOPC clusters and the neuronal cluster. Thus, it might be possible that higher expression levels sustain the directed differentiation. Thus, for genetic and chemical screens [41,42], safe harbor strategies may be a better choice to express OL-lineage-converting TFs and previous work could highlight that safe harbor strategies using SOX10 were sufficient to generate high yields of homogenous MBP[+] iOLs [19].

However, safe harbourstrategies will be complicated to apply in case-control comparisons, where many subjects/cell lines are to be compared. Nonetheless, a safe harbor-mediated CRISPR/Cas9-based genetic screen has been described for hiPSC-derived NGN2-directed iNeurons [41], showing the potential of this approach also for other cell types. Safe harbor strategies that apply CRISPR/Cas9 technology could also be applied to modify directed differentiation. In contrast to exogenous overexpression of TFs for directed differentiation, a recently published study applied CRISPR/Cas9-mediated activation of endogenous *Sox10*, *Olig2*, and *Nkx6.2* by specific gRNAs to differentiate mouse neural stem cells and mouse embryonic fibroblasts to O4[+] and MBP^{+} oligodendroglial cells [43].

In this study and previous studies that used the same neuronal patterning approach [13,19], the expression of early-stage OPCs markers, such as *CSPG4* (*NG2*) and *PDGFRA*, was barely detectable in iOPCs. Thus, with both SON and S this directed differentiation approach can be assumed to bypass early OPC stages. Chemical differentiation approaches may therefore be preferable for examining early-stage OPCs over a longer time period [44,45]. A study that used such an approach applied scRNAseq on PDGFRA-enriched, chemically transformed OL-lineage cells and uncovered several stages of OPCs [46]. The scRNAseq analysis of our study revealed that directed oligodendroglial-lineage conversion also reflects several aspects of known OPC and OL development [9,47]. For example, we observed an upregulation of *ST8STIA1* (A2B5), *ID2*, *ID4*, and *SOX9* in iOPCs. In addition, we found increased expression of the oligodendroglial markers *CNP* and *PLP1* during differentiation. In addition, in more mature iOLs we found an enhanced expression of marker genes for OL differentiation, such as *MBP* and *MYRF* that are crucial for myelination [47].

To investigate hiPSC-based oligodendroglial lineage differentiation, we applied RNA velocity analysis, a technique that was developed for investigating differentiation processes in scRNAseq datasets to infer temporal changes without needing to obtain samples at several time points [23]. Thereby, we described the transcriptional dynamics during fate decisions in induced oligodendroglial differentiation and identified *MBP*, for example, as a velocity gene. Nevertheless, our data are based on 3′UTR-enriched single-cell transcriptome libraries, which limits their information content in RNA velocity analysis. Full-length scRNAseq protocols, which cover more splicing sites, would detect a higher variety of splicing variants and thus increase the number of potential velocity genes and might be beneficial to improve velocity analysis [31]. Nonetheless, the RNA velocity-based analyses in this study provided additional insights. With the help of graph-based analysis methods such as PAGA [34], we could visualize the oligoden-

droglial differentiation stream from iOPC to iOL1 and iOL2, which could be validated independently in S- and SON-directed differentiation and which would not have been identified with standard scRNAseq analysis. To generate a pseudo-timeline, we used gene-shared latent time instead of common similarity-based Markovian diffusion models, as suggested by Bergen et al., (2020). This approach improved the resulting timeline dramatically because the diffusion-based pseudo-timeline forced a unidirectional 'time flow' onto the dataset, which clearly did not fit the existence of two distinct lineages in one dataset. We used latent time analysis to highlight the 'time'-dependent up- and downregulation of several oligodendroglial stage markers and to estimate the maturation state of a single cell within the whole span of oligodendroglial differentiation. Hereby, we observed a higher latent time distribution with SON than with S, indicating that oligodendroglial differentiation was faster in the SON- than in the S-directed differentiation. RNA velocity also uncovered a second neuronal leakage stream that was more prominent in S-directed differentiation. This leakage stream indicated that not only NPCs with low construct expression but also parts of the S-iOPC1s differentiated towards a neuronal state. Thus, we found evidence that S-directed differentiation might allow some iOPCs to 'escape' towards the neuronal lineage during the differentiation process, and that SON-directed differentiation seems to be less volatile and more efficient regarding OL differentiation under the applied conditions.

Differential gene expression analysis revealed that S-iOPC2 and SON-iOPC2 were quite similar and showed a substantial overlap in their differentially expressed genes when compared with iOPC1. This finding hints at a similar differentiation path with S and SON, although efficiency was higher with SON, as reflected by the abundance of more mature oligodendroglial cells, i.e., iOPC2, iOL1, and iOL2. On the other hand, iOPC1 constitutes a population of 'escaping' cells, giving us the opportunity to investigate the transcriptional networks and signaling machinery necessary for different steps of the differentiation process. Pathway analysis indicated greater expression of extracellular matrix components in iOPC2 cells than in iOPC1 cells; this difference may reflect a maturation step, as indicated by the change in direction of the velocity vectors towards the OL stage, or may represent a slight deflection towards other glial lineages [46].

Oligodendroglial-lineage cells represent a heterogeneous cell population with a high spatio-temporal diversity [3,6]. A limitation of directed protocols is that they most likely generate only a subset of OPC/OL sub-lineages, depending on which TFs or combination of TFs they use. An advantage of directed conversion, however, is that human cells from a defined differentiation state can be generated in virtually unlimited amounts for various applications.

Our work highlights that applied TFs for generating iOPCs or iOLs should be chosen depending on the intended application or research question. Our analysis suggests that differentiation directed by S offers a useful tool for research on OPC biology and earlier stages of oligodendroglial differentiation, including research that addresses the effects of external cues promoting OPC and OL differentiation, i.e., in a 3D/spheroid culture system; the same might be true for SOX9 [14]. On the other hand, applications, and research with a focus on more mature iOLs might benefit from the use of SON. TF combinations such as SON are likely to be better suited to studying OL biology and myelination-associated aspects, given the much higher conversion rate and easier access to much higher numbers of mature OLs with such combinations. Further investigations are certainly needed to unleash the potential of future cell therapies with engineered iOLs in myelin diseases, but a better understanding of the nature of induced cells via different TF-directed protocols will certainly be helpful to achieve this goal. We believe that the molecular and analysis tools applied in this study to force and dissect human oligodendrocyte development may support the understanding of dynamic aspects of cell-autonomous versus non-cell-autonomous contributions in in vivo disease models in the future, i.e., via grafting of iOLs generated from normal and diseased donors into mouse brains. The paradigmatic study on human iPSC-derived glia/mouse chimeras already revealed oligodendroglia-cell-autonomous

contributions to childhood-onset schizophrenia [48]. More such in vivo studies are needed that combine patient-derived oligodendoglial cell types with sophisticated single-cell level analyses to further increase our knowledge of disorders with myelination deficits.

References

1. Micu, I.; Plemel, J.R.; Caprariello, A.V.; Nave, K.-A.; Stys, P.K. Axo-Myelinic Neurotransmission: A Novel Mode of Cell Signalling in the Central Nervous System. *Nat. Rev. Neurosci.* **2018**, *19*, 49–58. [CrossRef]
2. Simons, M.; Nave, K.-A. Oligodendrocytes: Myelination and Axonal Support. *Cold Spring Harb. Perspect. Biol.* **2015**, *8*, a020479. [CrossRef] [PubMed]
3. Dimou, L.; Simons, M. Diversity of Oligodendrocytes and Their Progenitors. *Curr. Opin. Neurobiol.* **2017**, *47*, 73–79. [CrossRef] [PubMed]
4. Zonouzi, M.; Berger, D.; Jokhi, V.; Kedaigle, A.; Lichtman, J.; Arlotta, P. Individual Oligodendrocytes Show Bias for Inhibitory Axons in the Neocortex. *Cell Rep.* **2019**, *27*, 2799–2808.e3. [CrossRef] [PubMed]
5. Jäkel, S.; Agirre, E.; Mendanha Falcão, A.; van Bruggen, D.; Lee, K.W.; Knuesel, I.; Malhotra, D.; Ffrench-Constant, C.; Williams, A.; Castelo-Branco, G. Altered Human Oligodendrocyte Heterogeneity in Multiple Sclerosis. *Nature* **2019**, *566*, 543–547. [CrossRef] [PubMed]
6. Spitzer, S.O.; Sitnikov, S.; Kamen, Y.; Evans, K.A.; Kronenberg-Versteeg, D.; Dietmann, S.; de Faria, O.; Agathou, S.; Káradóttir, R.T. Oligodendrocyte Progenitor Cells Become Regionally Diverse and Heterogeneous with Age. *Neuron* **2019**, *101*, 459–471.e5. [CrossRef]
7. Schmitt, A.; Simons, M.; Cantuti-Castelvetri, L.; Falkai, P. A New Role for Oligodendrocytes and Myelination in Schizophrenia and Affective Disorders? *Eur. Arch. Psychiatry Clin. Neurosci.* **2019**, *269*, 371–372. [CrossRef]
8. Chanoumidou, K.; Mozafari, S.; Baron-Van Evercooren, A.; Kuhlmann, T. Stem Cell Derived Oligodendrocytes to Study Myelin Diseases. *Glia* **2020**, *68*, 705–720. [CrossRef]
9. Goldman, S.A.; Kuypers, N.J. How to Make an Oligodendrocyte. *Development* **2015**, *142*, 3983–3995. [CrossRef]
10. Raabe, F.J.; Galinski, S.; Papiol, S.; Falkai, P.G.; Schmitt, A.; Rossner, M.J. Studying and Modulating Schizophrenia-Associated Dysfunctions of Oligodendrocytes with Patient-Specific Cell Systems. *NPJ Schizophr.* **2018**, *4*, 23. [CrossRef]
11. Ehrlich, M.; Mozafari, S.; Glatza, M.; Starost, L.; Velychko, S.; Hallmann, A.-L.; Cui, Q.-L.; Schambach, A.; Kim, K.-P.; Bachelin, C.; et al. Rapid and Efficient Generation of Oligodendrocytes from Human Induced Pluripotent Stem Cells Using Transcription Factors. *Proc. Natl. Acad. Sci. USA* **2017**, *114*, E2243–E2252. [CrossRef] [PubMed]
12. Pawlowski, M.; Ortmann, D.; Bertero, A.; Tavares, J.M.; Pedersen, R.A.; Vallier, L.; Kotter, M.R.N. Inducible and Deterministic Forward Programming of Human Pluripotent Stem Cells into Neurons, Skeletal Myocytes, and Oligodendrocytes. *Stem Cell Rep.* **2017**, *8*, 803–812. [CrossRef] [PubMed]
13. García-León, J.A.; Kumar, M.; Boon, R.; Chau, D.; One, J.; Wolfs, E.; Eggermont, K.; Berckmans, P.; Gunhanlar, N.; de Vrij, F.; et al. SOX10 Single Transcription Factor-Based Fast and Efficient Generation of Oligodendrocytes from Human Pluripotent Stem Cells. *Stem Cell Rep.* **2018**, *10*, 655–672. [CrossRef] [PubMed]
14. Ng, A.H.M.; Khoshakhlagh, P.; Rojo Arias, J.E.; Pasquini, G.; Wang, K.; Swiersy, A.; Shipman, S.L.; Appleton, E.; Kiaee, K.; Kohman, R.E.; et al. A Comprehensive Library of Human Transcription Factors for Cell Fate Engineering. *Nat. Biotechnol.* **2021**, *39*, 510–519. [CrossRef] [PubMed]
15. Chanoumidou, K.; Hernández-Rodríguez, B.; Windener, F.; Thomas, C.; Stehling, M.; Mozafari, S.; Albrecht, S.; Ottoboni, L.; Antel, J.; Kim, K.-P.; et al. One-Step Reprogramming of Human Fibroblasts into Oligodendrocyte-like Cells by SOX10, OLIG2, and NKX6.2. *Stem Cell Rep.* **2021**, *16*, 771–783. [CrossRef]
16. Okita, K.; Yamakawa, T.; Matsumura, Y.; Sato, Y.; Amano, N.; Watanabe, A.; Goshima, N.; Yamanaka, S. An Efficient Nonviral Method to Generate Integration-Free Human-Induced Pluripotent Stem Cells from Cord Blood and Peripheral Blood Cells. *Stem Cells* **2013**, *31*, 458–466. [CrossRef]
17. Danecek, P.; McCarthy, S.A.; Consortium, H.; Durbin, R. A Method for Checking Genomic Integrity in Cultured Cell Lines from SNP Genotyping Data. *PLoS ONE* **2016**, *11*, e0155014. [CrossRef]
18. Bock, C.; Kiskinis, E.; Verstappen, G.; Gu, H.; Boulting, G.; Smith, Z.D.; Ziller, M.; Croft, G.F.; Amoroso, M.W.; Oakley, D.H.; et al. Reference Maps of Human ES and IPS Cell Variation Enable High-Throughput Characterization of Pluripotent Cell Lines. *Cell* **2011**, *144*, 439–452. [CrossRef]
19. García-León, J.A.; García-Díaz, B.; Eggermont, K.; Cáceres-Palomo, L.; Neyrinck, K.; Madeiro da Costa, R.; Dávila, J.C.; Baron-Van Evercooren, A.; Gutiérrez, A.; Verfaillie, C.M. Generation of Oligodendrocytes and Establishment of an All-Human Myelinating Platform from Human Pluripotent Stem Cells. *Nat. Protoc.* **2020**, *15*, 3716–3744. [CrossRef]
20. Schindelin, J.; Arganda-Carreras, I.; Frise, E.; Kaynig, V.; Longair, M.; Pietzsch, T.; Preibisch, S.; Rueden, C.; Saalfeld, S.; Schmid, B.; et al. Fiji: An Open-Source Platform for Biological-Image Analysis. *Nat. Methods* **2012**, *9*, 676–682. [CrossRef]
21. Longair, M.H.; Baker, D.A.; Armstrong, J.D. Simple Neurite Tracer: Open Source Software for Reconstruction, Visualization and Analysis of Neuronal Processes. *Bioinformatics* **2011**, *27*, 2453–2454. [CrossRef]
22. Romagnoli, D.; Boccalini, G.; Bonechi, M.; Biagioni, C.; Fassan, P.; Bertorelli, R.; De Sanctis, V.; Di Leo, A.; Migliaccio, I.; Malorni, L.; et al. DdSeeker: A Tool for Processing Bio-Rad DdSEQ Single Cell RNA-Seq Data. *BMC Genom.* **2018**, *19*, 960. [CrossRef]
23. La Manno, G.; Soldatov, R.; Zeisel, A.; Braun, E.; Hochgerner, H.; Petukhov, V.; Lidschreiber, K.; Kastriti, M.E.; Lönnerberg, P.; Furlan, A.; et al. RNA Velocity of Single Cells. *Nature* **2018**, *560*, 494–498. [CrossRef]

24. Satija, R.; Farrell, J.A.; Gennert, D.; Schier, A.F.; Regev, A. Spatial Reconstruction of Single-Cell Gene Expression Data. *Nat. Biotechnol.* **2015**, *33*, 495–502. [CrossRef] [PubMed]

25. Hafemeister, C.; Satija, R. Normalization and Variance Stabilization of Single-Cell RNA-Seq Data Using Regularized Negative Binomial Regression. *Genome Biol.* **2019**, *20*, 296. [CrossRef] [PubMed]

26. McInnes, L.; Healy, J.; Melville, J. UMAP: Uniform Manifold Approximation and Projection for Dimension Reduction. *arXiv* **2020**, arXiv:1802.03426.

27. Zhang, Y.; Chen, K.; Sloan, S.A.; Bennett, M.L.; Scholze, A.R.; O'Keeffe, S.; Phatnani, H.P.; Guarnieri, P.; Caneda, C.; Ruderisch, N.; et al. An RNA-Sequencing Transcriptome and Splicing Database of Glia, Neurons, and Vascular Cells of the Cerebral Cortex. *J. Neurosci.* **2014**, *34*, 11929–11947. [CrossRef]

28. Love, M.I.; Huber, W.; Anders, S. Moderated Estimation of Fold Change and Dispersion for RNA-Seq Data with DESeq2. *Genome Biol.* **2014**, *15*, 550. [CrossRef]

29. Stuart, T.; Butler, A.; Hoffman, P.; Hafemeister, C.; Papalexi, E.; Mauck, W.M.; Hao, Y.; Stoeckius, M.; Smibert, P.; Satija, R. Comprehensive Integration of Single-Cell Data. *Cell* **2019**, *177*, 1888–1902.e21. [CrossRef]

30. Eden, E.; Navon, R.; Steinfeld, I.; Lipson, D.; Yakhini, Z. GOrilla: A Tool for Discovery and Visualization of Enriched GO Terms in Ranked Gene Lists. *BMC Bioinform.* **2009**, *10*, 48. [CrossRef]

31. Bergen, V.; Lange, M.; Peidli, S.; Wolf, F.A.; Theis, F.J. Generalizing RNA Velocity to Transient Cell States through Dynamical Modeling. *Nat. Biotechnol.* **2020**, *38*, 1408–1414. [CrossRef]

32. Wolf, F.A.; Angerer, P.; Theis, F.J. SCANPY: Large-Scale Single-Cell Gene Expression Data Analysis. *Genome Biol.* **2018**, *19*, 15. [CrossRef]

33. Soneson, C.; Srivastava, A.; Patro, R.; Stadler, M.B. Preprocessing Choices Affect RNA Velocity Results for Droplet ScRNA-Seq Data. *PLoS Comput. Biol.* **2021**, *17*, e1008585. [CrossRef]

34. Wolf, F.A.; Hamey, F.K.; Plass, M.; Solana, J.; Dahlin, J.S.; Göttgens, B.; Rajewsky, N.; Simon, L.; Theis, F.J. PAGA: Graph Abstraction Reconciles Clustering with Trajectory Inference through a Topology Preserving Map of Single Cells. *Genome Biol.* **2019**, *20*, 59. [CrossRef]

35. Gossen, M.; Freundlieb, S.; Bender, G.; Müller, G.; Hillen, W.; Bujard, H. Transcriptional Activation by Tetracyclines in Mammalian Cells. *Science* **1995**, *268*, 1766–1769. [CrossRef]

36. Nectow, A.R.; Nestler, E.J. Viral Tools for Neuroscience. *Nat. Rev. Neurosci.* **2020**, *21*, 669–681. [CrossRef]

37. Sweeney, N.P.; Vink, C.A. The Impact of Lentiviral Vector Genome Size and Producer Cell Genomic to Gag-Pol MRNA Ratios on Packaging Efficiency and Titre. *Mol. Ther. Methods Clin. Dev.* **2021**, *21*, 574–584. [CrossRef] [PubMed]

38. Dodonova, S.O.; Zhu, F.; Dienemann, C.; Taipale, J.; Cramer, P. Nucleosome-Bound SOX2 and SOX11 Structures Elucidate Pioneer Factor Function. *Nature* **2020**, *580*, 669–672. [CrossRef] [PubMed]

39. Hoffmann, D.; Schott, J.W.; Geis, F.K.; Lange, L.; Müller, F.-J.; Lenz, D.; Zychlinski, D.; Steinemann, D.; Morgan, M.; Moritz, T.; et al. Detailed Comparison of Retroviral Vectors and Promoter Configurations for Stable and High Transgene Expression in Human Induced Pluripotent Stem Cells. *Gene Ther.* **2017**, *24*, 298–307. [CrossRef] [PubMed]

40. Liu, Z.; Chen, O.; Wall, J.B.J.; Zheng, M.; Zhou, Y.; Wang, L.; Ruth Vaseghi, H.; Qian, L.; Liu, J. Systematic Comparison of 2A Peptides for Cloning Multi-Genes in a Polycistronic Vector. *Sci. Rep.* **2017**, *7*, 2193. [CrossRef]

41. Tian, R.; Gachechiladze, M.A.; Ludwig, C.H.; Laurie, M.T.; Hong, J.Y.; Nathaniel, D.; Prabhu, A.V.; Fernandopulle, M.S.; Patel, R.; Abshari, M.; et al. CRISPR Interference-Based Platform for Multimodal Genetic Screens in Human IPSC-Derived Neurons. *Neuron* **2019**, *104*, 239–255.e12. [CrossRef]

42. Herholt, A.; Galinski, S.; Geyer, P.E.; Rossner, M.J.; Wehr, M.C. Multiparametric Assays for Accelerating Early Drug Discovery. *Trends Pharmacol. Sci.* **2020**, *41*, 318–335. [CrossRef]

43. Matjusaitis, M.; Wagstaff, L.J.; Martella, A.; Baranowski, B.; Blin, C.; Gogolok, S.; Williams, A.; Pollard, S.M. Reprogramming of Fibroblasts to Oligodendrocyte Progenitor-like Cells Using CRISPR/Cas9-Based Synthetic Transcription Factors. *Stem Cell Rep.* **2019**, *13*, 1053–1067. [CrossRef]

44. Wang, S.; Bates, J.; Li, X.; Schanz, S.; Chandler-Militello, D.; Levine, C.; Maherali, N.; Studer, L.; Hochedlinger, K.; Windrem, M.; et al. Human IPSC-Derived Oligodendrocyte Progenitor Cells Can Myelinate and Rescue a Mouse Model of Congenital Hypomyelination. *Cell Stem Cell* **2013**, *12*, 252–264. [CrossRef] [PubMed]

45. Douvaras, P.; Wang, J.; Zimmer, M.; Hanchuk, S.; O'Bara, M.A.; Sadiq, S.; Sim, F.J.; Goldman, J.; Fossati, V. Efficient Generation of Myelinating Oligodendrocytes from Primary Progressive Multiple Sclerosis Patients by Induced Pluripotent Stem Cells. *Stem Cell Rep.* **2014**, *3*, 250–259. [CrossRef] [PubMed]

46. Chamling, X.; Kallman, A.; Fang, W.; Berlinicke, C.A.; Mertz, J.L.; Devkota, P.; Pantoja, I.E.M.; Smith, M.D.; Ji, Z.; Chang, C.; et al. Single-Cell Transcriptomic Reveals Molecular Diversity and Developmental Heterogeneity of Human Stem Cell-Derived Oligodendrocyte Lineage Cells. *Nat. Commun.* **2021**, *12*, 652. [CrossRef] [PubMed]

47. Elbaz, B.; Popko, B. Molecular Control of Oligodendrocyte Development. *Trends Neurosci.* **2019**, *42*, 263–277. [CrossRef]

48. Windrem, M.S.; Osipovitch, M.; Liu, Z.; Bates, J.; Chandler-Militello, D.; Zou, L.; Munir, J.; Schanz, S.; McCoy, K.; Miller, R.H.; et al. Human IPSC Glial Mouse Chimeras Reveal Glial Contributions to Schizophrenia. *Cell Stem Cell* **2017**, *21*, 195–208.e6. [CrossRef]

Inventory of Supplemental Information

- Supplemental Figures
- Supplemental Tables
- Supplemental References
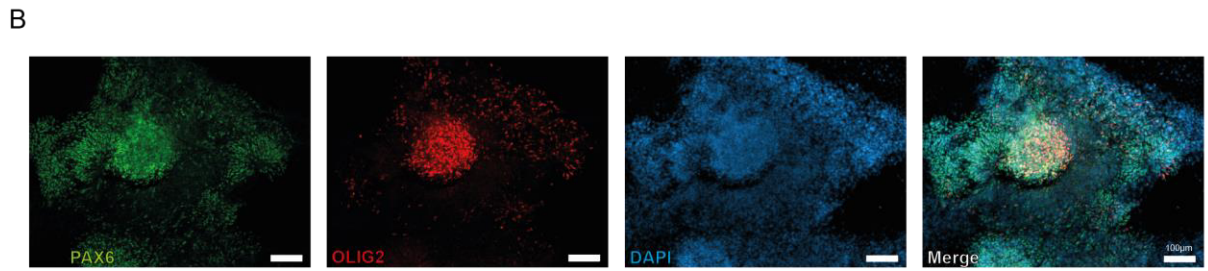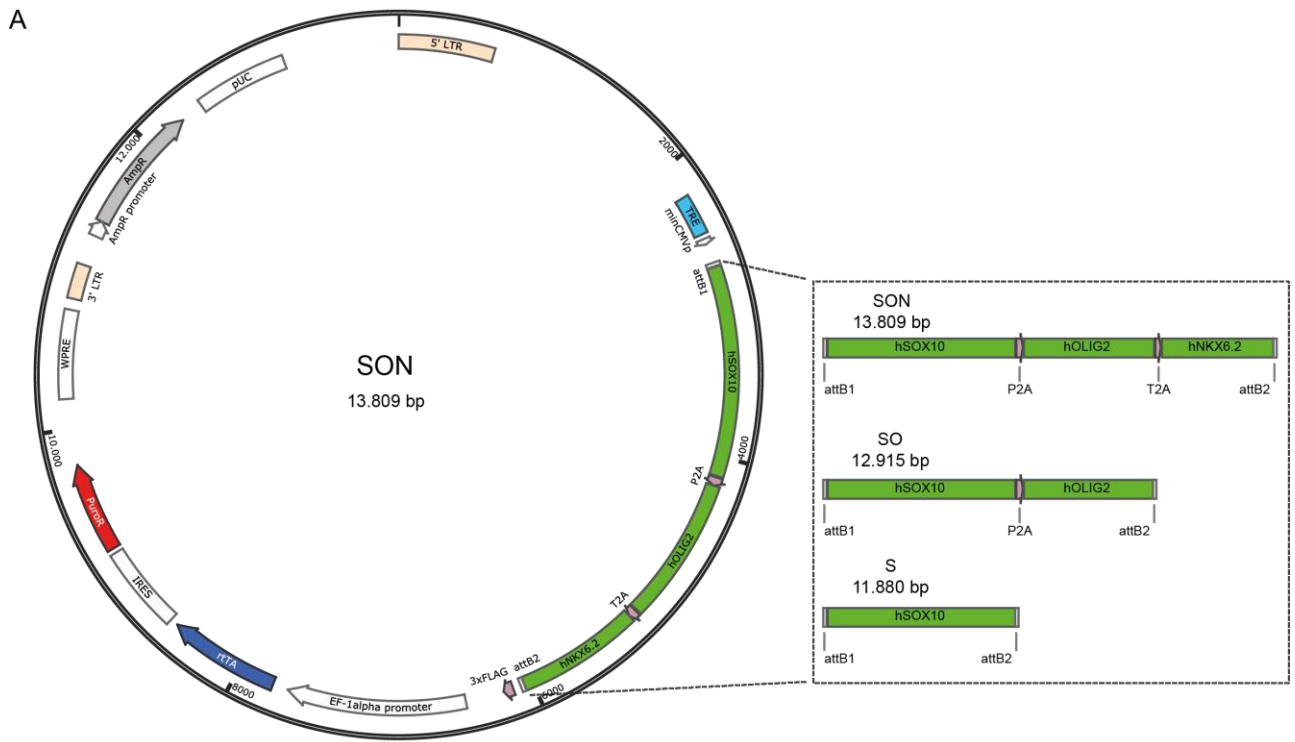
Figure S1. Detailed illustration of applied lentiviral construct and neural induction. Related to Figure 1.

(A) Schematic overview of the applied lentiviral vector containing constitutive expression units for the reversed tetracycline transactivator (rtTA) and puromycin N-acetyl-transferase (PuroR) and a tetracycline response element (TRE) for the doxycycline-dependent overexpression of the TFs. Magnification illustrates the different TFs combinations using SON, SO and S that are linked by the self-cleavage sites P2A and T2A. Plasmid maps of the constructs (S, SO, SON) are available in the supplemental files.

(B) Representative images of PAX6+ (green), OLIG2+ (red) neural precursor cells (NPC) 12 days after neural induction. Scale bar: 100μm.

2

A

| hiPSC donor 1 | hiPSC donor 2 | hiPSC donor 3 |
| hiPSC donor 4 | hiPSC donor 5 | hiPSC donor 6 |

O4
DAPI
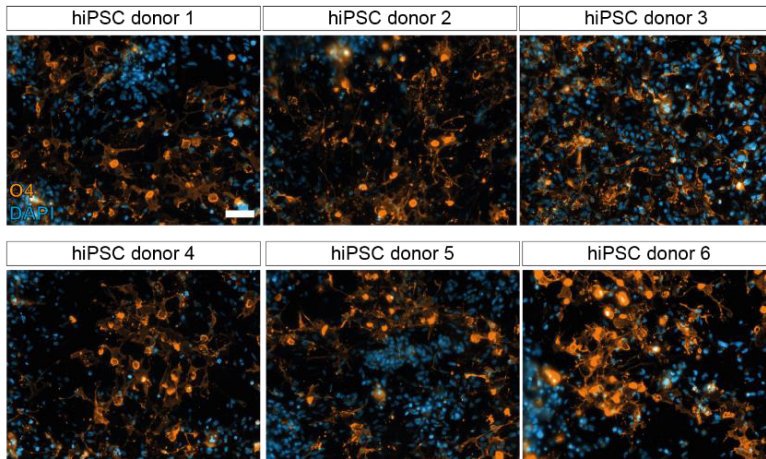
B
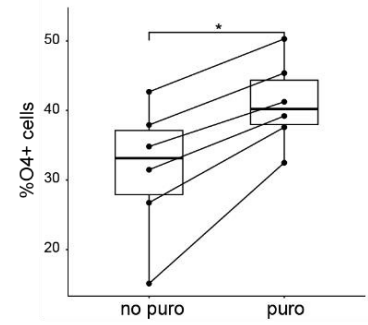
14

15 **Figure S2. SON-directed differentiation from different hiPSC lines and effect of intermediate selection.**

16 **Related to Figure 2.**

17 (A) Illustration of O4$^+$ cells (orange) from six different hiPSC lines of independent donors 10days of SON-

18   directed differentiation with intermediate puromycin selection (puro). Scale bar: 50µm.

19 (B) Quantification of O4$^+$ cells after 10 days of SON-directed differentiation with and without intermediate

20   puromycin selection between Day+2 and Day+4. 13 analysed fields of view for each condition, Dots

21   correspond to mean percentage of O4$^+$ cells per condition. Lines connects both conditions from one hiPSC

22   cell line. Statistical analysis by Wilcoxon signed-rank test, *p < 0.05.

23
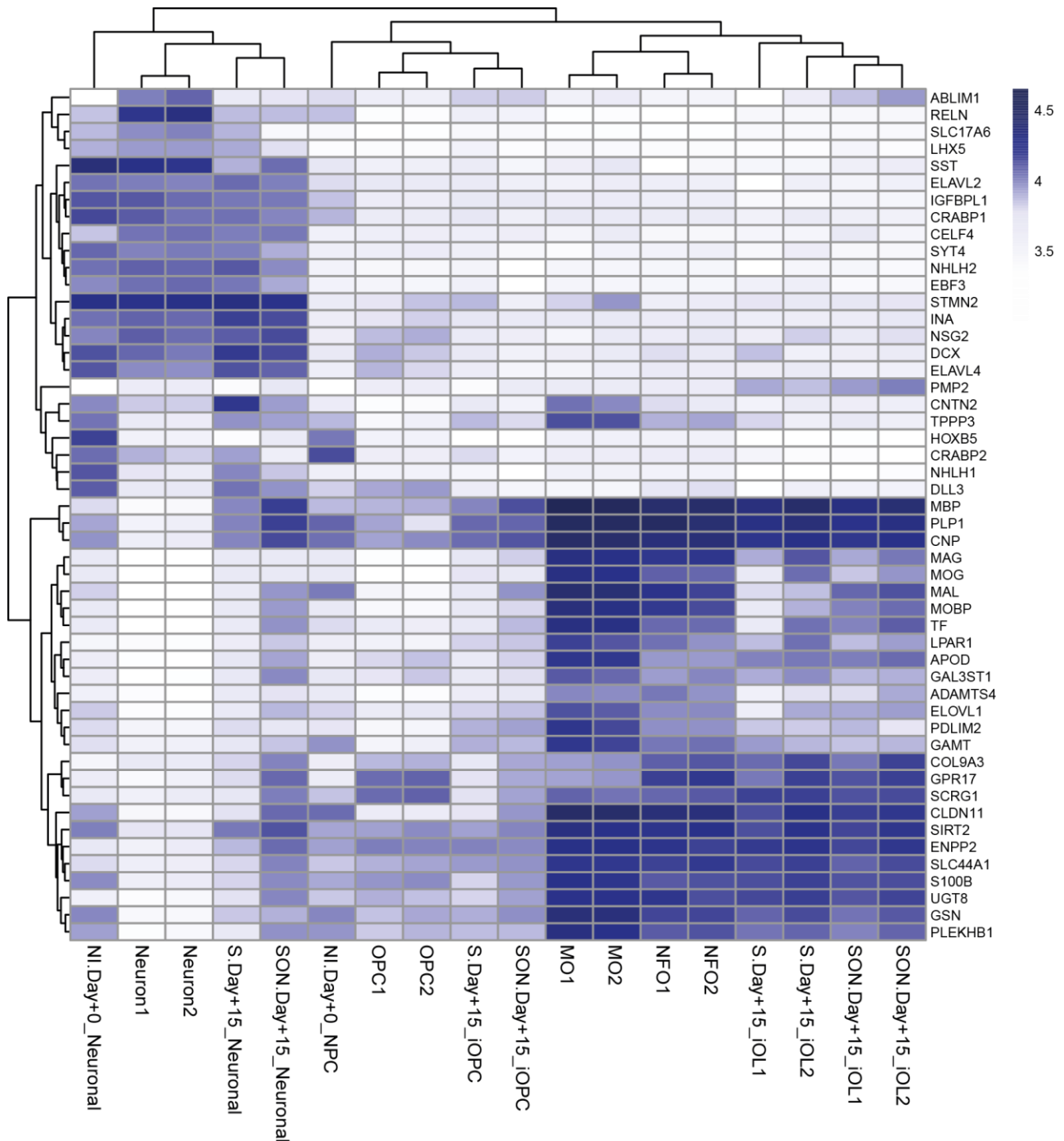
Figure S3. 50 most variable genes from co-clustering of iOPCs and iOLs with primary cells. Related to Figure 3.

Comparison of transcriptomes of hiPSC-derived cells with primary murine cells (Zhang et al., 2014). Expression heatmap of the 50 most variable genes in the analysis. Unsupervised hierarchical clustering based on Manhattan distances was performed on samples and genes and used for sorting of the heatmap. Abbreviations for primary reference samples: MO, myelinating oligodendrocytes; NFO, newly formed oligodendrocytes; OPC, oligodendrocyte precursor cells.
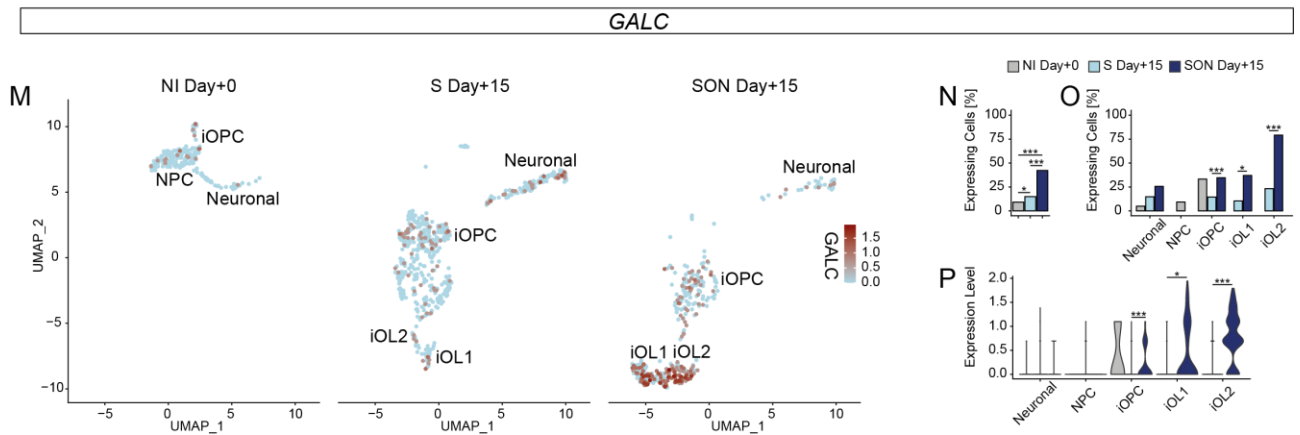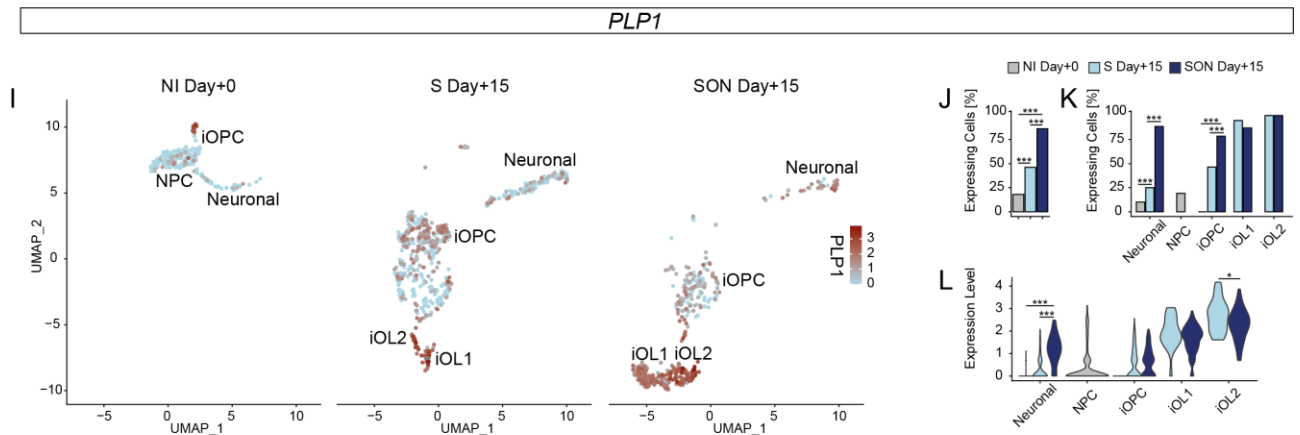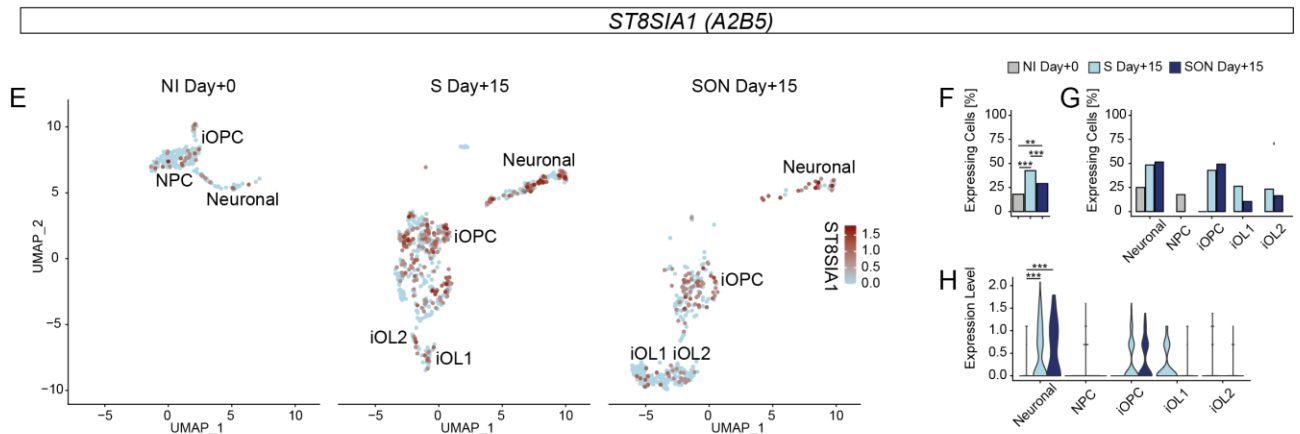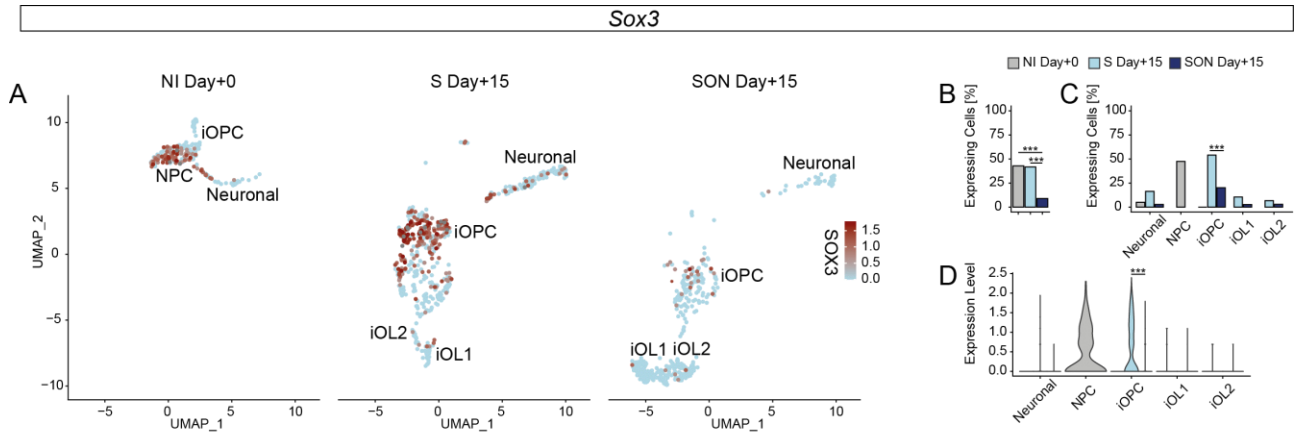
Figure S4. Illustration of extended marker gene expression from scRNAseq. Related to Figure 4.

(**A, E, I, M**) UMAP representation of selected marker genes (**A**) *SOX3*, (**E**) *ST8SIA1* (also known as A2B5), (**I**) *PLP1*, (**M**) *GALC* from scRNAseq of baseline sample after neural induction (NI Day+0, n = 217 cells, one independent experiment) and samples after 15 days of directed differentiation by SOX10 (S Day+15, n = 577 cells, one independent experiment) and SOX10-OLIG2-NKX6.2 (SON Day+15, n = 400 cells, one independent experiment) with annotated cell clusters of neural precursor cells (NPC), neuronal cells, induced oligodendrocyte precursor cells (iOPCs), induced oligodendrocyte cluster 1 (iOL1) and induced oligodendrocyte cluster 2 (iOL2). Expression value per cell plotted according to the colour intensity of the respective scale bar as indicated.

(**B, F, J, N**) Bar plots illustrate the abundance of expressing cells for each sample. * (p-value < 0.05), ** (p-value < 0.01), *** (p-value < 0.001) based on Fisher's exact tests (details provided in Table S5).

(**C, G, K, O**) Bar plots illustrate the abundance of expressing cells for each cluster split by sample. * (p-value < 0.05), ** (p-value < 0.01), *** (p-value < 0.001) based on Fisher's exact tests (details provided in Table S5).

(**D, H, L, P**) Violin plots of the normalized expression per sample within the respective cell type cluster. * (p-value < 0.05), ** (p-value < 0.01), *** (p-value < 0.001) based on Wilcoxon signed-rank test (details provided in Table S7).

6

A

B

C

D

Figure S5. Ratio of unspliced/spliced mRNA variants and sample-independent main differentiation trajectory analysis. Related to Figure 5.

(A) Overall ratio of spliced vs. unspliced mRNA

(B) Cluster-dependent ratio of spliced vs. unspliced mRNA

(C) Sample-dependent ratio of spliced vs. unspliced mRNA

(D) Sample independent main differentiation trajectory analysis using Partition-based graph abstraction (PAGA) to illustrate cluster-to-cluster transitions within the S- and SON-promoted oligodendroglial differentiation.
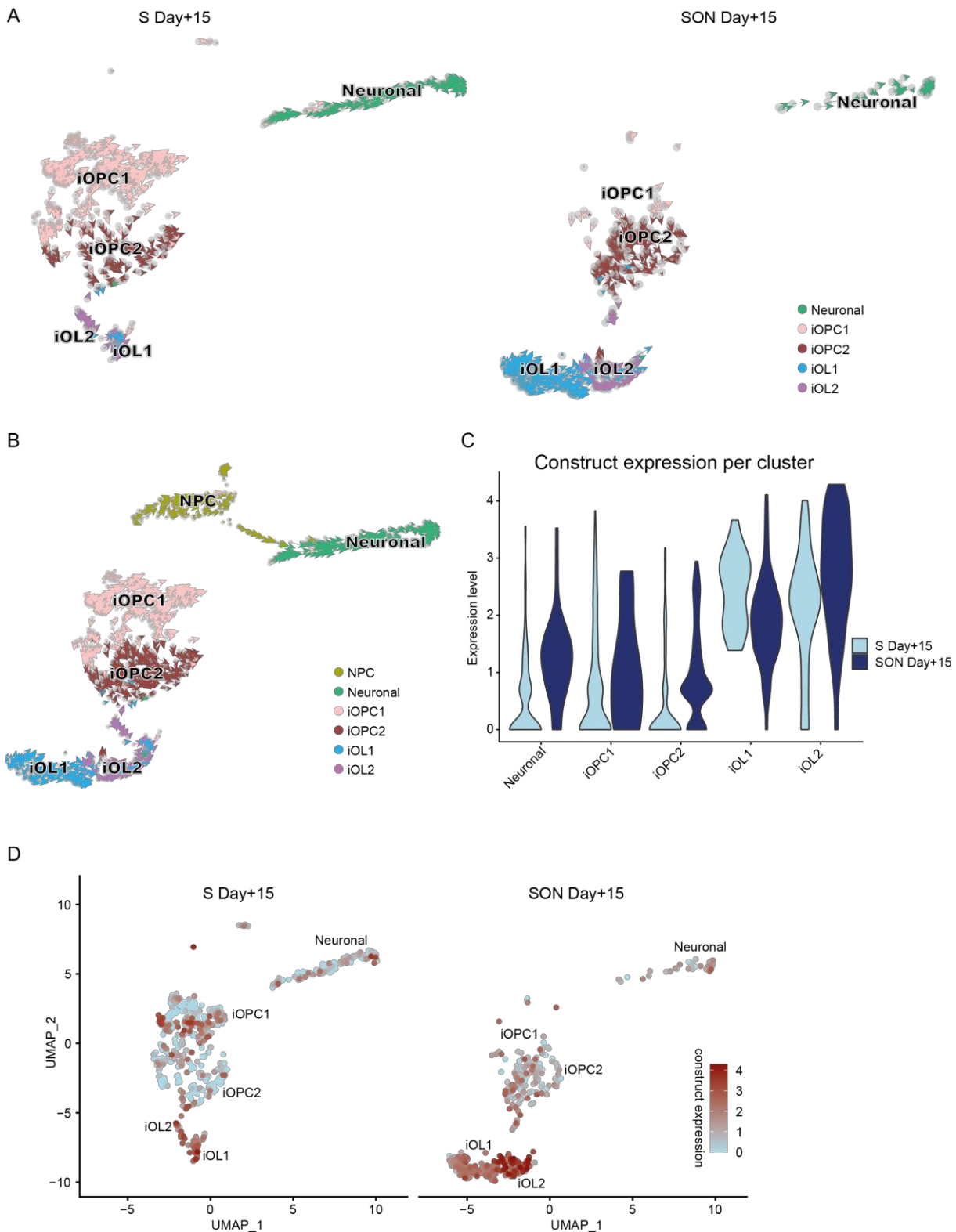
Figure S6. Differences of RNAvelocity between iOPC1 and iOPC2 are not based on different expression of directing TFs. Related to Figure 6.

(A) RNA velocity vectors projected on the single-cell UMAP-based dimension plot, indicating direction and speed of individual cells, including iOPC1 and iOPC2, in transcriptional space.

(B) Pooled Illustration of scVelocity of NI-, S- and SON-derived samples (NI Day+0, S Day+15, SON Day +15) including iOPC1 and iOPC2.

(C) Violin plots of normalized construct expression in Neuronal, iOPC1, iOPC2, iOL1 and iOL2 clusters split by S- and SON-sample (S Day+15, SON Day +15).

72   (D) Illustration of lentiviral construct expression from scRNAseq with UMAP dimension plot for S Day+15 and

73   SON Day+15 with the normalized expression level indicated by colour. Related to Figure S6C.

74
75 **Table S1. hiPSC lines in this study.**

hiPSC cell line	ID LMU	Donor age	Donor sex	Passage
hiPSC donor 0	PSYLMUi001-A	27	male	P17
hiPSC donor 1	PSYLMUi002-A	24	male	P18
hiPSC donor 2	PSYLMUi003-A	19	male	P17
hiPSC donor 3	PSYLMUi004-A	31	male	P18
hiPSC donor 4	PSYLMUi006-A	52	male	P21
hiPSC donor 5	PSYLMUi023-A	47	male	P19
hiPSC donor 6	PSYLMUi027-A	53	male	P15

76

77

78 **Table S2. Media, media supplements for cell cultivation and coating.**

Item	Supplier	Cat.No.
iPS-Brew	Miltenyi Biotec	130-104-368
mTeSR1	Stem Cell	85850
ProFreeze CDM	Lonza	BEBP12-769E
DMEM/F-12 with GlutaMAX™ supplement	ThermoFisherScientific	31331028
N-2 Supplement (100x)	ThermoFisherScientific	17502048
B-27® Supplement (50X), without vitamin A	ThermoFisherScientific	12587010
Non-Essential Amino Acids Solution (NEAA)	ThermoFisherScientific	11140035
ß-Mercaptoethanol	ThermoFisherScientific	21985023
Insulin solution human	Sigma	I9278-5ML
SB431542	StemCell	72232
LDN193189 (HCl) - superstock	StemCell	72147
Retinoic acid (RA)	Sigma	R2625-50MG
SAG	Millipore	566660
PDGFaa	PeproTech	100-13A
IGF1	PeproTech	100-11
HGF	PeproTech	100-39
NT3	Peprotech	AF-450-03
Biotin	Sigma	B4639-100MG
dbcAMP	Sigma	D0627-250MG
T3	Sigma	T6397-100MG
Doxycycline	Clontech	NC0424034
Puromycin	ThermoFisherScientific	A1113803
ROCK-Inhibitor (Y-27632)	Selleckchem	S 1049
RevitaCell	ThermoFisherScientific	A2644501
Vitronectin	ThermoFisherScientific	A14700
Matrigel	BD Bioscience	354277
Poly-L-ornithine solution	Sigma	P4957
Laminin (mouse)	Sigma	T6397-100MG
EDTA	ThermoFisherScientific	15575-020
Accutase	Sigma	A6964
Anti-O4 microbeads	Miltenyi Biotec	130-096-670

79

80 **Table S3. List of primary antibodies for immunostainings.** Related to Figure 1, 2, 6, S1, S2.

Antigen	Dilution	Supplier	Cat.No.	Serotype	Host
O4	1:200	R&D Systems	MAB1326	IgM, monoclonal	mouse
MBP	1:50	Millipore	AB9348	IgG, polyclonal	chicken
MBP	1:200	Abcam	ab40390	IgG, polyclonal	rat

Pax 6	1:500	Millipore	AB2237	IgG, polyclonal	rabbit
Olig2 (H-10)	1:100	Santa Cruz	sc-515947	IgG, monoclonal	mouse
Flag-M2	1:100	Sigma	3165	IgG, monoclonal	mouse

Table S4: Abundance of cell clusters, gene marker expressing cells per samples and cluster. Provided separately as Excel file. Related to Figure 3, 4 and S4. Provided separately as Excel file.

Table S5: Statistical analysis of cell clusters abundance per sample, abundance of gene expressing cells by sample and abundance of gene expressing cells per cluster split by sample. Related to Figure 3, 4 and S4. Provided separately as Excel file.

Table S6: Average expression of cell clusters. Related to Figure 3, 4 and S4. Provided separately as Excel file.

Table S7: Statistical analysis of normalized gene expression by cell cluster and by cell cluster split by sample. Related to Figure 3, 4 and S4. Provided separately as Excel file.

Table S8: Differential gene expression between iOPC1 and iOPC2. Related to Figure 6. Provided separately as Excel file.

Table S9: Hypergeometric gene ontology term enrichment analysis of iOPC1 and iOPC2. Related to Figure 6. Provided separately as Excel file.

Supplemental References

Zhang, Y., Chen, K., Sloan, S.A., Bennett, M.L., Scholze, A.R., O'Keeffe, S., Phatnani, H.P., Guarnieri, P., Caneda, C., Ruderisch, N., et al. (2014). An RNA-sequencing transcriptome and splicing database of glia, neurons, and vascular cells of the cerebral cortex. J. Neurosci. Off. J. Soc. Neurosci. *34*, 11929–11947.

References

Bernstein, H. G., Steiner, J., Guest, P. C., Dobrowolny, H., & Bogerts, B. (2015). Glial cells as key players in schizophrenia pathology: recent insights and concepts of therapy. *Schizophr Res, 161*(1), 4-18. doi:10.1016/j.schres.2014.03.035

Brandl, F., Avram, M., Weise, B., Shang, J., Simões, B., Bertram, T., . . . Sorg, C. (2019). Specific Substantial Dysconnectivity in Schizophrenia: A Transdiagnostic Multimodal Meta-analysis of Resting-State Functional and Structural Magnetic Resonance Imaging Studies. *Biological Psychiatry, 85*(7), 573-583. doi:10.1016/j.biopsych.2018.12.003

Brisch, R., Saniotis, A., Wolf, R., Bielau, H., Bernstein, H. G., Steiner, J., . . . Gos, T. (2014). The role of dopamine in schizophrenia from a neurobiological and evolutionary perspective: old fashioned, but still in vogue. *Front Psychiatry, 5*, 47. doi:10.3389/fpsyt.2014.00047

Cassoli, J. S., Guest, P. C., Malchow, B., Schmitt, A., Falkai, P., & Martins-de-Souza, D. (2015). Disturbed macro-connectivity in schizophrenia linked to oligodendrocyte dysfunction: from structural findings to molecules. *NPJ Schizophr, 1*, 15034. doi:10.1038/npjschz.2015.34

Chang, E. H., Argyelan, M., Aggarwal, M., Chandon, T. S., Karlsgodt, K. H., Mori, S., & Malhotra, A. K. (2017). Diffusion tensor imaging measures of white matter compared to myelin basic protein immunofluorescence in tissue cleared intact brains. *Data Brief, 10*, 438-443. doi:10.1016/j.dib.2016.12.018

Duncan, L. E., Holmans, P. A., Lee, P. H., O'Dushlaine, C. T., Kirby, A. W., Smoller, J. W., . . . Cohen, B. M. (2014). Pathway analyses implicate glial cells in schizophrenia. *PLoS One, 9*(2), e89441. doi:10.1371/journal.pone.0089441

Ehrlich, M., Mozafari, S., Glatza, M., Starost, L., Velychko, S., Hallmann, A. L., . . . Kuhlmann, T. (2017). Rapid and efficient generation of oligodendrocytes from human induced pluripotent stem cells using transcription factors. *Proc Natl Acad Sci U S A, 114*(11), E2243-E2252. doi:10.1073/pnas.1614412114

Falkai, P., Rossner, M. J., Schulze, T. G., Hasan, A., Brzozka, M. M., Malchow, B., . . . Schmitt, A. (2015). Kraepelin revisited: schizophrenia from degeneration to failed regeneration. *Mol Psychiatry, 20*(6), 671-676. doi:10.1038/mp.2015.35

Falkai, P., Schmitt, A., & Cannon, T. D. (2011). Pathophysiology of Schizophrenia. In H. Herrman & W. Gaebel (Eds.), *Schizophrenia* (pp. 31-65): Wiley-Blackwell.

Fields, R. D. (2008). White matter in learning, cognition and psychiatric disorders. *Trends Neurosci, 31*(7), 361-370. doi:10.1016/j.tins.2008.04.001

Fields, R. D., & Dutta, D. J. (2019). Treadmilling Model for Plasticity of the Myelin Sheath. *Trends Neurosci.* doi:10.1016/j.tins.2019.04.002

Garcia-Leon, J. A., Kumar, M., Boon, R., Chau, D., One, J., Wolfs, E., . . . Verfaillie, C. M. (2018). SOX10 Single Transcription Factor-Based Fast and Efficient Generation of Oligodendrocytes from Human Pluripotent Stem Cells. *Stem Cell Reports, 10*(2), 655-672. doi:10.1016/j.stemcr.2017.12.014

Goff, D. C., Hill, M., & Barch, D. (2011). The treatment of cognitive impairment in schizophrenia. *Pharmacol Biochem Behav, 99*(2), 245-253. doi:10.1016/j.pbb.2010.11.009

Goldman, S. A., & Kuypers, N. J. (2015). How to make an oligodendrocyte. *Development, 142*(23), 3983-3995. doi:10.1242/dev.126409

Gottesman, II, & Shields, J. (1967). A polygenic theory of schizophrenia. *Proc Natl Acad Sci U S A, 58*(1), 199-205. doi:10.1073/pnas.58.1.199

Green, M. F., Horan, W. P., & Lee, J. (2019). Nonsocial and social cognition in schizophrenia: current evidence and future directions. *World Psychiatry, 18*(2), 146-161. doi:10.1002/wps.20624

Haijma, S. V., Van Haren, N., Cahn, W., Koolschijn, P. C. M. P., Hulshoff Pol, H. E., & Kahn, R. S. (2013). Brain volumes in schizophrenia: a meta-analysis in over 18 000 subjects. *Schizophrenia Bulletin, 39*(5), 1129-1138. doi:10.1093/schbul/sbs118

Hilker, R., Helenius, D., Fagerlund, B., Skytthe, A., Christensen, K., Werge, T. M., . . . Glenthoj, B. (2017). Heritability of Schizophrenia and Schizophrenia Spectrum Based on the Nationwide Danish Twin Register. *Biol Psychiatry*. doi:10.1016/j.biopsych.2017.08.017

James, S. L., Abate, D., Abate, K. H., Abay, S. M., Abbafati, C., Abbasi, N., . . . Murray, C. J. L. (2018). Global, regional, and national incidence, prevalence, and years lived with disability for 354 diseases and injuries for 195 countries and territories, 1990–2017: a systematic analysis for the Global Burden of Disease Study 2017. *The Lancet, 392*(10159), 1789-1858. doi:10.1016/s0140-6736(18)32279-7

Kelly, S., Jahanshad, N., Zalesky, A., Kochunov, P., Agartz, I., Alloza, C., . . . Donohoe, G. (2018). Widespread white matter microstructural differences in schizophrenia across 4322 individuals: results from the ENIGMA Schizophrenia DTI Working Group. *Mol Psychiatry, 23*(5), 1261-1269. doi:10.1038/mp.2017.170

Klauser, P., Baker, S. T., Cropley, V. L., Bousman, C., Fornito, A., Cocchi, L., . . . Zalesky, A. (2017). White Matter Disruptions in Schizophrenia Are Spatially Widespread and Topologically Converge on Brain Network Hubs. *Schizophrenia Bulletin, 43*(2), 425-435. doi:10.1093/schbul/sbw100

Kraepelin, E. (1899). *Psychiatrie: ein Lehrbuch für Studirende und Aertze [Psychiatry: A Textbook for Students and Doctors]* (6th edn ed.). Leipzig: JA Barth.

Kristensen, T. D., Mandl, R. C. W., Raghava, J. M., Jessen, K., Jepsen, J. R. M., Fagerlund, B., . . . Ebdrup, B. H. (2019). Widespread higher fractional anisotropy associates to better cognitive functions in individuals at ultra-high risk for psychosis. *Hum Brain Mapp*. doi:10.1002/hbm.24765

Kuroki, N., Kubicki, M., Nestor, P. G., Salisbury, D. F., Park, H. J., Levitt, J. J., . . . Shenton, M. E. (2006). Fornix integrity and hippocampal volume in male schizophrenic patients. *Biol Psychiatry, 60*(1), 22-31. doi:10.1016/j.biopsych.2005.09.021

Li, T., Wang, Q., Zhang, J., Rolls, E. T., Yang, W., Palaniyappan, L., . . . Feng, J. (2017). Brain-Wide Analysis of Functional Connectivity in First-Episode and Chronic Stages of Schizophrenia. *Schizophrenia Bulletin, 43*(2), 436-448. doi:10.1093/schbul/sbw099

Lim, K. O., Ardekani, B. A., Nierenberg, J., Butler, P. D., Javitt, D. C., & Hoptman, M. J. (2006). Voxelwise correlational analyses of white matter integrity in multiple cognitive domains in schizophrenia. *Am J Psychiatry, 163*(11), 2008-2010. doi:10.1176/ajp.2006.163.11.2008

Lopez Juarez, A., He, D., & Richard Lu, Q. (2016). Oligodendrocyte progenitor programming and reprogramming: Toward myelin regeneration. *Brain Res, 1638*(Pt B), 209-220. doi:10.1016/j.brainres.2015.10.051

McCutcheon, R. A., Reis Marques, T., & Howes, O. D. (2020). Schizophrenia-An Overview. *JAMA Psychiatry, 77*(2), 201-210. doi:10.1001/jamapsychiatry.2019.3360

McGrath, J., Saha, S., Chant, D., & Welham, J. (2008). Schizophrenia: a concise overview of incidence, prevalence, and mortality. *Epidemiol Rev, 30*, 67-76. doi:10.1093/epirev/mxn001

McPhie, D. L., Nehme, R., Ravichandran, C., Babb, S. M., Ghosh, S. D., Staskus, A., . . . Cohen, B. M. (2018). Oligodendrocyte differentiation of induced pluripotent stem cells derived from subjects with schizophrenias implicate abnormalities in development. *Transl Psychiatry, 8*(1), 230. doi:10.1038/s41398-018-0284-6

Micu, I., Plemel, J. R., Caprariello, A. V., Nave, K. A., & Stys, P. K. (2018). Axo-myelinic neurotransmission: a novel mode of cell signalling in the central nervous system. *Nat Rev Neurosci, 19*(1), 49-58. doi:10.1038/nrn.2017.128

Nave, K. A. (2010). Myelination and support of axonal integrity by glia. *Nature, 468*(7321), 244-252. doi:10.1038/nature09614

Oh, Y., & Jang, J. (2019). Directed Differentiation of Pluripotent Stem Cells by Transcription Factors. *Mol Cells, 42*(3), 200-209. doi:10.14348/molcells.2019.2439

Pardinas, A. F., Holmans, P., Pocklington, A. J., Escott-Price, V., Ripke, S., Carrera, N., . . . Consortium, C. (2018). Common schizophrenia alleles are enriched in mutation-intolerant genes and in regions under strong background selection. *Nat Genet*. doi:10.1038/s41588-018-0059-2

Pawlowski, M., Ortmann, D., Bertero, A., Tavares, J. M., Pedersen, R. A., Vallier, L., & Kotter, M. R. N. (2017). Inducible and Deterministic Forward Programming of Human Pluripotent Stem Cells into Neurons, Skeletal Myocytes, and Oligodendrocytes. *Stem Cell Reports, 8*(4), 803-812. doi:10.1016/j.stemcr.2017.02.016

Prytkova, I., & Brennand, K. J. (2017). Prospects for Modeling Abnormal Neuronal Function in Schizophrenia Using Human Induced Pluripotent Stem Cells. *Front Cell Neurosci, 11*, 360. doi:10.3389/fncel.2017.00360

Raabe, F. J., Galinski, S., Papiol, S., Falkai, P. G., Schmitt, A., & Rossner, M. J. (2018). Studying and modulating schizophrenia-associated dysfunctions of oligodendrocytes with patient-specific cell systems. *NPJ Schizophr, 4*(1), 23. doi:10.1038/s41537-018-0066-4

Raabe, F. J., Slapakova, L., Rossner, M. J., Cantuti-Castelvetri, L., Simons, M., Falkai, P. G., & Schmitt, A. (2019). Oligodendrocytes as A New Therapeutic Target in Schizophrenia: From Histopathological Findings to Neuron-Oligodendrocyte Interaction. *Cells, 8*(12). doi:10.3390/cells8121496

Raabe, F. J., Stephan, M., Waldeck, J. B., Huber, V., Demetriou, D., Kannaiyan, N., . . . Rossner, M. J. (2022). Expression of Lineage Transcription Factors Identifies Differences in Transition States of Induced Human Oligodendrocyte Differentiation. *Cells, 11*(2). doi:10.3390/cells11020241

Rasanen, N., Tiihonen, J., Koskuvi, M., Lehtonen, S., & Koistinaho, J. (2022). The iPSC perspective on schizophrenia. *Trends Neurosci, 45*(1), 8-26. doi:10.1016/j.tins.2021.11.002

Ripke, S., Walters, J. T. R., & O'Donovan, M. C. (2020). doi:10.1101/2020.09.12.20192922

Schizophrenia Working Group of the Psychiatric Genomics, C. (2014). Biological insights from 108 schizophrenia-associated genetic loci. *Nature, 511*(7510), 421-427. doi:10.1038/nature13595

Schmitt, A., Hasan, A., Gruber, O., & Falkai, P. (2011). Schizophrenia as a disorder of disconnectivity. *Eur Arch Psychiatry Clin Neurosci, 261 Suppl 2*(2), S150-154. doi:10.1007/s00406-011-0242-2

Simons, M., & Nave, K. A. (2015). Oligodendrocytes: Myelination and Axonal Support. *Cold Spring Harb Perspect Biol, 8*(1), a020479. doi:10.1101/cshperspect.a020479

Skene, N. G., Bryois, J., Bakken, T. E., Breen, G., Crowley, J. J., Gaspar, H. A., . . . Hjerling-Leffler, J. (2018). Genetic identification of brain cell types underlying schizophrenia. *Nat Genet, 50*(6), 825-833. doi:10.1038/s41588-018-0129-5

Soliman, M. A., Aboharb, F., Zeltner, N., & Studer, L. (2017). Pluripotent stem cells in neuropsychiatric disorders. *Mol Psychiatry, 22*(9), 1241-1249. doi:10.1038/mp.2017.40

Takahashi, K., & Yamanaka, S. (2006). Induction of pluripotent stem cells from mouse embryonic and adult fibroblast cultures by defined factors. *Cell, 126*(4), 663-676. doi:10.1016/j.cell.2006.07.024

Tansey, K. E., & Hill, M. J. (2018). Enrichment of schizophrenia heritability in both neuronal and glia cell regulatory elements. *Transl Psychiatry, 8*(1), 7. doi:10.1038/s41398-017-0053-y

The Network Pathway Analysis Subgroup of the Psychiatric Genomics, C. (2015). Psychiatric genome-wide association study analyses implicate neuronal, immune and histone pathways. *Nat Neurosci, 18*(2), 199-209. doi:10.1038/nn.3922

van Erp, T. G. M., Walton, E., Hibar, D. P., Schmaal, L., Jiang, W., Glahn, D. C., . . . Turner, J. A. (2018). Cortical Brain Abnormalities in 4474 Individuals With Schizophrenia and 5098

Control Subjects via the Enhancing Neuro Imaging Genetics Through Meta Analysis (ENIGMA) Consortium. *Biological Psychiatry, 84*(9), 644-654. doi:10.1016/j.biopsych.2018.04.023

Voineskos, A. N., Felsky, D., Kovacevic, N., Tiwari, A. K., Zai, C., Chakravarty, M. M., . . . Kennedy, J. L. (2013). Oligodendrocyte genes, white matter tract integrity, and cognition in schizophrenia. *Cereb Cortex, 23*(9), 2044-2057. doi:10.1093/cercor/bhs188

Vos, T., Lim, S. S., Abbafati, C., Abbas, K. M., Abbasi, M., Abbasifard, M., . . . Murray, C. J. L. (2020). Global burden of 369 diseases and injuries in 204 countries and territories, 1990–2019: a systematic analysis for the Global Burden of Disease Study 2019. *The Lancet, 396*(10258), 1204-1222. doi:10.1016/s0140-6736(20)30925-9

Wang, D., Liu, S., Warrell, J., Won, H., Shi, X., Navarro, F. C. P., . . . Gerstein, M. B. (2018). Comprehensive functional genomic resource and integrative model for the human brain. *Science (New York, N.Y.), 362*(6420), eaat8464. doi:10.1126/science.aat8464

Windrem, M. S., Osipovitch, M., Liu, Z., Bates, J., Chandler-Militello, D., Zou, L., . . . Goldman, S. A. (2017). Human iPSC Glial Mouse Chimeras Reveal Glial Contributions to Schizophrenia. *Cell Stem Cell, 21*(2), 195-208 e196. doi:10.1016/j.stem.2017.06.012

Yamada, S., Takahashi, S., Malchow, B., Papazova, I., Stocklein, S., Ertl-Wagner, B., . . . Keeser, D. (2021). Cognitive and functional deficits are associated with white matter abnormalities in two independent cohorts of patients with schizophrenia. *Eur Arch Psychiatry Clin Neurosci*. doi:10.1007/s00406-021-01363-8

Appendix A: Review Paper

Studying and modulating schizophrenia-associated dysfunctions of oligodendrocytes with patient-specific cell systems

Florian J. Raabe[1,2,*], Sabrina Galinski[1], Sergi Papiol[1,3], Peter G. Falkai[1], Andrea Schmitt[1,4], Moritz J. Rossner[1,*]

[1] Molecular and Behavioural Neurobiology, Department of Psychiatry and Psychotherapy, University Hospital, LMU Munich, Germany

[2] International Max Planck Research School for Translational Psychiatry (IMPRS-TP), Munich, Germany

[3] Institute of Psychiatric Phenomics and Genomics (IPPG), University Hospital, LMU Munich, Germany

[4] Laboratory of Neuroscience (LIM27), Institute of Psychiatry, University of Sao Paulo, Sao Paulo, Brazil

*Correspondence:

Florian J. Raabe (florian.raabe@med.uni-muenchen.de) or

Moritz J. Rossner (moritz.rossner@med.uni-muenchen.de)

REVIEW ARTICLE   OPEN

Studying and modulating schizophrenia-associated dysfunctions of oligodendrocytes with patient-specific cell systems

Florian J. Raabe[1,2], Sabrina Galinski[1], Sergi Papiol [1,3], Peter G. Falkai[1], Andrea Schmitt[1,4] and Moritz J. Rossner[1]

Postmortem studies in patients with schizophrenia (SCZ) have revealed deficits in myelination, abnormalities in myelin gene expression and altered numbers of oligodendrocytes in the brain. However, gaining mechanistic insight into oligodendrocyte (OL) dysfunction and its contribution to SCZ has been challenging because of technical hurdles. The advent of individual patient-derived human-induced pluripotent stem cells (hiPSCs), combined with the generation of in principle any neuronal and glial cell type, including OLs and oligodendrocyte precursor cells (OPCs), holds great potential for understanding the molecular basis of the aetiopathogenesis of genetically complex psychiatric diseases such as SCZ and could pave the way towards personalized medicine. The development of neuronal and glial co-culture systems now appears to enable the in vitro study of SCZ-relevant neurobiological endophenotypes, including OL dysfunction and myelination, with unprecedented construct validity. Nonetheless, the meaningful stratification of patients before the subsequent functional analyses of patient-derived cell systems still represents an important bottleneck. Here, to improve the predictive power of ex vivo disease modelling we propose using hiPSC technology to focus on representatives of patient subgroups stratified for genomic and/or phenomic features and neurobiological cell systems. Therefore, this review will outline the evidence for the involvement of OPCs/OLs in SCZ in the context of their proposed functions, including myelination and axon support, the implications for hiPSC-based cellular disease modelling and potential strategies for patient selection.

INTRODUCTION

Schizophrenia (SCZ) is a severe, disabling neuropsychiatric disorder with a lifetime prevalence of 0.3%–2.3%.[1–4] The substantial disability associated with this disorder, together with its early onset and chronicity, places an enormous burden on patients. This burden was quantified in the Global Burden of Disease Study 2013, which found a remarkably high number of disability-adjusted life years (DALY) and years lived with disability (YLD) in SCZ compared with other medical conditions.[5–7] The clinical features of SCZ have been subdivided into positive, negative and cognitive symptoms. Positive symptoms are likely to be associated with a hyper-dopaminergic state. Neuroleptics that act mainly at the dopamine receptor 2 (DRD2), which is highly expressed in the basal ganglia, are effective in reducing positive symptoms in many patients.[8] An increasing body of evidence indicates that negative and cognitive symptoms are functionally associated with an excitation/inhibition dysbalance in the function of glutamatergic and ɣ-aminobutyric acid (GABA)ergic synapses. This dysbalance is proposed to eventually lead to a disconnection of critical cortico-cortical and cortico-subcortical projection systems, although the underlying mechanisms are not fully understood.[9] No effective pharmacological treatment is available for negative and cognitive symptoms.[8]

So far, all attempts to target the synapse-associated glutamatergic system have failed and thus other mechanisms need to be explored to identify novel treatment options.[10] The lack of human neurobiological test systems to study the consequences of genetic and pharmacological perturbation, for example, has been a major limitation in the field of psychiatry to date. Research has been mainly restricted to peripheral tissues, such as blood, correlative imaging studies, genetics and molecular and histological analyses of postmortem brain samples. Taken together, these approaches have revealed strong evidence for a synaptic dysfunction. In addition, current evidence of altered white matter (WM) structures and reduced myelin gene expression in SCZ suggests that dysfunctional oligodendrocyte precursor cells (OPCs) and/or oligodendrocytes (OLs) may also contribute to the dysconnectivity of brain regions seen in this disorder.[11–14] Moreover, despite compelling advances in the understanding of genetic factors that contribute to the risk for SCZ, little is still known about the final mechanistic consequences of such risk factors in the biological systems involved in the genesis of SCZ.[15–17]

The unavailability of proper model systems to accurately assess the functional consequences for and contribution of dedicated molecular and cellular signatures to these disorders is one possible reason for the lack of biological insight. Animal models,

---

[1]Molecular and Behavioural Neurobiology, Department of Psychiatry and Psychotherapy, University Hospital, LMU Munich, Munich, Germany; [2]International Max Planck Research School for Translational Psychiatry (IMPRS-TP), Munich, Germany; [3]Institute of Psychiatric Phenomics and Genomics (IPPG), University Hospital, LMU Munich, Munich, Germany and [4]Laboratory of Neuroscience (LIM27), Institute of Psychiatry, University of Sao Paulo, Sao Paulo, Brazil
Correspondence: Florian J. Raabe (florian.raabe@med.uni-muenchen.de) or Moritz J. Rossner (moritz.rossner@med.uni-muenchen.de)
These authors contributed equally: Sabrina Galinski, Sergi Papiol, Peter G. Falkai, Andrea Schmitt.

np̄j
Studying and modulating schizophrenia-associated dysfunctions…
F.J. Raabe et al.

2

especially inbred genetic mouse models, are well-suited to characterize the molecular and phenotypic (i.e. behavioural) impact of one or a few risk genes but cannot capture the complex genetic risk architecture of SCZ. However, recent developments in the methodologies for the induction of pluripotent stem cells and their differentiation into neuronal and glial cell types have paved the way for the generation of patient-specific cellular systems.[18–20] These systems hold promise for comparing cellular phenotypes in patients and healthy controls, whereas keeping the individual genomic risk background of each individual. Likewise, such cellular models have some characteristics that make them especially well-suited to assessing how pharmacological treatments may restore affected pathways in patient-specific cell types.[21,22]

This review aims to (i) revisit dysfunctions of OPCs/OLs in SCZ, including and beyond myelination, and (ii) discuss strategies for patient selection towards stem-cell generation and cellular modelling as a pre-requisite to target OPC/OL deficits with pharmacological approaches.

OLIGODENDROCYTE DYSFUNCTION AND WHITE MATTER DEFICITS IN SCHIZOPHRENIA

Neurodevelopment, myelination and axonal support

Puberty and adolescence are vulnerable periods of brain development and are characterized by a multitude of psychosocial challenges related to work and interpersonal relationships. Adolescence coincides with the average age of onset of affective and non-affective psychoses.[23] The hypothesis that SCZ is not a neurodegenerative but a neurodevelopmental disease that alters brains circuits was proposed nearly 40 years ago[24,25], but was recently rediscovered and is gaining increasing influence.[26–29]

An important process that takes place during early postnatal human brain development is myelination. The development of WM tracts occurs at a high rate in the first years of childhood and continues during puberty and even young adulthood.[30,31] Postmortem analyses of human brain tissues have revealed that myelination follows a defined chronological and topographical order along the caudal to rostral axis.[32,33] The fact that associative cortical areas such as the prefrontal cortex are among the latest to become myelinated, i.e. not until early adulthood, and are generally less myelinated has potential implications for SCZ.[14] The developmental aspects of myelination that may be affected in SCZ remain largely unclear, however, because most studies have been performed in adult postmortem samples.[34] Defects in myelination during development could be caused by a failed or delayed differentiation of the OPC lineage and/or by failed or delayed OL maturation. On the other hand, myelin deficits in SCZ could also reflect failures in the adaptive mechanism termed 'myelin plasticity'. It has been known for a long time that electrical activity stimulates myelination and that many structural aspects of myelin-axon interactions can modulate for example conduction velocity, including myelination per se; myelin thickness; the spacing and size of the nodes of Ranvier and the clustering of ion channels.[35] It has recently been established that several of these mechanisms are plastic and likely to contribute to the overall plasticity of the brain.[36] In addition, segmented or partial myelination and the pattern and relationship of myelination by individual OLs of functionally distinct or potentially synchronized axons (coupled myelin bundles) have been mentioned as being important, as yet unanswered questions in the field that add additional opportunities for remodelling and plasticity.[37] Finally, disturbances in myelination impair connectivity and coherence between brain regions by causing improper spike timing and desynchronized signal processing.[38,39] Thus, the consequences of deficits in developmental and adaptive myelination align well with the prevailing hypothesis of schizophrenia as a 'dysconnectivity

disease'.[40] More recently, OLs have been proven to metabolically support axons,[41,42] an essential biological mechanism that is important for brain function and that can be uncoupled from myelination. Myelination coincides with the maturation of brain networks, which is mainly driven by the integration of interneurons into local cortical microcircuits. It has thus been hypothesized that, in addition to optimizing action potential fidelity, the segmented myelination of fast-spiking parvalbumin-positive (Parv+) interneurons may help to cope with the high energy demands of these cells.[43] Strikingly, in the cortex of rodents most myelinated axons of interneurons belong to the Parv+ subtype.[44] The suggestion that dysfunctions of Parv+ interneurons are associated with SCZ also led to the idea that failure of both processes, i.e. optimizing of action potential fidelity and metabolic support, may together precipitate the network dysfunctions associated with SCZ.[45] However, this view was recently challenged because the most comprehensive analysis of the contribution of cell type-associated SCZ risk variants so far did not point to an involvement of Parv+ interneurons in the aetiology of SCZ, but rather highlighted the role of reelin-positive cortical interneurons.[46] Also, neither OPC- nor OL-specific gene sets were enriched in SCZ risk genes identified in genome-wide association studies (GWASs).[46] Although these observations cannot be considered as definitive, they suggest that OL dysfunctions in SCZ may rather be a secondary consequence of genetic risk factors operating primarily in glutamatergic neurons. This does not, however, exclude 'myelin plasticity' as a potential target for research into treatment options. On the other hand, a study where glial precursors isolated from childhood-onset SCZ patients were transplanted into mice also provided evidence for a direct and 'primary' contribution of OLs to SCZ[47] (see below for details).

Disturbed oligodendrocyte function and myelin: impact on cognition in schizophrenia

A series of studies with different techniques provided much evidence for disturbed OL function and myelin deficits in schizophrenia, which has been reviewed in detail elsewhere.[12,34] In short, in vivo brain imaging studies revealed decreased fractional anisotropy as a sign of impaired WM tract integrity,[48,49] a lower myelin water fraction in the WM of the frontal lobe and corpus callosum[50] and functional dysconnectivity in relevant neuronal networks,[51] which is supported by electrophysiological measurements.[40] Studies in SCZ patients that combined imaging and neurocognitive testing revealed associations between impaired cognitive performance and decreased fractional anisotropy,[52,53] disturbed connectivity[54,55] and reduced volume of specific brain areas (hippocampus and nucleus accumbens).[56] Furthermore, histopathological findings in postmortem brain tissue indicated a decreased number of OLs in the dorsolateral prefrontal cortex (DLPFC) and cornu ammonis (CA) 4 region of the anterior and posterior hippocampus,[57–59] and reduced OL number was correlated with cognitive dysfunction.[60] Moreover, a reduced density of perineuronal OLs,[61] lower myelin basic protein (MBP) immunohistochemical staining intensities[62] and damaged myelin sheaths and apoptosis of OLs[63,64] have also been documented in light microscopy and electron microscopy studies. Transcriptomic studies in postmortem tissues reported reduced expression of myelin- and OL-related genes, such as MAG and MBP, in several relevant brain regions,[65,66] and myelin-associated proteins have been shown to be decreased in proteomic studies.[67,68]

Taken together, accumulating evidence suggests that disturbances of OL function and myelination likely contribute to the dysconnectivity of brain regions and cognitive impairments seen in SCZ. Whether the deficits in OL functions and their impact on cognition is a primary causative mechanism or a secondary consequence of neuronal and synaptic alterations, or both, is still unclear, although evidence exists for both options.[46,47]

Studying and modulating schizophrenia-associated dysfunctions…
F.J. Raabe et al.

npj

3

GENETIC AND CELLULAR COMPLEXITY OF SCZ - NEW INTERPRETATIONS FROM THE LATEST GWASS AND SCRNASEQ ANALYSES

GWASs and exome sequencing approaches have provided outstanding and solid results regarding the role of common and rare genetic variations in psychiatric disorders, such as SCZ. In SCZ, an increasing number (so far around 150) of genetic risk *loci* have been unequivocally identified after controlling for multiple testing and for sources of confounding, such as population stratification.[16,17,69] Likewise, these studies have provided compelling evidence of the polygenic architecture of this disorder. Polygenic risk scores (PRSs) can be calculated for everyone and summarize in a single risk score the effects of many single nucleotide polymorphisms (SNPs) under an additive model. PRSs have shown an excellent replicability across independent samples of SCZ patients, although they lack predictive value as regards disease risk.[70]

An important proportion of *loci* associated with SCZ contain at least one expression quantitative trait locus (eQTL) for a gene within 1 Mb. Active brain enhancers are enriched in these associations, highlighting the regulatory nature of such associations with SCZ risk. Further analysis revealed that several risk SNPs are associated with genes of known regulatory function in neurons and also with genes relevant for glial cells and OPCs/OLs.[16,17,71–73] SCZ risk variants are enriched within genomic regions that are marked by histone H3-K4 methylation (H3K4me3), which points to the impact of processes related to the control of gene expression.[73] Pathway analyses have shown the aggregation of risk variants in pathways related to neuronal signalling, postsynaptic density, FMRP-bound transcripts and mitochondrial and glial function.[74,75] Interestingly, Duncan et al. revealed a stronger association of an expert-curated glia-OL pathway (comprising 52 genes) with SCZ than with bipolar disorder.[74] Worth mentioning in this context is the fact that, numerically, most pathway analyses underline the best evidence of disturbed neuronal function in SCZ.

The contribution of brain cell types to SCZ was recently addressed in a sophisticated analysis combining the most comprehensive list of SCZ GWAS hits with a series of single cell (sc) and single nucleus (sn) RNAseq analyses from mouse and human brain tissues, which provide dramatically enhanced cell-type resolution.[46] In contrast to the previous, above mentioned pathway analyses, which relied on lists of expert curated cell type markers,[74,75] Skene et al.[46] computed cell type-specific gene expression metrics on the basis of scRNAseq and snRNAseq data. Moreover, they weighted risk gene contributions for genetic association probabilities on the basis of GWAS data. With this approach, the group made several observations with respect to brain cell types associated with SCZ: (i) cell-type profiles from mature (e.g. pyramidal and cortical interneurons) but not from immature cell types (e.g. neuronal progenitors, radial glia) were associated with SCZ; (ii) a dedicated set of mature neuronal cell types (medium spiny neurons, cortical and hippocampal glutamatergic projection neurons and cortical GABAergic interneurons) showed greater association with SCZ than any other neuronal and glial cell type; and (iii) human, but not mouse, reference mRNA cell type profiles indicated that OPCs and OLs also showed a moderate enrichment. These observations likely helped to shape the current hypotheses on SCZ aetiology, which highlight late cortical developmental processes, including microcircuit maturation ('micro-connectivity'), rather than early neurodevelopmental processes. Moreover, the association of gene sets from cortical and hippocampal projection neurons support the idea that the connectivity between brain regions ('macro-connectivity') may also be critical. Because both 'micro-connectivity' and 'macro-connectivity' essentially depend on trophic support and myelination (see above), it appears possible that the 'intermediate'

enrichment of OPC-/OL-specific gene sets further supports these assumptions. Although the analyses by Skene et al.[46] made use of the most comprehensive data sets available so far, the conclusions of their study are not definite because of some technical limitations: (i) non-cell type-specific gene sets may operate to a variable, disease-relevant extent in different cell types (e.g. alteration of gene expression by the H3-K4 methylation pathway, see above); (ii) so far, human brain region- and cell type-specific RNA reference profiles are only available as nuclear transcriptomes, which generates a bias on transcripts involved in cellular processes, such as those associated with dendrites and/or synapses (compartmentalized transcription has also been described in cellular processes of OLs[76,77]); and (iii) although scRNAseq and snRNAseq data sets offer an unprecedented cell type definition and resolution, in general the depth of sequencing per individual transcriptome is low and low abundance transcripts coding for transcription factors or signalling components, for example, may be underrepresented. Besides these limitations, the above findings give the impression that common risk variants of SCZ primarily target dysfunctions of striatal and cortical neurons, which may cooperate with a minor fraction of risk factors operating in OPCs/OLs to disturb the local and remote connectivity of brain networks (Fig. 1).

PHENOMICS-BASED PATIENT STRATIFICATION

On the phenomics side, the use of a case-control condition as a target phenotype has inherent limitations, including patient heterogeneity and overlap of the symptom spectrum. A potentially more promising strategy might be to use alternative or
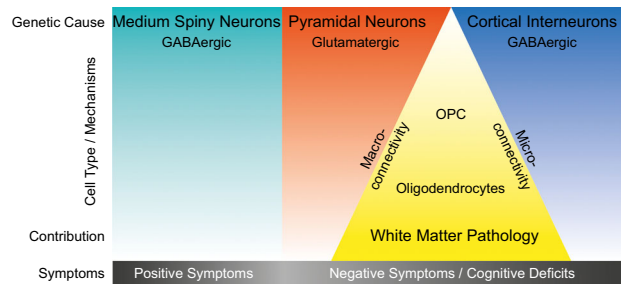
Fig. 1 Primary and secondary cell types and mechanisms of schizophrenia (SCZ)—combining results of the latest genome-wide association studies (GWASs) with cell type-specific transcriptomics. Most recent GWASs combined with single-cell RNAseq profiles identified SCZ risk genes that may primarily operate in three neuronal cell types: GABAergic medium spiny neurons (cyan), glutamatergic pyramidal neurons (red) and GABAergic cortical interneurons (blue). A minor fraction of single nucleotide polymorphisms associated with increased risk for SCZ may affect oligodendrocyte precursor cells (OPCs) and oligodendrocytes and their function (yellow). Nonetheless, oligodendroglia intensively interact with pyramidal projection neurons and cortical interneurons at the level of myelination and metabolic support. Myelination of long-range projection neurons supports the connectivity between brain regions ('macro-connectivity'). Myelination and trophic support of interneurons may support the function of local circuits ('micro-connectivity'). Therefore, we hypothesize that the disturbed functional connectivity in SCZ results from the interaction of cell types and mechanisms where the primary effects occur (e.g. directed at synapses in glutamatergic and GABAergic neurons), with secondary effects on OPCs and oligodendrocytes finally causing white matter alterations. It is tempting to speculate that (i) positive symptoms are likely more connected to the dysfunction of dopamine-responsive medium spiny neurons and (ii) excitation-inhibition dysbalances of cortical glutamatergic and GABAergic neurons and disturbed connectivity, including oligodendroglia functions, may rather be associated with higher order cognitive impairments and negative symptoms

npj Studying and modulating schizophrenia-associated dysfunctions…
F.J. Raabe et al.

4

additional (sub)phenotypes within these patients that may be closer to the aetiological roots of psychotic disorders.[78]

Cognition-based patient stratification

Cognitive impairments are a key aspect of SCZ[79] and an attractive but still mainly untapped target for drug development.[29] Several aspects of cognition, including working memory, attention and executive performance, are affected in SCZ and are already detectable in early-onset SCZ and high-risk individuals.[80] Moreover, cognitive impairments that occur during the first episode are very stable and improvements or deteriorations are hardly detectable in SCZ patients even after 10 years.[81,82] Besides the clinical aspects of cognitive impairment as one of the main symptoms in SCZ, there is also a genetic relationship between cognition and SCZ risk genes. Thus, an increased PRS for SCZ is associated with reduced spatial visualization (measured by a block design test) in a cohort of patients, relatives and healthy controls.[83] Assessment of cognitive abilities with the Brief Assessment of Cognition in Schizophrenia (BACS) also showed an association of PRS with cognitive performance in both SCZ patients and healthy controls.[84] Besides a general association between increased polygenic risk for SCZ and impaired cognition, a large study identified 21 independent SCZ risk loci that influence cognitive functioning.[85] Furthermore, cognitive performance was found to be slightly worse in adult healthy carriers of risk copy number variations that are associated with SCZ than in healthy non-carriers.[86,87] On the functional level, a higher PRS is associated with hypoactivity in the prefrontal cortex during working memory tests in healthy controls.[88,89] Most recently, the largest GWAS on human intelligence performed so far identified hundreds of genes involved in this trait.[90] The same study reported a negative genetic correlation between intelligence and SCZ ($r_g = -0.21$, $P = 3.82 \times 10^{-17}$). Remarkably, most prominent gene sets associated with cognition are enriched in medium spiny neurons and hippocampal projection neurons.[90]

In summary, this body of clinical and genetic evidence suggests that cognitive dysfunction in SCZ is an integral part of the disorder rather than a consequence of it. Therefore, using cognition as a stratification criterion for patient selection has the potential to capture key elements in the genetic/molecular architecture of SCZ that are measurable in cellular systems. The results of the aforementioned studies based on SCZ PRS and cognition further support this notion. However, the amount of variation in cognition explained by the SCZ PRS is very modest, which strongly advises against using it as the only patient selection criterion. Although the SCZ PRS is currently the best measure of genetic risk available, the score alone may not yet allow a proper stratification of patient subgroups for decisions regarding iPSC generation and follow-up analyses.

Imaging-based patient stratification

Patients with early-onset and first-episode SCZ already display widely distributed reduced WM homogeneity, as indicated by a substantial reduction of fractional anisotropy in most brain areas, including several fibre tracts; this reduced WM homogeneity has been associated with disturbed higher order cognitive function.[53,91–93] These findings were recently verified by the largest imaging study conducted so far, which analysed 29 independent and international imaging studies that included a total of 4322 individuals with SCZ.[94] Moreover, individuals at high risk for psychosis already display altered WM integrity similar to the pattern of first-episode patients.[95] Systematic reviews and meta-analyses substantiate a pattern of WM impairments and structural dysconnectivity in patients with early-onset SCZ, drug-naive patients and clinical high-risk individuals[96] and link disturbed WM in first-episode SCZ to cognitive deficits.[97] A pioneering study identified a strong association between two risk SNPs in genes

important for OL function (MAG and *OLIG2*), the integrity of WM tracts and cognitive performance.[98] The use of genome-wide analyses will likely provide stronger confidence about which genetic factors and pathways may link WM deficits with cognitive impairments in SCZ. In terms of identifying novel drug targets, understanding the biological pathways that modulate the course of the disease over time will provide additional opportunities beyond current genetic approaches.[99]

Accumulating evidence suggests that WM pathology and functional dysconnectivity are key aspects of SCZ pathophysiology that contribute to cognitive impairments. Thus, the combined use of phenotypes related to cognition and neuroimaging holds great potential for patient stratification and may be less affected by experimental noise than current genetic classifiers. A critical issue for improving selection strategies even further in the future could be to include environmental stress factors, if available. The additional stratification tools, i.e. cognitive and imaging-related phenotypes and environmental stress factors, might help to identify representatives of (sub)groups with verified WM pathophysiology and subsequently to investigate their underlying mechanisms and their impact on cognition in SCZ, e.g. with hiPSC-based cellular modelling (Fig. 2a).

GENERATION OF HIPSC-BASED NEUROBIOLOGICAL CELL SYSTEMS

Until recently, most insights into psychiatric diseases, including SCZ, have been generated from postmortem tissue samples, brain imaging, genetic and pharmacological studies and animal models. Cellular reprogramming methods now provide a new opportunity to model the complex polygenetic conditions in diseases such as SCZ by generating patient-derived hiPSC-based systems.

Generation of hiPSCs from patients

The first successful reprogramming into iPSCs was performed with murine fibroblasts[101] and was awarded the Nobel Prize in Physiology or Medicine 2012. Multiple subsequent studies in humans successfully reprogrammed diverse somatic cell types that are more accessible than fibroblasts, such as keratinocytes,[102] urine cells[103] and (cord) blood samples.[104–108] Peripheral blood mononuclear cells (PMBCs) can be reprogrammed even after cryopreservation.[109] Initial reprogramming methods relied on constitutive retroviral and lentiviral expression systems that were limited by insufficient genomic integration and insertional mutagenesis.[110] In recent years, integration-free reprogramming methods have been developed on the basis of adenovirus,[111] mRNA,[112] sendai virus[113] and episomal vectors.[114] Episomal reprogramming is highly reliable for different somatic cell lines, and the rapid loss of the reprogramming factors from the host genome over short time periods makes this method highly attractive.[115] For translational clinical research, it is crucial to choose the best reprogramming method and the most suitable primary cell type, i.e. the cell type that is most easily accessible and can be stored for long periods.[116] Because PMBC sampling and cryopreservation are standard procedures and less invasive than skin biopsies, PBMCs represent the best choice for human cell-based studies on psychiatric diseases. Moreover, setting up large PBMC repositories for clinical studies is a routine procedure that might allow post hoc access to patient data, e.g. for validation purposes beyond the 'subgroup representatives' selected in first-round reprogramming. Thus, the use of PBMCs (e.g. CD34+ hematopoietic stem cells and erythroid progenitor cells)[117–119] and episomal reprogramming enables hiPSCs to be generated in a safe, efficient and scalable approach.

Once generated, hiPSCs can be differentiated in principle to all specific brain cell types by providing a lineage-specific chemical environment and/or transient overexpression of transcription

Studying and modulating schizophrenia-associated dysfunctions...
F.J. Raabe et al.

npj

5
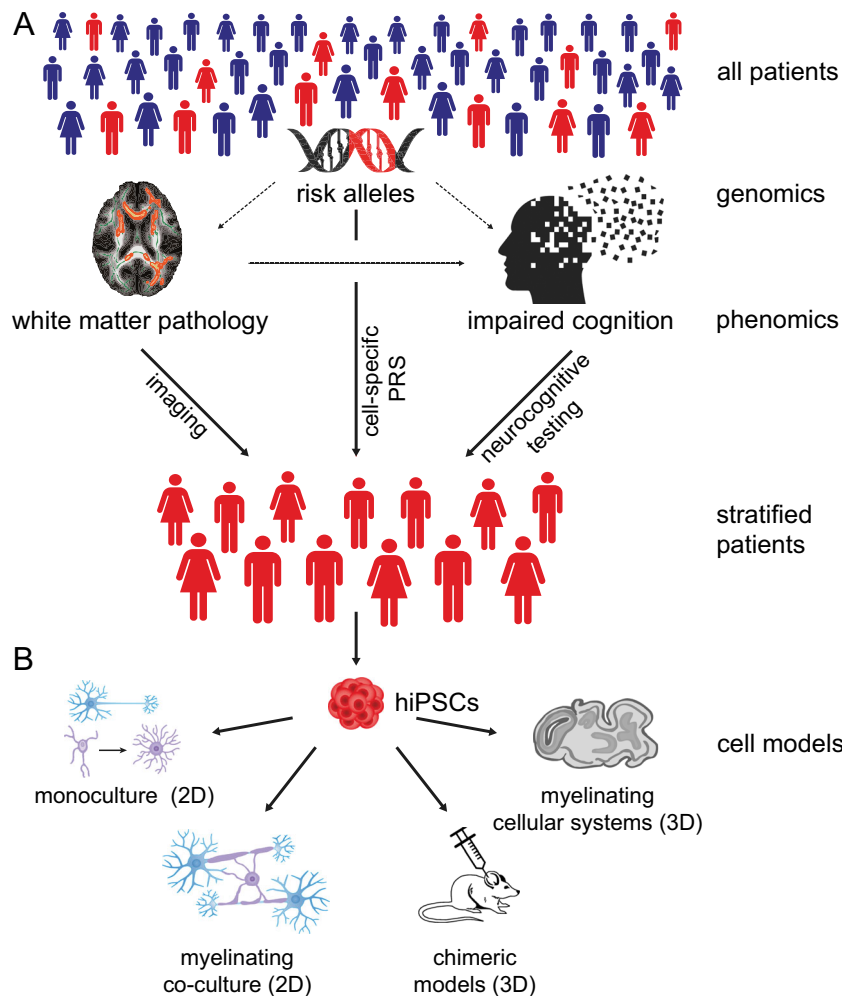
Fig. 2 Principals of patient stratification for subsequent human-induced pluripotent stem cell (hiPSC-)-based cellular disease modelling combining genetics, white matter pathology and cognitive impairments. **a** Subsets of SCZ risk genes (as indicated by the red part of the DNA symbol) impair cognitive performance. Red human icons illustrate such risk gene carriers. Recent evidence suggests that the effect of these 'cognitive' risk genes is at least in part connected to white matter pathology. Sufficient patient stratification is needed to reveal the underlining mechanisms of white matter pathology. Clinical deep phenotyping, with a focus on neurocognitive testing, combined with imaging of white matter is probably a suitable approach to identify the corresponding subgroup of patients. Additional stratification based on cell-specific PRSs might further increase stratification precision. **b** hiPSC technology enables the generation of a toolbox of patient-derived cell systems. Monocultures of glial cells and neurons and myelinating co-culture systems may simulate disease-relevant aspects of SCZ in 2D and 3D cellular systems in vitro. Moreover, hiPSC-derived cells can be tested in chimeric mouse models in vivo. NB: The illustrations of the 'chimeric mouse' and the DNA 'risk alleles' have been published previously[100]

factors that determine the cell lineage. Protocols have been developed for hiPSC-derived neuronal stem cells (iPSC NSCs), hiPSC-derived glutamatergic and GABAergic neurons (hiPSC neurons), hiPSC astrocytes, hiPSC OPCs and hiPSC OLs (see below). The generation of disease-relevant cell types represents a major step forward in studying aspects of the neuronal and glial contribution to SCZ in 2D or 3D cellular systems without losing the genetic complexity (Fig. 2b).

Differentiation of hiPSCs to neuronal cells

The most prominent cell types with significant importance in the modelling of psychiatric diseases are the hiPSC neurons. By using different protocols, glutamatergic excitatory neurons can be generated with similar properties as those of the cortex[120] and hippocampus.[121] Specific overexpression of certain transcription factors alone,[122,123] or in combination with small molecules,[124] enables more homogeneous and scalable populations of gluta-matergic iNeurons to be obtained. Besides excitatory neurons,

stem cells can also be differentiated into cortical GABAergic interneurons similar to medium spiny striatal interneurons[125] or Parv+ interneurons.[126,127] For more details, we refer readers to comprehensive reviews on the differentiation of iPSC-derived neurons[120] and iPSC-derived astrocytes[128] or microglia.[129]

Differentiation of hiPSCs into the oligodendroglial lineage

The initial approaches employed to generate 'first-generation' OPCs from stem cells used small molecule cocktails that inhibited or activated restrictive signalling pathways. These approaches are comprehensively reviewed in detail elsewhere.[130–132] In general, the main disadvantages of such chemical differentiation approaches are the very protracted protocols, which can take up to several months and are expensive, the high variability in the generated OPCs and the limited numbers of differentiated cells produced with the desired properties. Consequently, these approaches are hardly suitable for diagnostic and empirical perturbation purposes. Another strategy to generate OPCs/OLs is

npj

Studying and modulating schizophrenia-associated dysfunctions…
F.J. Raabe et al.

6

Table 1. Fast differentiation of human-induced pluripotent stem cells (hiPSCs) or predifferentiated hiPSC neuronal stem cells (NSCs) to induced oligodendrocyte precursor cells (iOPCs) or induced oligodendrocytes (iOLs) by using selected expression of transcription factors

Cells used	Transcription factors	Generated cell stage	Days	References
hiPSCs	SOX10, OLIG2	iOPC (PDGFRα+/O4+)	14	Li et al.[135]
		iOL (CNP+)	42	
hiPSC NSCs	SOX10, OLIG2, NKX6.2[a]	iOPC (O4+)	28	Ehrlich et al.[136]
		iOL (MBP+/CNP+)	35	
hiPSCs	SOX10, OLIG2	iOPC (PDGFRα+/O4+)	10	Pawlowski et al.[137]
		iOL (MBP+/PLP+/CNP+)	20	
hiPSCs	NKX2.2	pre-iOPC (PDGFRα+)	30	Rodrigues et al.[138]
		iOPC (O4+)	55	
hiPSCs	SOX10[a]	iOL (O4+/MBP+/PLP+)	22	García-León et al.[139]

[a]Best combination of transcription factors to reach (different) endpoint

the forced overexpression of lineage-determining transcription factors (as pioneered for iNeurons, see above). Rodent fibroblasts have been successfully trans-differentiated in this way.[133,134] Furthermore, several combinations of certain transcription factors can differentiate hiPSCs or predifferentiated hiPSC NSCs into iOPCs and iOLs relatively quickly and efficiently (Table 1).

Thus, several combinations of stage-specific transcription factors seem to be sufficient to differentiate hiPSCs into the OPC/OL lineage by directed overexpression. The studies listed in Table 1 used different combinations of transcription factors and applied different cell media and supplement compositions. Although the major focus of Pawlowski et al. and Rodrigues et al. was to generate and characterize the iOPC stage,[137,138] Li et al., Ehrlich et al. and García-León et al. tried to reach the iOL stage as part of the main protocol.[135,136,139] Indeed, it is unclear whether protocol differences may have affected the properties of iOPCs or iOLs, e.g. with respect to kinetics and the efficiency of differentiation and myelination. Thus far, no study has compared the protocols by applying a comprehensive battery of molecular and morphological assessments, but such a study could help to identify potential (dis)advantages of the different conditions.

Myelinating 2D culture systems

hiPSC OPCs and hiPSC OLs not only express state-specific markers, but are also able to myelinate axon-like structures,[136] human foetal neurons[140] and hiPSC neurons.[136,139] They can be used in co-culture systems to investigate axoglial interactions or, for example, to assess pro-myelinating drugs with potential relevance also for SCZ. After pioneer experiments in mouse pluripotent epiblast stem-cell-derived OPCs,[141] studies have also shown that clobetasol, miconazole and pranlukast promote myelination of hiPSC OPCs[136,139,141] (Fig. 2B).

Myelinating 3D culture systems

As a highly advanced in vivo test system, hiPSC OPCs have been used in human-mouse chimeric models. hiPSC OPCs have the capacity to myelinate mouse brain slices ex vivo[139] and brain regions in living animals.[136,138,140] Chimeric hiPSC-based systems thus allow glial pathophysiology to be investigated in complex organisms up to the behavioural level (Fig. 2B).[47] Newly developed 3D cell culture systems enable disease biology to be studied at the circuit level in an experimentally accessible and complex cellular environment.[142,143] The 3D organoid culture systems, termed cerebral organoids, recapitulate some critical features of human cortical development. To date, maturation of circuits by spine pruning or myelination cannot be studied in cerebral organoids because of the lack of OLs and microglia.[144]

Another, technically 'less challenging' approach uses hiPSC-derived cortical spheroids, which consist of a cerebral cortex-like structure and include astrocytes and interneurons.[145] Recently, Madhavan et al. generated hiPSC-derived 'oligocortical spheroids',[146] in which 20% of the contained cell were part of the oligodendroglial lineage after 14 weeks of maturation. Early-stage myelination of neurons occurred after 20 weeks, but myelin maturation, refinement and myelin compaction were not complete until 30 weeks of maturation. Thus, higher level processes such as myelination can be studied in 3D hiPSC-derived cerebral spheroids. However, the time and costs of generating them are still quite challenging.

An additional, less complex but much faster approach is the generation of an hiPSC-derived 3D brain microphysiological system (BMPS).[147] The key accelerating step in this approach is the pre-differentiation of hiPSC to hiPSC NSCs before the 3D generation of the BMPS. In just 2 weeks Pamies et al.[148] generated a BMPS that contained GABAergic, dopaminergic and glutamatergic neurons, astroglia and oligodendroglia. Intriguingly, this approach allowed Pamies et al. to observe complex processes such as synaptogenesis and myelination within only 4 weeks, and 42% of axons were myelinated after 8 weeks. The above mentioned pioneering studies have limitations regarding intra- and inter-individual variability, cellular robustness, reproducibility, scalability and affordability. However, the field of 3D cellular systems, as well as the whole-hiPSC field, is rapidly evolving. Thus, in the near future we might expect more robust protocols for 3D hiPSC-based cell systems that contain OPCs and OLs (Fig. 2B).

RECENT OBSERVATIONS AND CHALLENGES OF PATIENT-SPECIFIC NEUROBIOLOGICAL TEST SYSTEMS

The landmark study by Brennand et al. in 2011 that characterized hiPSC neurons from SCZ patients was performed in a mixed population of glutamatergic, dopaminergic and GABAergic neurons that showed decreased neuronal connectivity, decreased neurites and decreased levels of post-synaptic protein PSD95.[148] Recent studies have focused more on specific neuronal subtypes, such as pyramidal cortical interneurons, cortical interneurons and dentate gyrus (DG) granule neurons; these studies are reviewed in detail elsewhere.[20,149]

Studying and modulating schizophrenia-associated dysfunctions…
F.J. Raabe et al.

npj

7

Disturbed OPC/O function and impaired myelination in SCZ-relevant iPSC cell systems

In contrast to the large number of studies on hiPSC-derived neurons, so far only a few studies have investigated the oligodendroglial impact in SCZ-related iPSC models. Chen et al. focused on the known schizophrenia risk gene FEZ1 in murine and human iPSC-derived oligodendroglial cells and showed that FEZ1 knockdown impaired OL development[150]. Additional analysis revealed that potential SCZ-relevant pathways governed FEZ1 expression and post-transcriptional stability[150]. Lee et al. used hiPSC neurons and hiPSC OPCs from two individuals with a large (289 kb) heterozygous deletion in CNTNAP2 that affected exons 14–15, whereby both the patient with SCZ and the patient's healthy father, who carried the allele, were heterozygous[151]. The research group showed that the expression of exons 14–15 was significantly decreased in hiPSC-derived neurons and OPCs, but not in fibroblasts, whereas the expression of other exons was upregulated, indicating cell-type-specific mechanism[151]. Another family-based approach investigated the contribution of two rare missense mutations in CSPG4 (A131T and V901G)[152]. CSPG4 codes for NG2, a marker of proliferating OPCs, which are frequently termed NG2-glia[153,154]. hiPSC OPCs derived from CSPG4 mutation carriers revealed dysregulated posttranslational processing, different cellular NG2 location, impaired OPC survival and reduced differentiation to mature OLs[152]. Transfection of the two risk variants into OPCs generated from healthy non-carrier siblings revealed similar deficits, underlining the contribution of the described mutations to the OPC pathology. By using diffusion tensor imaging (DTI), the investigators observed impairments of white matter integrity in affected mutation carriers but not in unaffected siblings or the general population[152]. Interestingly, no pathological signs were detected in carrier-derived hiPSC neurons, underlining the OPC-specific effect of the CSPG4 mutations[152].

These studies were either prototypical, hypothesis-driven or single-gene interference approaches or they evaluated 'rare' variants that are thought to reflect high-penetrance and 'high-impact' mutations; thus, the studies are limited in their dissecting mechanisms and restricted to the dysfunction of a single gene or locus. The generation of iPSCs and derived cell systems from patients who are carriers of polygenic risk assemblies could enable a deeper understanding of common molecular roots of SCZ in a given cell type, such as OLs. Moreover, the differentiation protocols applied in the studies mentioned above were solely based on small molecule differentiation protocols, which may be compromised by having a higher level of variability than directed protocols. Nonetheless, direct cell lineage conversion may possibly override subtle developmental deficits, which may be better accessible with chemical protocols (see below).

In the seminal study by Windrem et al., glial precursor cells, which could mature into both oligodendroglial and astroglial lineage cells, were generated from patients with childhood-onset SCZ and unaffected controls[47]. SCZ-derived precursor cells displayed impaired glial maturation, altered transcriptomic signatures in vitro and hypomyelination; when grafted into brains of immune-deficient mice, the mice showed psychosis-related behaviours, such as deficits in sensory motor gating[47]. This study provides the strongest evidence so far that glial precursor cells have a cell-autonomous effect that is thus a potentially 'primary' cause of the disease or at least contributes to it. It seems likely that the majority of SCZ-relevant endophenotypes detected by Windrem et al. were caused by glial dysfunction and related to disturbed myelination and impaired functional connectivity. Nonetheless, more studies are needed to dissect the relative impact of the cell-type-dependent risk in individual patients.

## Challenges for the future of disease-relevant cell systems

To date, hiPSC-based studies in psychiatric disorders have mainly been performed on adherent monolayer cultures and have focused on cell-autonomous molecular and cellular abnormalities. Most protocols applied to generate neuronal cell types also contained cells of mixed temporal and spatial identities and other cell types of glial and non-neural origin[155]. The large heterogeneity of these mixed cell cultures leads to a substantial and hard-to-control level of variability, even when the cells are obtained from the same individual, and decreases the confidence and robustness of the results (i.e. observed SCZ vs. control samples). One very costly and potentially impracticable strategy to tackle this issue is to increase the technical and biological replicates[156]. Another, possibly more feasible strategy to increase levels of reliability is to reduce the cellular heterogeneity of hiPSC-based cell systems. This may be possible by the directed generation of cell types via overexpression of defined cell- and stage-specific transcription factors, as described above. These paradigms may bypass certain maturation processes, which might be a disadvantage when studying psychiatric diseases, in which neurodevelopmental aspects are hypothesized to play a role, such as SCZ. As regards SCZ, however, recent analyses of GWAS data did not provide evidence for a strong association between early developmental cell stages and the disease (see above[46]).

Although great progress has been made with 3D cell-based neurobiological model systems, they still have major limitations. Current protocols for organoids mimic early neurodevelopment but lack mature OLs and do not develop to postnatal maturation stages, including myelination and synapse pruning. However, recent landmark studies have managed to generate myelinating spheroids and brain microphysiological systems and we can expect more elaborated protocols in the future. One of the current challenges is to develop procedures to establish more mature 3D cell systems. For both 2D and 3D cell systems, scalability is an important issue to enable genetic and chemical screenings at high throughput. Another important topic is intra- and inter-patient variability[157,158]. To increase reliability, multiple hiPSC clones should be analysed. An alternative strategy could be to initially focus on a pool of clones and to subsequently validate the obtained effects in individual cell clones to substantiate robust findings. In any case, modern array-based genotyping tools should be applied to verify the genomic integrity and genotype beyond karyotyping at the chromosome level.

Even if further progress is made in 2D and 3D cellular systems, they will always be limited regarding construct validity in brain disorders where circuit-level dysfunctions precipitate behavioural and cognitive deficits. We must accept that even patient-specific cellular models, which reflect the genetic background of an individual, only allow us to study certain disease-associated endophenotypes, such as axonal support or multiple aspects of myelination, in isolation. The possibility to generate iOLs and myelinating 3D systems with patient-derived OLs simply will expand the experimental repertoire in psychiatric research.

PATIENT SELECTION AS A PRE-REQUISITE TO OVERCOME THE BOTTLENECK OF LIMITED HIPSC-BASED CELLULAR TEST SYSTEMS

One of the major questions that researchers face is how to select representatives of subgroups from whom hiPSC will be derived for empirical testing. An approach that may yield successful results is to use different analytical methods to select individuals according to phenotypical characteristics. This approach requires the availability of deeply phenotyped samples. Whereas selection based on a simple clinical feature may have limitations, clustering individuals according to different clinical subdomains (e.g. psychopathology, neurocognition or response to treatment) and

npj

Studying and modulating schizophrenia-associated dysfunctions…
F.J. Raabe et al.

8
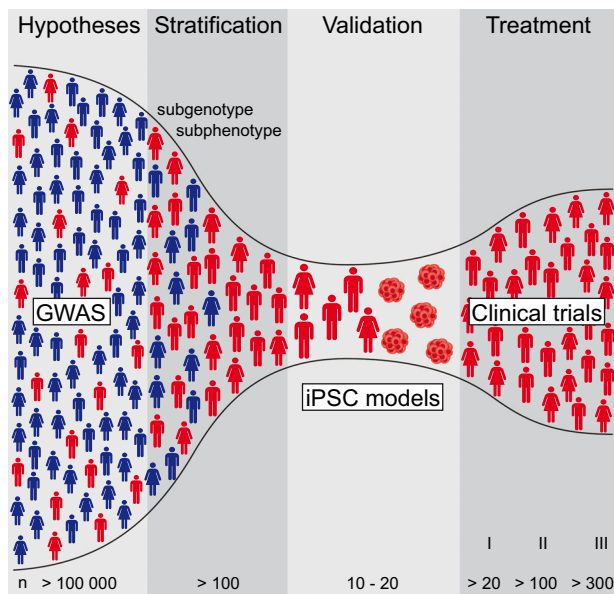
Fig. 3 hiPSC models are the bottleneck for molecular validation of hypotheses driven by genome-wide association studies (GWASs). Analyses based on GWASs ($n > 100,000$ individuals) in combination with clinical investigations allow for definition of causal hypotheses in complex diseases, such as SCZ. The next major step is sufficient patient stratification for the genetic subtype and corresponding subphenotype ($n > 100$). Subsequent iPSC reprogramming from the identified representative patients remains the bottleneck because the process is so cost and labour intensive. hiPSC models enable experimental validation and evaluation of GWAS-driven hypotheses. These patient-derived cell systems allow researchers to screen treatment options and pave the way for new therapies that can be introduced after being verified in clinical studies with increasing numbers of patients; these studies are best performed in patient subgroups that align with the initial stratification strategy

imaging (e.g. DTI) may yield more valid clusters of individuals with an enhanced biological validity, similar to the Research Domain Criteria (RDoC) concept.[159,160] Moreover, including longitudinal information into such a clustering will undoubtedly enrich the validity of the clusters in terms of disease progression/trajectory and potentially also treatment response. However, an important limitation of this approach is the high degree of uncertainty regarding the role of the environment in determining the clinical and neurocognitive profile of a patient. Another method of selecting patients is to leverage the current knowledge on the genetic architecture of complex disorders, such as SCZ.[78] Given their polygenic nature, one could select those individuals who are carriers of the largest/lowest genetic burden on the basis of their individual PRS and subsequently analyse the characteristics of their cellular systems.[78] Such a polygenic score could also be biologically informed on the basis of pathways or cell-type information (cell-type-specific PRS). This approach would be extremely relevant if the hypotheses and cellular systems are based on a specific cell type (Fig. 2B). Here again, however, caution is advised when using the PRS as a stratification criterion, given the modest amount of variation in clinical diagnosis explained by SCZ PRS.

Imaging techniques might allow patients with impaired white matter tract integrity to be included; these patients might hold the promise of having oligodendroglial pathology, which could be confirmed by combining imaging with cognitive profiling, for example. The subsequent generation of hiPSC cell systems will be very labour- and cost-intensive and represents the bottleneck in the process. This strongly argues for a stringent, at best hypothesis-driven pre-selection of relevant subgroup

representatives, which might enable investigators to reveal corresponding molecular mechanisms in SCZ. There is a chance that hiPSC technology might be a future key technology to find new cellular targets by performing genetic and chemical perturbation screenings with relevance for a given subgroup and/or trait, even with very limited numbers of test systems. Ideally, subsequent validation of candidate drugs in clinical trials and approved treatment should be restricted to those patients who fit the initial classifiers used for 'empirical validation', such as white matter abnormalities combined with cognitive deficits (Fig. 3).

OUTLOOK

The advent of hiPSCs combined with the generation of in principle any neuronal or glial cell type holds great potential for ex vivo disease modelling. A wide range of disease modelling iPSC-based systems have been developed, ranging from 2D monocultures to complex 3D myelinating multicellular systems, and we can expect that many more protocols and conditions will be explored in the future. However, the high costs and cellular variability are important limitations and represent crucial challenges, as does the issue of reproducibility. Besides these technical limitations, meaningful patient stratification is another important issue to be addressed in the future. Despite important limitations and challenges, in principle hiPSC-based cellular disease modelling offers a possibility to address cellular phenotypes in patients with SCZ, whereas retaining the genetic background of each individual. This approach, however, requires stringent experimental proof of the stability of the respective genotype throughout the process of reprogramming, cell-line establishment and differentiation. Unfortunately, experiments to prove stability have not yet been implemented in the field. Epigenetic signatures may also introduce an as yet unknown layer of variability. Nonetheless, the decrease in costs for genomic and epigenetic profiling technologies should allow the field to cope with these sources of variability when setting up batteries of iPSC lines that may complement clinical studies. If successful, personalized strategies that include these new technologies might help to address old questions and reveal new molecular pathways that contribute to neuropsychiatric diseases such as SCZ[161] and might also enable targeted drug development.[162] The field of hiPSC technology in neuroscience is rapidly evolving and constantly progressing. We are witnessing a new era of psychiatry research that brings new challenges, new solutions and new possibilities.

AUTHOR CONTRIBUTIONS

F.J.R., A.S. and M.J.R. conceived the review. F.J.R., S.G., S.P., P.G.F., A.S. and M.J.R. wrote and reviewed the manuscript. F.J.R. and M.J.R. conceived and designed the figures and table. Images that were not open source were drawn by F.J.R.

Studying and modulating schizophrenia-associated dysfunctions…
F.J. Raabe et al.

npj

9

ADDITIONAL INFORMATION

REFERENCES

1. van Os, J. & Kapur, S. Schizophrenia. *Lancet* **374**, 635–645 (2009).
2. Grande, I., Berk, M., Birmaher, B. & Vieta, E. Bipolar disorder. *Lancet* **387**, 1561–1572 (2016).
3. Charlson, F. J. et al. Global epidemiology and burden of schizophrenia: findings from the Global Burden of Disease study 2016. *Schizophr. Bull.* https://doi.org/10.1093/schbul/sby058 (2018).
4. McGrath, J., Saha, S., Chant, D. & Welham, J. Schizophrenia: a concise overview of incidence, prevalence, and mortality. *Epidemiol. Rev.* **30**, 67–76 (2008).
5. GBD 2013 DALYs and HALE Collaborators et al. Global, regional, and national disability-adjusted life years (DALYs) for 306 diseases and injuries and healthy life expectancy (HALE) for 188 countries, 1990–2013: quantifying the epidemiological transition. *Lancet* **386**, 2145–2191 (2015).
6. Global Burden of Disease Study 2013 Collaborators. Global, regional, and national incidence, prevalence, and years lived with disability for 301 acute and chronic diseases and injuries in 188 countries, 1990–2013: a systematic analysis for the Global Burden of Disease Study 2013. *Lancet* **386**, 743–800 (2015).
7. Vigo, D., Thornicroft, G. & Atun, R. Estimating the true global burden of mental illness. *Lancet Psychiatry* **3**, 171–178 (2016).
8. Hasan, A. et al. World Federation of Societies of Biological Psychiatry (WFSBP) Guidelines for Biological Treatment of Schizophrenia, part 1: update 2012 on the acute treatment of schizophrenia and the management of treatment resistance. *World J. Biol. Psychiatry* **13**, 318–378 (2012).
9. Falkai, P., Schmitt, A. & Cannon, T. D. Pathophysiology of Schizophrenia. in *Schizophrenia* 31–65 (Wiley-Blackwell, 2011) https://doi.org/10.1002/9780470978672.ch2
10. Hashimoto, K., Malchow, B., Falkai, P. & Schmitt, A. Glutamate modulators as potential therapeutic drugs in schizophrenia and affective disorders. *Eur. Arch. Psychiatry Clin. Neurosci.* **263**, 367–377 (2013).
11. Gandal, M. J. et al. Shared molecular neuropathology across major psychiatric disorders parallels polygenic overlap. *Science* **359**, 693–697 (2018).
12. Bernstein, H.-G., Steiner, J., Guest, P. C., Dobrowolny, H. & Bogerts, B. Glial cells as key players in schizophrenia pathology: recent insights and concepts of therapy. *Schizophr. Res.* **161**, 4–18 (2015).
13. Chew, L.-J., Fusar-Poli, P. & Schmitz, T. Oligodendroglial alterations and the role of microglia in white matter injury: relevance to schizophrenia. *Dev. Neurosci.* **35**, 102–129 (2013).
14. Höistad, M. et al. Linking white and grey matter in schizophrenia: oligodendrocyte and neuron pathology in the prefrontal cortex. *Front Neuroanat.* **3**, 9 (2009).
15. Birnbaum, R. & Weinberger, D. R. Genetic insights into the neurodevelopmental origins of schizophrenia. *Nat. Rev. Neurosci.* **18**, 727–740 (2017).
16. Schizophrenia Working Group of the Psychiatric Genomics Consortium. Biological insights from 108 schizophrenia-associated genetic loci. *Nature* **511**, 421–427 (2014).
17. Pardiñas, A. F. et al. Common schizophrenia alleles are enriched in mutation-intolerant genes and in regions under strong background selection. *Nat. Genet.* **50**, 381–389 (2018).
18. Brennand, K. J. & Gage, F. H. Modeling psychiatric disorders through reprogramming. *Dis. Models Mech.* **5**, 26–32 (2012).
19. Hoffman, G. E., Schrode, N., Flaherty, E. & Brennand, K. J. New considerations for hiPSC-based models of neuropsychiatric disorders. *Mol. Psychiatry* https://doi.org/10.1038/s41380-018-0029-1 (2018).
20. Soliman, M. A., Aboharb, F., Zeltner, N. & Studer, L. Pluripotent stem cells in neuropsychiatric disorders. *Mol. Psychiatry* **22**, 1241–1249 (2017).
21. Zhang, J., Li, H., Trounson, A., Wu, J. C. & Nioi, P. Combining hiPSCs and human genetics: major applications in drug development. *Cell Stem Cell* **21**, 161–165 (2017).
22. Schadt, E. E., Buchanan, S., Brennand, K. J. & Merchant, K. M. Evolving toward a human-cell based and multiscale approach to drug discovery for CNS disorders. *Front Pharmacol.* **5**, 252 (2014).
23. Paus, T., Keshavan, M. & Giedd, J. N. Why do many psychiatric disorders emerge during adolescence? *Nat. Rev. Neurosci.* **9**, 947–957 (2008).
24. Feinberg, I. Schizophrenia: caused by a fault in programmed synaptic elimination during adolescence? *J. Psychiatr. Res* **17**, 319–334 (1982).
25. Weinberger, D. R. Implications of normal brain development for the pathogenesis of schizophrenia. *Arch. Gen. Psychiatry* **44**, 660–669 (1987).
26. Lewis, D. A. & Levitt, P. Schizophrenia as a disorder of neurodevelopment. *Annu. Rev. Neurosci.* **25**, 409–432 (2002).
27. Insel, T. R. Rethinking schizophrenia. *Nature* **468**, 187–193 (2010).
28. Falkai, P. et al. Kraepelin revisited: schizophrenia from degeneration to failed regeneration. *Mol. Psychiatry* **20**, 671–676 (2015).
29. Millan, M. J. et al. Altering the course of schizophrenia: progress and perspectives. *Nat. Rev. Drug Discov.* **15**, 485–515 (2016).
30. Hermoye, L. et al. Pediatric diffusion tensor imaging: normal database and observation of the white matter maturation in early childhood. *NeuroImage* **29**, 493–504 (2006).
31. Miller, D. J. et al. Prolonged myelination in human neocortical evolution. *Proc. Natl. Acad. Sci. USA* **109**, 16480–16485 (2012).
32. Brody, B. A., Kinney, H. C., Kloman, A. S. & Gilles, F. H. Sequence of central nervous system myelination in human infancy. I. An Autopsy study of myelination. *J. Neuropathol. Exp. Neurol.* **46**, 283–301 (1987).
33. Kinney, H. C., Brody, B. A., Kloman, A. S. & Gilles, F. H. Sequence of central nervous system myelination in human infancy. II Patterns of myelination in autopsied infants. *J. Neuropathol. Exp. Neurol.* **47**, 217–234 (1988).
34. Cassoli, J. S. et al. Disturbed macro-connectivity in schizophrenia linked to oligodendrocyte dysfunction: from structural findings to molecules. *NPJ Schizophr.* **1**, 15034 (2015).
35. Micu, I., Plemel, J. R., Caprariello, A. V., Nave, K.-A. & Stys, P. K. Axo-myelinic neurotransmission: a novel mode of cell signalling in the central nervous system. *Nat. Rev. Neurosci.* **19**, 49–58 (2018).
36. Fields, R. D. A new mechanism of nervous system plasticity: activity-dependent myelination. *Nat. Rev. Neurosci.* **16**, 756–767 (2015).
37. de Hoz, L. & Simons, M. The emerging functions of oligodendrocytes in regulating neuronal network behaviour. *Bioessays* **37**, 60–69 (2015).
38. Fields, R. D. White matter in learning, cognition and psychiatric disorders. *Trends Neurosci.* **31**, 361–370 (2008).
39. Eroglu, C. & Barres, B. A. Regulation of synaptic connectivity by glia. *Nature* **468**, 223–231 (2010).
40. Schmitt, A., Hasan, A., Gruber, O. & Falkai, P. Schizophrenia as a disorder of disconnectivity. *Eur. Arch. Psychiatry Clin. Neurosci.* **261**, S150–154 (2011).
41. Fünfschilling, U. et al. Glycolytic oligodendrocytes maintain myelin and long-term axonal integrity. *Nature* **485**, 517–521 (2012).
42. Lee, Y. et al. Oligodendroglia metabolically support axons and contribute to neurodegeneration. *Nature* **487**, 443–448 (2012).
43. Stedehouder, J. et al. Fast-spiking parvalbumin interneurons are frequently myelinated in the cerebral cortex of mice and humans. *Cereb. Cortex* **27**, 5001–5013 (2017).
44. Micheva, K. D. et al. A large fraction of neocortical myelin ensheaths axons of local inhibitory neurons. *Elife* **5**, e15784 (2016).
45. Stedehouder, J. & Kushner, S. A. Myelination of parvalbumin interneurons: a parsimonious locus of pathophysiological convergence in schizophrenia. *Mol. Psychiatry* **22**, 4–12 (2017).
46. Skene, N. G. et al. Genetic identification of brain cell types underlying schizophrenia. *Nat. Genet.* **50**, 825–833 (2018).
47. Windrem, M. S. et al. Human iPSC glial mouse chimeras reveal glial contributions to schizophrenia. *Cell Stem Cell* **21**, 195–208.e6 (2017).
48. Kubicki, M. et al. A review of diffusion tensor imaging studies in schizophrenia. *J. Psychiatr. Res* **41**, 15–30 (2007).
49. Ellison-Wright, I. & Bullmore, E. Meta-analysis of diffusion tensor imaging studies in schizophrenia. *Schizophr. Res.* **108**, 3–10 (2009).
50. Flynn, S. W. et al. Abnormalities of myelination in schizophrenia detected in vivo with MRI, and post-mortem with analysis of oligodendrocyte proteins. *Mol. Psychiatry* **8**, 811–820 (2003).
51. Li, T. et al. Brain-wide analysis of functional connectivity in first-episode and chronic stages of schizophrenia. *Schizophr. Bull.* **43**, 436–448 (2017).
52. Epstein, K. A. et al. White matter abnormalities and cognitive impairment in early-onset schizophrenia-spectrum disorders. *J. Am. Acad. Child Adolesc. Psychiatry* **53**, 362–372.e1–2 (2014).
53. Kochunov, P. et al. Association of white matter with core cognitive deficits in patients with schizophrenia. *JAMA Psychiatry* **74**, 958–966 (2017).
54. Giraldo-Chica, M., Rogers, B. P., Damon, S. M., Landman, B. A. & Woodward, N. D. Prefrontal-thalamic anatomical connectivity and executive cognitive function in schizophrenia. *Biol. Psychiatry* **83**, 509–517 (2018).
55. Viviano, J. D. et al. Resting-state connectivity biomarkers of cognitive performance and social function in individuals with schizophrenia spectrum disorder and healthy control subjects. *Biol. Psychiatry* https://doi.org/10.1016/j.biopsych.2018.03.013 (2018).
56. Koshiyama, D. et al. Subcortical association with memory performance in schizophrenia: a structural magnetic resonance imaging study. *Transl. Psychiatry* **8**, 20 (2018).

Studying and modulating schizophrenia-associated dysfunctions…
F.J. Raabe et al.

10

57. Hof, P. R. et al. Loss and altered spatial distribution of oligodendrocytes in the superior frontal gyrus in schizophrenia. *Biol. Psychiatry* **53**, 1075–1085 (2003).

58. Schmitt, A. et al. Stereologic investigation of the posterior part of the hippocampus in schizophrenia. *Acta Neuropathol.* **117**, 395–407 (2009).

59. Falkai, P. et al. Decreased oligodendrocyte and neuron number in anterior hippocampal areas and the entire hippocampus in schizophrenia: a Stereological Postmortem study. *Schizophr. Bull.* **42**, S4–S12 (2016).

60. Falkai, P. et al. Oligodendrocyte and interneuron density in hippocampal subfields in schizophrenia and Association of Oligodendrocyte Number with Cognitive Deficits. *Front Cell Neurosci.* **10**, 78 (2016).

61. Vostrikov, V. M., Uranova, N. A. & Orlovskaya, D. D. Deficit of perineuronal oligodendrocytes in the prefrontal cortex in schizophrenia and mood disorders. *Schizophr. Res.* **94**, 273–280 (2007).

62. Parlapani, E. et al. Association between myelin basic protein expression and left entorhinal cortex pre-alpha cell layer disorganization in schizophrenia. *Brain Res.* **1301**, 126–134 (2009).

63. Uranova, N. et al. Electron microscopy of oligodendroglia in severe mental illness. *Brain Res. Bull.* **55**, 597–610 (2001).

64. Uranova, N. A. et al. Ultrastructural damage of capillaries in the neocortex in schizophrenia. *World J. Biol. Psychiatry* **11**, 567–578 (2010).

65. Hakak, Y. et al. Genome-wide expression analysis reveals dysregulation of myelination-related genes in chronic schizophrenia. *Proc. Natl Acad. Sci. USA* **98**, 4746–4751 (2001).

66. Haroutunian, V., Katsel, P., Dracheva, S., Stewart, D. G. & Davis, K. L. Variations in oligodendrocyte-related gene expression across multiple cortical regions: implications for the pathophysiology of schizophrenia. *Int. J. Neuropsychopharmacol.* **10**, 565–573 (2007).

67. Martins-de-Souza, D. et al. Proteomic analysis of dorsolateral prefrontal cortex indicates the involvement of cytoskeleton, oligodendrocyte, energy metabolism and new potential markers in schizophrenia. *J. Psychiatr. Res.* **43**, 978–986 (2009).

68. Saia-Cereda, V. M. et al. Proteomics of the corpus callosum unravel pivotal players in the dysfunction of cell signaling, structure, and myelination in schizophrenia brains. *Eur. Arch. Psychiatry Clin. Neurosci.* **265**, 601–612 (2015).

69. O'Donovan, M. C. et al. Identification of loci associated with schizophrenia by genome-wide association and follow-up. *Nat. Genet.* **40**, 1053–1055 (2008).

70. The International Schizophrenia Consortium. Common polygenic variation contributes to risk of schizophrenia and bipolar disorder. *Nature* **460**, 748–752 (2009).

71. Silberberg, G., Darvasi, A., Pinkas-Kramarski, R. & Navon, R. The involvement of ErbB4 with schizophrenia: association and expression studies. *Am. J. Med. Genet. B Neuropsychiatr. Genet.* **141B**, 142–148 (2006).

72. Agim, Z. S. et al. Discovery, validation and characterization of erbb4 and nrg1 haplotypes using data from three genome-wide association studies of schizophrenia. *PLoS ONE* **8**, e53042 (2013).

73. Tansey, K. E. & Hill, M. J. Enrichment of schizophrenia heritability in both neuronal and glia cell regulatory elements. *Transl. Psychiatry* **8**, 7 (2018).

74. Duncan, L. E. et al. Pathway analyses implicate glial cells in schizophrenia. *PLoS ONE* **9**, e89441 (2014).

75. The Network and Pathway Analysis Subgroup of the Psychiatric Genomics Consortium. Psychiatric genome-wide association study analyses implicate neuronal, immune and histone pathways. *Nat. Neurosci.* **18**, 199–209 (2015).

76. Baraban, M., Koudelka, S. & Lyons, D. A. Ca 2+ activity signatures of myelin sheath formation and growth in vivo. *Nat. Neurosci.* **21**, 19–23 (2018).

77. Krasnow, A. M., Ford, M. C., Valdivia, L. E., Wilson, S. W. & Attwell, D. Regulation of developing myelin sheath elongation by oligodendrocyte calcium transients in vivo. *Nat. Neurosci.* **21**, 24–28 (2018).

78. Hoekstra, S. D., Stringer, S., Heine, V. M. & Posthuma, D. Genetically-informed patient selection for iPSC studies of complex diseases may aid in reducing cellular heterogeneity. *Front Cell Neurosci.* **11**, 164 (2017).

79. Lesh, T. A., Niendam, T. A., Minzenberg, M. J. & Carter, C. S. Cognitive control deficits in schizophrenia: mechanisms and meaning. *Neuropsychopharmacology* **36**, 316–338 (2011).

80. Bora, E. et al. Cognitive deficits in youth with familial and clinical high risk to psychosis: a systematic review and meta-analysis. *Acta Psychiatr. Scand.* **130**, 1–15 (2014).

81. Hoff, A. L., Svetina, C., Shields, G., Stewart, J. & DeLisi, L. E. Ten year longitudinal study of neuropsychological functioning subsequent to a first episode of schizophrenia. *Schizophr. Res.* **78**, 27–34 (2005).

82. Rund, B. R. et al. Neurocognition and duration of psychosis: a 10-year follow-up of first-episode patients. *Schizophr. Bull.* **42**, 87–95 (2016).

83. Ranlund, S. et al. A polygenic risk score analysis of psychosis endophenotypes across brain functional, structural, and cognitive domains. *Am. J. Med. Genet. B Neuropsychiatr. Genet.* **177**, 21–34 (2018).

84. Shafee, R. et al. Polygenic risk for schizophrenia and measured domains of cognition in individuals with psychosis and controls. *Transl. Psychiatry* **8**, 78 (2018).

85. Smeland, O. B. et al. Identification of genetic loci jointly influencing schizophrenia risk and the cognitive traits of verbal-numerical reasoning, reaction time, and general cognitive function. *JAMA Psychiatry* **74**, 1065–1075 (2017).

86. Stefansson, H. et al. CNVs conferring risk of autism or schizophrenia affect cognition in controls. *Nature* **505**, 361–366 (2014).

87. Kendall, K. M. et al. Cognitive performance among carriers of pathogenic copy number variants: analysis of 152,000 UK Biobank subjects. *Biol. Psychiatry* **82**, 103–110 (2017).

88. Miller, J. A. et al. Effects of schizophrenia polygenic risk scores on brain activity and performance during working memory subprocesses in healthy young adults. *Schizophr. Bull.* **44**, 844–853 (2018).

89. Krug, A. et al. Polygenic risk for schizophrenia affects working memory and its neural correlates in healthy subjects. *Schizophr. Res.* https://doi.org/10.1016/j.schres.2018.01.013 (2018).

90. Savage, J. E. et al. Genome-wide association meta-analysis in 269,867 individuals identifies new genetic and functional links to intelligence. *Nat. Genet.* https://doi.org/10.1038/s41588-018-0152-6 (2018).

91. Kyriakopoulos, M., Vyas, N. S., Barker, G. J., Chitnis, X. A. & Frangou, S. A diffusion tensor imaging study of white matter in early-onset schizophrenia. *Biol. Psychiatry* **63**, 519–523 (2008).

92. Melicher, T. et al. White matter changes in first episode psychosis and their relation to the size of sample studied: a DTI study. *Schizophr. Res.* **162**, 22–28 (2015).

93. Zhang, X. Y. et al. Extensive white matter abnormalities and clinical symptoms in drug-naive patients with first-episode schizophrenia: a voxel-based diffusion tensor imaging study. *J. Clin. Psychiatry* **77**, 205–211 (2016).

94. Kelly, S. et al. Widespread white matter microstructural differences in schizophrenia across 4322 individuals: results from the ENIGMA Schizophrenia DTI Working Group. *Mol. Psychiatry* **23**, 1261–1269 (2018).

95. Rigucci, S. et al. White matter microstructure in ultra-high risk and first episode schizophrenia: a prospective study. *Psychiatry Res Neuroimaging* **247**, 42–48 (2016).

96. Samartzis, L., Dima, D., Fusar-Poli, P. & Kyriakopoulos, M. White matter alterations in early stages of schizophrenia: a systematic review of diffusion tensor imaging studies. *J. Neuroimaging* **24**, 101–110 (2014).

97. Kuswanto, C. N., Teh, I., Lee, T.-S. & Sim, K. Diffusion tensor imaging findings of white matter changes in first episode schizophrenia: a systematic review. *Clin. Psychopharmacol. Neurosci.* **10**, 13–24 (2012).

98. Voineskos, A. N. et al. Oligodendrocyte genes, white matter tract integrity, and cognition in schizophrenia. *Cereb. Cortex* **23**, 2044–2057 (2013).

99. Heilbronner, U., Samara, M., Leucht, S., Falkai, P. & Schulze, T. G. The longitudinal course of schizophrenia across the lifespan: clinical, cognitive, and neurobiological aspects. *Harv. Rev. Psychiatry* **24**, 118–128 (2016).

100. Raabe, F. J. & Spengler, D. Epigenetic risk factors in PTSD and depression. *Front Psychiatry* **4**, 80 (2013).

101. Takahashi, K. & Yamanaka, S. Induction of pluripotent stem cells from mouse embryonic and adult fibroblast cultures by defined factors. *Cell* **126**, 663–676 (2006).

102. Aasen, T. et al. Efficient and rapid generation of induced pluripotent stem cells from human keratinocytes. *Nat. Biotechnol.* **26**, 1276–1284 (2008).

103. Zhou, T. et al. Generation of human induced pluripotent stem cells from urine samples. *Nat. Protoc.* **7**, 2080–2089 (2012).

104. Loh, Y.-H. et al. Generation of induced pluripotent stem cells from human blood. *Blood* **113**, 5476–5479 (2009).

105. Loh, Y.-H. et al. Reprogramming of T cells from human peripheral blood. *Cell Stem Cell* **7**, 15–19 (2010).

106. Seki, T. et al. Generation of induced pluripotent stem cells from human terminally differentiated circulating T cells. *Cell Stem Cell* **7**, 11–14 (2010).

107. Staerk, J. et al. Reprogramming of human peripheral blood cells to induced pluripotent stem cells. *Cell Stem Cell* **7**, 20–24 (2010).

108. Seki, T., Yuasa, S. & Fukuda, K. Generation of induced pluripotent stem cells from a small amount of human peripheral blood using a combination of activated T cells and Sendai virus. *Nat. Protoc.* **7**, 718–728 (2012).

109. Zhou, H. et al. Rapid and efficient generation of transgene-free iPSC from a small volume of cryopreserved blood. *Stem Cell Rev. Rep.* **11**, 652–665 (2015).

110. Takahashi, K. et al. Induction of pluripotent stem cells from adult human fibroblasts by defined factors. *Cell* **131**, 861–872 (2007).

111. Stadtfeld, M., Nagaya, M., Utikal, J., Weir, G. & Hochedlinger, K. Induced pluripotent stem cells generated without viral integration. *Science* **322**, 945–949 (2008).

112. Warren, L. et al. Highly efficient reprogramming to pluripotency and directed differentiation of human cells with synthetic modified mRNA. *Cell Stem Cell* **7**, 618–630 (2010).

113. Fusaki, N., Ban, H., Nishiyama, A., Saeki, K. & Hasegawa, M. Efficient induction of transgene-free human pluripotent stem cells using a vector based on Sendai

Studying and modulating schizophrenia-associated dysfunctions...
F.J. Raabe et al.

npj

11

virus, an RNA virus that does not integrate into the host genome. *Proc. Jpn. Acad., Ser. B Phys. Biol. Sci.* **85**, 348–362 (2009).

114. Okita, K. et al. A more efficient method to generate integration-free human iPS cells. *Nat. Methods* **8**, 409–412 (2011).

115. Schlaeger, T. M. et al. A comparison of non-integrating reprogramming methods. *Nat. Biotechnol.* **33**, 58–63 (2015).

116. Brouwer, M., Zhou, H. & Nadif Kasri, N. Choices for induction of pluripotency: recent developments in human induced pluripotent stem cell reprogramming strategies. *Stem Cell Rev.* **12**, 54–72 (2016).

117. Mack, A. A., Kroboth, S., Rajesh, D. & Wang, W. B. Generation of induced pluripotent stem cells from CD34+ cells across blood drawn from multiple donors with non-integrating episomal vectors. *PLoS ONE* **6**, e27956 (2011).

118. Chou, B.-K. et al. Efficient human iPS cell derivation by a non-integrating plasmid from blood cells with unique epigenetic and gene expression signatures. *Cell Res.* **21**, 518–529 (2011).

119. Dowey, S. N., Huang, X., Chou, B.-K., Ye, Z. & Cheng, L. Generation of integration-free human induced pluripotent stem cells from postnatal blood mononuclear cells by plasmid vector expression. *Nat. Protoc.* **7**, 2013–2021 (2012).

120. Paşca, S. P., Panagiotakos, G. & Dolmetsch, R. E. Generating human neurons in vitro and using them to understand neuropsychiatric disease. *Annu. Rev. Neurosci.* **37**, 479–501 (2014).

121. Yu, D. X. et al. Modeling hippocampal neurogenesis using human pluripotent stem cells. *Stem Cell Rep.* **2**, 295–310 (2014).

122. Zhang, Y. et al. Rapid single-step induction of functional neurons from human pluripotent stem cells. *Neuron* **78**, 785–798 (2013).

123. Busskamp, V. et al. Rapid neurogenesis through transcriptional activation in human stem cells. *Mol. Syst. Biol.* **10**, 760 (2014).

124. Nehme, R. et al. Combining NGN2 programming with developmental patterning generates human excitatory neurons with NMDAR-mediated synaptic transmission. *Cell Rep.* **23**, 2509–2523 (2018).

125. Ma, L. et al. Human embryonic stem cell-derived gaba neurons correct locomotion deficits in quinolinic acid-lesioned mice. *Cell Stem Cell* **10**, 455–464 (2012).

126. Maroof, A. M. et al. Directed differentiation and functional maturation of cortical interneurons from human embryonic stem cells. *Cell Stem Cell* **12**, 559–572 (2013).

127. Tyson, J. A. et al. Duration of culture and sonic hedgehog signaling differentially specify PV versus SST cortical interneuron fates from embryonic stem cells. *Development* **142**, 1267–1278 (2015).

128. Chandrasekaran, A., Avci, H. X., Leist, M., Kobolák, J. & Dinnyés, A. Astrocyte differentiation of human pluripotent stem cells: new tools for neurological disorder research. *Front Cell Neurosci.* **10**, 215 (2016).

129. Pocock, J. M. & Piers, T. M. Modelling microglial function with induced pluripotent stem cells: an update. *Nat. Rev. Neurosci.* https://doi.org/10.1038/s41583-018-0030-3 (2018).

130. Alsanie, W. F., Niclis, J. C. & Petratos, S. Human embryonic stem cell-derived oligodendrocytes: protocols and perspectives. *Stem Cells Dev.* **22**, 2459–2476 (2013).

131. Goldman, S. A. & Kuypers, N. J. How to make an oligodendrocyte. *Development* **142**, 3983–3995 (2015).

132. Lopez Juarez, A., He, D. & Richard Lu, Q. Oligodendrocyte progenitor programming and reprogramming: toward myelin regeneration. *Brain Res.* **1638**, 209–220 (2016).

133. Yang, N. et al. Generation of oligodendroglial cells by direct lineage conversion. *Nat. Biotechnol.* **31**, 434–439 (2013).

134. Najm, F. J. et al. Transcription factor-mediated reprogramming of fibroblasts to expandable, myelinogenic oligodendrocyte progenitor cells. *Nat. Biotechnol.* **31**, 426–433 (2013).

135. Li, P. et al. Accelerated generation of oligodendrocyte progenitor cells from human induced pluripotent stem cells by forced expression of Sox10 and Olig2. *Sci. China Life Sci.* **59**, 1131–1138 (2016).

136. Ehrlich, M. et al. Rapid and efficient generation of oligodendrocytes from human induced pluripotent stem cells using transcription factors. *Proc. Natl Acad. Sci. USA* **114**, E2243–E2252 (2017).

137. Pawlowski, M. et al. Inducible and deterministic forward programming of human pluripotent stem cells into neurons, skeletal myocytes, and oligodendrocytes. *Stem Cell Rep.* **8**, 803–812 (2017).

138. Rodrigues, G. M. C. et al. Defined and scalable differentiation of human oligodendrocyte precursors from pluripotent stem cells in a 3D culture system. *Stem Cell Rep.* **8**, 1770–1783 (2017).

139. García-León, J. A. et al. SOX10 single transcription factor-based fast and efficient generation of oligodendrocytes from human pluripotent stem cells. *Stem Cell Rep.* **10**, 655–672 (2018).

140. Wang, S. et al. Human iPSC-derived oligodendrocyte progenitor cells can myelinate and rescue a mouse model of congenital hypomyelination. *Cell Stem Cell* **12**, 252–264 (2013).

141. Najm, F. J.et al. Drug-based modulation of endogenous stem cells promotes functional remyelination in vivo. *Nature* https://doi.org/10.1038/nature14335 (2015).

142. Mariani, J. et al. Modeling human cortical development in vitro using induced pluripotent stem cells. *Proc. Natl Acad. Sci. USA* **109**, 12770–12775 (2012).

143. Lancaster, M. A. et al. Cerebral organoids model human brain development and microcephaly. *Nature* **501**, 373–379 (2013).

144. Quadrato, G., Brown, J. & Arlotta, P. The promises and challenges of human brain organoids as models of neuropsychiatric disease. *Nat. Med.* **22**, 1220–1228 (2016).

145. Birey, F. et al. Assembly of functionally integrated human forebrain spheroids. *Nature* **545**, 54–59 (2017).

146. Madhavan, M. et al. Induction of myelinating oligodendrocytes in human cortical spheroids. *Nat. Methods* **15**, 700–706 (2018).

147. Pamies, D. et al. A human brain microphysiological system derived from induced pluripotent stem cells to study neurological diseases and toxicity. *ALTEX* **34**, 362–376 (2017).

148. Brennand, K. J. et al. Modelling schizophrenia using human induced pluripotent stem cells. *Nature* **473**, 221–225 (2011).

149. Prytkova, I. & Brennand, K. J. Prospects for modeling abnormal neuronal function in schizophrenia using human induced pluripotent stem cells. *Front. Cell Neurosci.* **11**, 360 (2017).

150. Chen, X. et al. Novel schizophrenia risk factor pathways regulate FEZ1 to advance oligodendroglia development. *Transl. Psychiatry* **7**, 1293 (2017).

151. Lee, I. S. et al. Characterization of molecular and cellular phenotypes associated with a heterozygous CNTNAP2 deletion using patient-derived hiPSC neural cells. *NPJ Schizophr.* **1**, 15019 (2015).

152. de Vrij, F. M. et al. Candidate CSPG4 mutations and induced pluripotent stem cell modeling implicate oligodendrocyte progenitor cell dysfunction in familial schizophrenia. *Mol. Psychiatry* https://doi.org/10.1038/s41380-017-0004-2 (2018).

153. Küspert, M. & Wegner, M. SomethiNG 2 talk about-Transcriptional regulation in embryonic and adult oligodendrocyte precursors. *Brain Res.* **1638**, 167–182 (2016).

154. Sakry, D. & Trotter, J. The role of the NG2 proteoglycan in OPC and CNS network function. *Brain Res.* **1638**, 161–166 (2016).

155. Brennand, K. J., Landek-Salgado, M. A. & Sawa, A. Modeling heterogeneous patients with a clinical diagnosis of schizophrenia with induced pluripotent stem cells. *Biol. Psychiatry* **75**, 936–944 (2014).

156. Hoffman, G. E. et al. Transcriptional signatures of schizophrenia in hiPSC-derived NPCs and neurons are concordant with post-mortem adult brains. *Nat. Commun.* **8**, 2225 (2017).

157. Carcamo-Orive, I. et al. Analysis of transcriptional variability in a large human iPSC library reveals genetic and non-genetic determinants of heterogeneity. *Cell Stem Cell* **20**, 518–532.e9 (2017).

158. Schwartzentruber, J. et al. Molecular and functional variation in iPSC-derived sensory neurons. *Nat. Genet.* **50**, 54–61 (2018).

159. Insel, T. R. & Cuthbert, B. N. Endophenotypes: bridging genomic complexity and disorder heterogeneity. *Biol. Psychiatry* **66**, 988–989 (2009).

160. NIMH. NIMH » Definitions of the RDoC Domains and Constructs. (2018). Available at: https://www.nimh.nih.gov/research-priorities/rdoc/definitions-of-the-rdoc-domains-and-constructs.shtml. (Accessed 12th July 2018).

161. Willsey, A. J. et al. The psychiatric cell map initiative: a convergent systems biological approach to illuminating key molecular pathways in neuropsychiatric disorders. *Cell* **174**, 505–520 (2018).

162. Gibbs, R. M. et al. Toward precision medicine for neurological and neuropsychiatric disorders. *Cell Stem Cell* **23**, 21–24 (2018).

Acknowledgements

This thesis was possible thank to the great scientific environment that enabled and supported me to perform translational research for my PhD in parallel to my residency and specialization in psychiatry. Herby, I would like to express my special thanks…

…to my preclinical supervisor *Moritz Rossner* for his openness to integrate me as only clinician in his research group, for inspiring visions of future biological psychiatry, for introducing me to new dimensions of science, and the 100ends of intensive and long discussions. Above all, I would like to thank him for allowing and supporting me to pursue my own ideas and develop projects that were not originally in his focus.

…to my clinical supervisor *Andrea Schmitt* for her great support that I was able to combine both sides, bed and bench, of the translational bridge. She picked up on my interest in translational research, paved the way for my PhD and opened up her large scientific network to me.

…to *Michael Ziller* for his scientific sprit, his invitation to team up and initiate a scaled collaborative project in parallel to my core PhD project, and the unique opportunity of an outstanding lab rotation at his *Lab for Genomics of Complex Diseases, Department of Translational Research, Max Planck Institute of Psychiatry.*

…to *Peter Falkai* for creating a unique scientific environment for translational psychiatry at the Department of Psychiatry and for being very supportive of wet lab projects during my residency.

I am especially grateful to the enthusiastic research team of *Molecular and Behavioural Neurobiology* at the Department of Psychiatry and Psychotherapy for their intensive support, exchange of ideas, great research discussions and their humour that carried me through the PhD even in challenging times.

Finally, this work would never have happened without the excellent and continuous support and patience of my wife *Nadja* and *my family*, who never stopped believing in my abilities.